



UNIVERSITY OF SOUTHERN DENMARK

MASTER THESIS

June 1, 2018

Synchronisation in Stochastic Oscillatory Networks

Bonnie Liefting

supervised by

Prof. dr. Kristian Debrabant
Prof. dr. Holger Waalkens¹

Abstract

Fænomenet synkronisering er blevet undersøgt ved hjælp af Kuramoto modellen samt med forskellige tilpasninger deraf. Denne model beskriver en stor population af koblede oscillatorer. Tilpasningerne som er undersøgt her inkluderer en bimodal frekvens fordeling, tilføjelse af hvid støj, kobling afhængig af beliggenhed og en uniform faseforskydning. Vi reproducerer analyser og udfører simulationer, hvor blandt andet Monte Carlo metoder er brugt. Ved hjælp af tid-frekvens analyse baseret på wavelets er vi i stand til at opdage partiell synkronisering.

¹University of Groningen

Introduction

We introduce the concept of synchronisation and the model that Kuramoto used to describe it as well as various adaptations of it. We are interested in the behaviour of the oscillators for different distributions of their natural frequencies and different types of coupling between them. How strong should the oscillators be coupled to each other in order for them to synchronise? What is the effect of adding white-noise? How can we use time-frequency analysis to detect (partial) synchronisation? What conditions does a system need to satisfy for chimera states to appear?

This Thesis and our Results

In order to answer these and more questions about synchronisation we followed analyses of various models that were performed previously. We start with the analysis of the Kuramoto model based on the works of Kuramoto, Battogtokh and Okuda [1, 2]. We then look at the Kuramoto model with added white noise based on the works of Acebrón and Bonilla [3, 4]. Our study of those models with bimodal frequency distributions as well as a model in which Chimera states appear are based on the works of Sakaguchi [5], Strogatz, Mirello, Martens, Abrams and Pannagio [6, 7, 8, 9, 10] and those of Ott and Antonsen [11]. In addition to this we performed numerical analyses on all models discussed using Monte Carlo simulations to make a comparison between each of the models with and without a white noise forcing term. We also performed time-frequency analysis based on wavelets using the Matlab Wavelet toolbox [12, 13] on those results, which to our knowledge has not been performed before on the models discussed here.

Motivational Examples

Well known examples of collective synchronisation in biology are those of fireflies flashing and crickets chirping in sync. Collective synchronisation also appears within organism. For example in insulin-secreting cells in the pancreas and in pacemaker cells in the heart. Furthermore there are cells in the brain and spinal cord that synchronise in order to control the rhythm of breathing and running. [14]

The interaction between fireflies, crickets or neurons happens through pulses. The insects or cells respond to sudden impulses of their neighbours. This behaviour is difficult to model mathematically. We would like to model continuous behaviour rather than the discontinuous pulses. Thus we consider only the rhythm of an individual or neuron. We might think of this as oscillators with a certain natural frequency. When their periods (or frequencies) coincide, they are said to be in sync.

We will consider a large collection of coupled oscillators and study the behaviour of the system. Such a large collection of oscillators might spontaneously lock into a common frequency. In other words, without force put upon them, the oscillators will take on the same frequency despite having different natural frequencies. When the coupling is location dependent and furthermore a phase lag is introduced, even more interesting behaviour can appear. We study the appearance of chimera states in which some of the oscillators are synchronised whilst the others move incoherently.

Organisation of the Thesis

The network we will study in Section 1 is the Kuramoto model. The coupling strength between the oscillators depends only on the relative phase between the oscillators. In this Section we also introduce the order parameter, which is an important measure of synchronisation that is used throughout the paper. We continue by studying the Kuramoto model with added white noise in Section 2. In this model the coupling depends on the oscillators' relative phase as well as a white-noise term. The phase of each oscillator is described by a stochastic differential equation.

The analytics of considering a bimodal frequency distribution are discussed in Section 3. We consider the Kuromoto model with added white noise where the natural frequencies have a discrete bimodal distribution. Furthermore we consider the Kuramoto model where the oscillators have a Lorentzian bimodal frequency distribution.

Another adaptation is implementing a coupling that is location dependent in addition to be depending on relative phases. The model we study analytically in Section 4 was proposed by Abrams, Mirello and Strogatz [6]. The oscillators are divided into two groups where the intra-group coupling is stronger than the intergroup coupling. Apart from location dependent coupling, this model also includes a phase-lag as described by Sakaguchi [5]. In such models an interesting phenomena, named a chimera state, can appear in which some oscillators are synchronised while others move incoherently.

In the limit of infinitely many oscillators we can study the behaviour of such a network analytically. To confirm the stability properties that can be found analytically, we perform Monte Carlo simulations of the model. The resulting paths of the oscillators can then be analysed using time-frequency analysis. In particular, we will use time-frequency analysis based on wavelets as described in Section 5 on the order parameter of the Kuramoto model. This parameter gives the general rhythm of the oscillators and with our time-frequency analysis we should be able to detect partial synchronisation. This is relevant when we for example consider a bimodal distribution of the oscillators frequencies. The results of the simulations as well as the time-frequency analysis on the order parameters for different models described in this thesis can be found in Section 6.

Contents

Introduction	1
This Thesis and our Results	1
Motivational Examples	1
Organisation of the Thesis	2
List of Symbols	3
1 The Original Kuramoto Model	5
1.1 Winfree's Research on Synchronisation	5
1.2 Introducing the Kuramoto Model	5
1.3 Order Parameter	6
1.4 Kuramoto's Analysis	7
2 The Kuramoto Model with added White Noise	11

2.1	Introducing the Model	11
2.2	Fokker-Planck Equation	11
2.3	Stability Analysis around the Incoherent Solution	12
2.3.1	Derivation of the Evolution Equations	12
2.3.2	Analysis of the Fundamental Harmonic (Eigenvalues)	16
2.3.3	Analysis of the Fundamental Harmonic (Continuous Spectrum)	17
3	Bimodal Frequency Distribution	20
3.1	Discrete Bimodal Frequency Distribution	20
3.2	Lorenzian Bimodal Frequency Distribution	21
3.2.1	Derivation	21
3.2.2	Bifurcation Analysis around the Incoherent Solution	26
4	Chimera State	28
4.1	Derivation	28
4.2	Analysis of Chimera State	32
4.3	Bifurcation Analysis for Chimera State	35
4.3.1	Phase Plane Analysis	35
4.3.2	Bifurcation Curves	37
5	Time-frequency Analysis	39
5.1	Basic Fourier Transform	39
5.2	Windowed Fourier Transform	40
5.3	Continuous Wavelet Transform	40
5.4	Time-frequency Analysis: Some Examples	41
6	Numerical Solutions	42
6.1	The Original Kuramoto Model	43
6.2	The Kuramoto Model with added White-Noise	46
6.3	Bimodal Frequency Distribution	47
6.4	Chimera State	50
7	Concluding remarks	53
A	Calculation of r^2 for Chimera Model	55
B	Matlab Code for Simulations	56
C	Matlab Code for Phase Plots	65

List of Symbols

Here we present the symbols used in order of appearance.

N	number of oscillators
ω	natural frequency
θ	phase
K	coupling strength (Kuramoto model)

z	complex order parameter
r	$r = z $, measure of phase coherence ²
ψ	average phase
ρ	distribution of oscillators
g	distribution of natural frequencies
ξ	white noise
D	noise strength
W	Wiener / Brownian process
η	function with which we perturb ρ
c	first harmonic of η 's Fourier series
η^\perp	second and higher order harmonics of η 's Fourier series
<i>c.c.</i>	complex conjugate of the preceding term
λ	eigenvalue
δ	Dirac delta
σ_c	continuous spectrum
K_c	critical coupling
K^*	coupling at which $D = -\lambda$
ω_0	mean (or means $\pm\omega_0$) of (bimodal) frequency distribution
Δ	width parameter in (bimodal) Lorenzian distribution
*	complex conjugation
a	term in the Ott-Antonsen ansatz $c_n = a^n$ for the Fourier expansion terms of ρ
α	phase lag
β	$\frac{\pi}{2} - \alpha$
μ	intragroup coupling
ν	intergroup coupling
A	parameter determining intra- / intergroup coupling strength
φ	radial coordinate of order parameter z
ϕ	angular coordinate of order parameter z
$\psi(t)$	mother wavelet
$\psi_{a,b}(t)$	daughter wavelet
$L_\psi S(a, b)$	wavelet transform of a signal $S(t)$

²Either of the whole oscillator population or (only in Section 4) a local order parameter for the second group.

1 The Original Kuramoto Model

In this section we introduce the Kuramoto model as well as the order parameter. This order parameter can be seen as the average of a group of oscillators and turns out to be useful when studying synchronisation. We start by defining synchronisation and briefly discuss Winfree's research before we introduce Kuramoto's ideas.

We will now formally define what we mean by synchronisation. Consider a system of N oscillators with phases θ_i for $i = 1, \dots, N$. These oscillators are said to synchronise if $\dot{\theta}_i - \dot{\theta}_j \rightarrow 0$ as $t \rightarrow \infty$ for every $i, j = 1, \dots, N$, where a dot denotes the derivative with respect to time. Synchronisation thus means that the oscillators travel with the same speed as $t \rightarrow \infty$. They are said to be exactly synchronised when moreover $\theta_i - \theta_j \rightarrow 0$ as $t \rightarrow \infty$ for every $i, j = 1, \dots, N$. Thus next to having the same speed, the oscillators will follow the exact same path as $t \rightarrow \infty$.

1.1 Winfree's Research on Synchronisation

Winfree started his research on large populations of limit-cycle oscillators in 1966 [14]. He used computer simulations, mathematical analysis and experiments with electrically coupled neon-tube oscillators. In his mathematical analysis Winfree considered a large population of limit-cycle oscillators. Such oscillators are periodic in time, meaning that the phase corresponds to a closed curve called a limit cycle in the phase plane. Trajectories close to this limit cycle will converge to it. In particular this means that when an oscillator is slightly perturbed it will still tend to move along its limit cycle, i.e. move with its natural frequency.

Winfree allowed for interaction between all oscillators and applied some simplifications in order to analyse the behaviour. Firstly he assumed that the coupling between the oscillators was weak and secondly he assumed that the oscillators were nearly identical. A third simplification made by Winfree was that the natural frequencies are taken from some narrow probability function. Furthermore the oscillators are assumed to be coupled to the collective rhythm of the population. That is, rather than being coupled to each of the other oscillators it is coupled to some average of the frequencies.

1.2 Introducing the Kuramoto Model

Inspired by the works of Winfree, Kuramoto decided to study the phenomenon as well [15]. He expanded on the ideas of Winfree and derived a model that describes the long term dynamics of any system of nearly identical weakly coupled limit-cycle oscillators. In spite of the assumptions made in order to simplify the model, the oscillators described by the Kuramoto model will still synchronise under certain conditions. Therefore the model can and has been used to study collective synchronisation.

The Kuramoto model describes a system of N oscillators that are coupled by means of their phase differences. A general form for the rate of change of the i 'th oscillator is given by

$$\dot{\theta}_i = \omega_i + \sum_{j=1}^N L_{i,j}(\theta_j - \theta_i),$$

for $i = 1, \dots, N$. Here ω_i is the natural frequency of the respective oscillator and $L_{i,j}$ denotes the interaction function. Kuramoto considered purely sinusoidal coupling between all oscillators.

Thus he obtained

$$\dot{\theta}_i = \omega_i + \sum_{j=1}^N K_{i,j} \sin(\theta_j - \theta_i), \quad i = 1, \dots, N, \quad (1)$$

where $K_{i,j}$ denote the coupling constants. For small coupling constants the model approximately describes a system of independent oscillators moving at frequencies ω_i . Because the model is closely related to this solvable system, it is a useful tool in our study. As we will find out, the coupling constants should be sufficiently great in order for synchronisation to occur.

Different types of coupling may be considered. Some possibilities are next-neighbour coupling, mean-field coupling and long-range coupling [4]. We will consider mean-field coupling, each oscillator is coupled to some average frequency. The coupling constants $K_{i,j}$ are identically equal to $\frac{K}{N}$ for all $i, j = 1, \dots, N$. The model then becomes

$$\dot{\theta}_i = \omega_i + \frac{K}{N} \sum_{j=1}^N \sin(\theta_j - \theta_i), \quad i = 1, \dots, N. \quad (2)$$

Each oscillator is coupled to the collective rhythm, as was also assumed by Winfree. This is not evident from the equations for the Kuramoto model as introduced above (1). To get a better idea of the model and the dependence between the oscillators we therefore introduce the *order parameter*.

1.3 Order Parameter

Let θ_i describe the angle of a point running around the unit circle. The model then describes a collection of N points running around this unit circle. We can define a collective rhythm for this collection of points as

$$z = r e^{i\psi} = \frac{1}{N} \sum_{j=1}^N e^{i\theta_j}. \quad (3)$$

Here ψ is the average phase and r measures the phase coherence of the oscillators. The order parameter z will have a value located in the unit circle. If the points are spread around the circle, r will be close to zero. If the points are located closer to each other, r will be closer to 1. So values of $r e^{i\psi}$ close to zero indicate absence of synchronisation whereas values close to the unit circle indicate (partial) synchronisation.

We can write equations (2) in terms of the order parameter. First we rewrite (3) by multiplying both sides by $e^{-i\theta_i}$ to obtain

$$r e^{i(\psi - \theta_i)} = \frac{1}{N} \sum_{j=1}^N e^{i(\theta_j - \theta_i)}.$$

We then equate imaginary parts:

$$r \sin(\psi - \theta_i) = \frac{1}{N} \sum_{j=1}^N \sin(\theta_j - \theta_i).$$

By this result equation (2) can be rewritten to

$$\dot{\theta}_i = \omega_i + Kr \sin(\psi - \theta_i), \quad i = 1, \dots, N.$$

Modifying the model using this order parameter leads us to the conclusion that each oscillator is coupled to the others only through the mean-field quantities r and ψ . As the population becomes more coherent, r increases and therefore the effective coupling term Kr increases. This leads to more and more oscillators becoming part of the synchronised group of oscillators. This behaviour was first discovered by Winfree and specifically stands out in the Kuramoto model.

Kuramoto used this order parameter to study the behaviour of the model. We will have a look at his analysis in the next subsection. In Section 5 we will analyse the order parameter in a different manner. Namely by using time-frequency analysis.

1.4 Kuramoto's Analysis

In this section, we will follow Kuramoto's analysis of the model as described by Strogatz [16]. We have rewritten (3) in terms of the mean-field quantities in the following way:

$$\dot{\theta}_i = \omega_i + Kr \sin(\psi - \theta_i), \quad \text{for } i = 1, \dots, N.$$

We will now analyse the model following Kuramoto's procedures. In his analysis, Kuramoto sought for particular solutions, namely those in which $r(t)$ is constant and $\psi(t)$ rotates uniformly at some frequency Ω . By then moving into a rotating frame with this frequency Ω we can set $\psi = 0$ to obtain

$$\dot{\theta}_i = \omega_i - Kr \sin(\theta_i), \quad \text{for } i = 1, \dots, N.$$

This equation has two different types of solutions. One corresponding to the oscillators that are in the synchronised pack, the other corresponding to the oscillators that are not.

Oscillators for which their natural frequency satisfies $|\omega_i| \leq Kr$ have solutions approaching a stable fixed point. This fixed point satisfies $\dot{\theta}_i = 0$ and can therefore be implicitly described by

$$\omega_i = Kr \sin(\theta_i), \quad \text{where } |\theta_i| \leq \frac{1}{2}\pi.$$

These are the oscillators that are part of the synchronised pack. With respect to the original frame, these oscillators are locked to the frequency Ω . For coupling constants great enough (relative to the natural frequencies), each oscillator will tend to a fixed point. Hence they will all synchronise when we take the limit $K \rightarrow \infty$.

However, this is not necessarily the case. Some of the oscillators might have natural frequencies such that $|\omega_i| > Kr$. These will not lock to the frequency Ω . Instead, they will run around the circle in an incoherent manner. As they interact with the other oscillators, they will speed up at some of the phases and slow down at others.

Recall that we are considering solutions such that the order parameter (3) is constant. To ensure that the order parameter is constant even though not all oscillators lock their phase, Kuramoto required the drifting oscillators to form a stationary distribution. He required that oscillators pile up at slow places and thin out at fast places. The fraction of oscillators whose natural frequency is given by ω that lie between θ and $\theta + d\theta$ is denoted by $\rho(\theta, \omega)d\theta$. The

incoherent solution is for example represented by a phase distribution $\rho(\theta, \omega)$ has a constant value of $\frac{1}{2\pi}$ for each ω when we normalise the integral using

$$\int_{-\pi}^{\pi} \rho(\theta, \omega) d\theta = 1 \quad (4)$$

for each ω . Then we should have that it is inversely proportional to the speed at θ . Hence,

$$\rho(\theta, \omega) = \frac{C}{|\dot{\theta}|} = \frac{C}{|\omega - Kr \sin(\theta)|}. \quad (5)$$

The normalisation condition (4) thus results in

$$\begin{aligned} 1 &= \lim_{n \rightarrow \pi} \int_{-n}^n \frac{C}{|\omega - Kr \sin(\theta)|} d\theta \\ &= \lim_{n \rightarrow \pi} \frac{-2C \tan^{-1} \left(\frac{Kr - \omega \tan(\frac{n}{2})}{\sqrt{\omega^2 - (Kr)^2}} \right) \text{sign}(\omega - Kr \sin(n))}{\sqrt{\omega^2 - (Kr)^2}} \Big|_{-n}^n \\ &= \frac{2C \left(\frac{\pi}{2} + \frac{\pi}{2} \right) \text{sign}(\omega) \cdot \text{sign}(\omega)}{\sqrt{\omega^2 - (Kr)^2}} \\ &= \frac{2C\pi}{\sqrt{\omega^2 - (Kr)^2}}. \end{aligned}$$

The normalisation constant C is determined to be

$$C = \frac{1}{2\pi} \sqrt{\omega^2 - (Kr)^2}.$$

Since we are in the rotating frame such that $\psi = 0$, we can rewrite the order parameter to $re^{i\psi} = r$. The order parameter should describe the collective rhythm of the oscillators. As we take the limit $N \rightarrow \infty$, we denote the order parameter by

$$r = \langle e^{i\theta} \rangle_{\text{lock}} + \langle e^{i\theta} \rangle_{\text{drift}}, \quad (6)$$

where $\langle e^{i\theta} \rangle_{\text{lock}}$ and $\langle e^{i\theta} \rangle_{\text{drift}}$ denote the averages of the oscillators locked to the phase $\psi = 0$ and the drifting oscillators respectively. For a locked state θ_{lock} , we have that $\dot{\theta}_{\text{lock}} = 0$ and hence

$$\sin(\theta_{\text{lock}}) = \frac{\omega}{Kr}. \quad (7)$$

Kuramoto assumes that the natural frequency distribution of the oscillators satisfies $g(\omega) = g(-\omega)$ in the limit of infinitely many oscillators. This implies that the number of oscillators at θ_{lock} is equal to the number of oscillators at $-\theta_{\text{lock}}$ and therefore $\langle \sin(\theta_{\text{lock}}) \rangle = 0$. Thus the average of the locked phases is given by

$$\langle e^{i\theta} \rangle_{\text{lock}} = \langle \cos \theta \rangle_{\text{lock}}, \quad (8)$$

where the drifting oscillators have natural frequencies satisfying $|\omega| > Kr$. Their contribution to the average of the population is given by

$$\begin{aligned}
\langle e^{i\theta} \rangle_{\text{drift}} &= \int_{-\pi}^{\pi} \int_{|\omega| > Kr} e^{i\theta} \rho(\theta, \omega) g(\omega) d\omega d\theta \\
&= \int_{-\pi}^{\pi} \int_{-\infty}^{-Kr} e^{i\theta} \rho(\theta, \omega) g(\omega) d\omega d\theta \\
&\quad + \int_{-\pi}^{\pi} \int_{Kr}^{\infty} e^{i\theta} \rho(\theta, \omega) g(\omega) d\omega d\theta \\
&= \int_{-\pi}^{\pi} \int_{Kr}^{\infty} e^{i\theta} \rho(\theta, -\omega) g(\omega) d\omega d\theta \\
&\quad + \int_{-\pi}^{\pi} \int_{Kr}^{\infty} e^{i\theta} \rho(\theta, \omega) g(\omega) d\omega d\theta. \tag{9}
\end{aligned}$$

Where we rewrote the first integral by changing variables from ω to $-\omega$. This implies the change of variables for the phase $\theta \rightarrow \theta + \pi$ as follows: $\omega = Kr \sin(\theta) \rightarrow -Kr \sin(\theta) = Kr \sin(\theta + \pi)$. Thus (9) becomes

$$\begin{aligned}
\langle e^{i\theta} \rangle_{\text{drift}} &= \int_0^{2\pi} \int_{Kr}^{\infty} \left(e^{i\theta} \rho(\theta, \omega) g(\omega) + e^{i(\theta+\pi)} \rho(\theta + \pi, -\omega) g(-\omega) \right) d\omega d\theta \\
&= \int_0^{2\pi} \int_{Kr}^{\infty} (e^{i\theta} \rho(\theta, \omega) g(\omega) - e^{i\theta} \rho(\theta, \omega) g(\omega)) d\omega d\theta \\
&= 0.
\end{aligned}$$

Here we have used the symmetry $\rho(\theta + \pi, -\omega) = \rho(\theta, \omega)$ implied by (5). Combining this result with (6) and (8), we find that r only depends on the cosine of the phase of the locked oscillators. For locked oscillators, the integral over θ is non zero only for one particular phase $\theta(\omega)$. We obtain

$$\begin{aligned}
r &= \langle \cos \theta \rangle_{\text{lock}} \\
&= \int_{|\omega| \leq Kr} \cos(\theta(\omega)) g(\omega) d\omega.
\end{aligned}$$

For the locked oscillators, we can use the expression for ω given by (7) to change variables to θ .

$$\begin{aligned}
r &= \int_{|\theta| \leq \frac{1}{2}\pi} \cos(\theta) g(Kr \sin(\theta)) Kr \cos(\theta) d\theta \\
&= Kr \int_{|\theta| \leq \frac{1}{2}\pi} \cos^2(\theta) g(Kr \sin(\theta)) d\theta. \tag{10}
\end{aligned}$$

First of all, this equation has the trivial solution with $r = 0$. The distribution of the oscillators is then given by $\rho(\theta, \omega) = \frac{C}{|\omega|} = \frac{1}{2\pi}$ for all θ and ω . The corresponding state is completely incoherent, it exhibits no kind of synchrony.

The non-trivial solutions of equation (10) satisfies

$$1 = K \int_{|\theta| \leq \frac{1}{2}\pi} \cos^2(\theta) g(Kr \sin(\theta)) d\theta. \tag{11}$$

From this condition Kuramoto derived an exact formula for the critical coupling K_c , that is the value for the coupling K below which no synchronisation occurs and above which (partial) synchronisation occurs. We obtain this value by letting $r \rightarrow 0^+$. Then equation (11) becomes

$$\begin{aligned} 1 &= K \int_{|\theta| \leq \frac{1}{2}\pi} \cos^2(\theta) g(0) d\theta \\ &= K \int_{|\theta| \leq \frac{1}{2}\pi} \frac{1}{2}(\cos(2\theta) + 1) g(0) d\theta \\ &= K \left[\left(\frac{1}{4} \sin(2\theta) + \frac{1}{2}\theta \right) g(0) \right]_{\theta=-\frac{\pi}{2}}^{\theta=\frac{\pi}{2}} \\ &= K \frac{\pi}{2} g(0). \end{aligned}$$

Thus we obtain the critical coupling

$$K_c = \frac{2}{\pi g(0)}. \quad (12)$$

If we consider for example a normal distribution

$$g(\omega) = \frac{1}{\sigma 2\pi} \exp\left(-\frac{\omega^2}{2\sigma^2}\right),$$

we obtain the critical coupling constant $K_c = 4\sigma$. If instead we consider the Lorenzian distribution

$$g(\omega) = \frac{\Delta}{\pi} \frac{1}{\omega^2 + \Delta^2},$$

then the critical coupling will be $K_c = 2\Delta$. We can integrate (10) exactly for the Lorenzian distribution:

$$\begin{aligned} r &= Kr \lim_{n \rightarrow \frac{\pi}{2}} \int_{-n}^n \cos^2(\theta) g(Kr \sin(\theta)) d\theta \\ &= \frac{Kr\Delta}{\pi} \lim_{n \rightarrow \frac{\pi}{2}} \int_{-n}^n \frac{\cos^2(\theta)}{K^2 r^2 \sin^2(\theta) + \Delta^2} d\theta \\ &= \frac{Kr\Delta}{\pi} \lim_{n \rightarrow \frac{\pi}{2}} \int_{-n}^n \frac{1}{\Delta K^2 r^2} \left[\sqrt{\Delta^2 + K^2 r^2} \tan^{-1} \left(\frac{\tan(\theta)\sqrt{\Delta^2 + K^2 r^2}}{\Delta} \right) - \Delta\theta \right]_{\theta=-n}^n \\ &= \frac{1}{\pi Kr} \left(\sqrt{\Delta^2 + K^2 r^2} \frac{\pi}{2} - \Delta \frac{\pi}{2} - \sqrt{\Delta^2 + K^2 r^2} \left(-\frac{\pi}{2} \right) + \Delta \left(-\frac{\pi}{2} \right) \right) \\ &= \frac{1}{Kr} \left(\sqrt{\Delta^2 + K^2 r^2} - \Delta \right). \end{aligned}$$

Rearranging terms we obtain

$$\begin{aligned} Kr^2 + \Delta &= \sqrt{\Delta^2 + K^2 r^2} \\ \Rightarrow K^2 r^4 + 2\Delta Kr^2 + \Delta^2 &= \Delta^2 + K^2 r^2 \\ \Rightarrow Kr^2 + 2\Delta &= K. \end{aligned}$$

Since $0 \leq r \leq 1$ by definition, we obtain

$$r = \sqrt{1 - \frac{K_c}{K}}. \quad (13)$$

2 The Kuramoto Model with added White Noise

Now we will study the Kuramoto model as introduced before but with added white noise. Considering the model as the number of oscillators N goes to infinity, we study the evolution of the density distribution of the oscillators. Adding white noise results in equations of Langevin type for which the evolution of the density is known to follow a Fokker-Planck equation. This equation is more easy to analyse than the continuity equation that is followed by the density when there is no white noise added. Including white noise terms does not only make the model more physical. It also leads to a model that is mathematically more tractable.

By perturbing from the incoherent solution we will proceed to study the system. We write this incoherent solution in terms of its Fourier series and consider the fundamental node only. This node is the only one contributing to the coherence $r(t)$ which will be explained in detail later (in Subsection 2.3.1). The basis is in that we assumed the coupling to be purely sinusoidal. We start by introducing the model as well as the Fokker-Planck equation in Subsections 2.1 and 2.2 respectively. We then perform the stability analysis as done by Strogatz and Mirello [7] in Subsection 2.3.

2.1 Introducing the Model

Adding a white-noise term ξ_i to the mean-field Kuramoto model in Equation 2, considering purely sinusoidal mean field coupling $\Gamma_{i,j} = \frac{K}{N} \sin(\theta_j - \theta_i)$, we obtain the stochastic differential equations:

$$\dot{\theta}_i = \omega_i + \frac{K}{N} \sum_{j=1}^N \sin(\theta_j - \theta_i) + \xi_i, \quad i = 1, \dots, N, \quad (14)$$

where ξ_i denotes the so-called white noise. Its expectation values are $E(\xi_i(t)) = 0$, and the correlations are $E(\xi_i(t)\xi_j(t)) = 2D\delta(t-t')\delta_{ij}$. Where $\delta(t)$ is the Dirac delta distribution; and δ_{ij} equals 1 for $i = j$ and 0 elsewhere. Thus the values ξ_i are independent and taken from a normal distribution with mean $\mu = 0$ and standard deviation $\sigma^2 = 2D$.

In the notation more common in probability theory we can rewrite Equation 14 as

$$d\theta_i = \left[\omega_i + \frac{K}{N} \sum_{j=1}^N \sin(\theta_j - \theta_i) - \frac{1}{2} \frac{\partial}{\partial \theta_i} D \right] dt + \sqrt{2D} dW, \quad i = 1, \dots, N,$$

where dW denotes a Wiener process. Each increment of a Wiener process is independent and normally distributed with mean $\mu = 0$ and standard deviation $\sigma^2 = 2D$. We will only consider constant noise strengths D in which case the above equation reduces to

$$d\theta_i = \left[\omega_i + \frac{K}{N} \sum_{j=1}^N \sin(\theta_j - \theta_i) \right] dt + \sqrt{2D} dW, \quad i = 1, \dots, N.$$

2.2 Fokker-Planck Equation

In our analysis of the model given by (14), we look at the evolution of the density distribution of the oscillators. For Langevin type equations such as Equations 14, it is known that the the

probability density satisfies a Fokker-Planck equation. The model (14) satisfies the following Fokker-Planck equation (see for example Appendix A of [4] for a derivation of (15))

$$\frac{\partial \rho}{\partial t} = D \frac{\partial^2 \rho}{\partial \theta^2} - \frac{\partial}{\partial \theta}(\rho v), \quad (15)$$

where we ignore the subscripts i . The velocity v is given by $v = \omega + Kr \sin(\psi - \theta)$, where ψ is the average phase as in (3). In the case where $D = 0$, this reduces to the continuity equation that we will use in the analysis of the Kuramoto model without noise in Sections 3.2 and 4.1. We assume that the density is 2π -periodic (e.g. $\rho(\theta + 2\pi, \omega, t) = \rho(\theta, \omega, t)$), and we normalize the density by

$$\int_{-\pi}^{\pi} \rho(\theta, \omega, t) d\theta = 1, \quad \forall t. \quad (16)$$

Thus with $\rho(\theta, \omega, t)d\theta$ we denote the fraction of oscillators with frequency ω at time t between θ and $\theta + d\theta$. In the completely asynchronous case where all oscillators are distributed evenly over the interval from $-\pi$ to π , the density is given by $\rho(\theta, \omega, t) = \frac{1}{2\pi}$. This is a trivial solution to Equation 15 which we refer to as the incoherent solution.

As we consider the N -infinite case of the Kuramoto model with added white noise, we rewrite the order parameter as follows:

$$re^{i\psi} = \int_{-\pi}^{\pi} \int_{-\infty}^{+\infty} e^{i\theta} \rho(\theta, \omega, t) g(\omega) d\omega d\theta, \quad (17)$$

where $g(\omega)$ is the distribution of the frequencies ω_i as in Section 1 and the oscillators should be initially independent.

2.3 Stability Analysis around the Incoherent Solution

To study the behaviour of the Kuramoto model with added white noise we first consider the trivial solution of the system and look at what happens in the neighbourhood of it. With the trivial solution we mean the case where all oscillators move incoherently and are evenly distributed over the interval $(-\pi, \pi)$. We then perturb this solution slightly and write out its Fourier series.

We then look only at the fundamental harmonics and derive the evolution equations for these Fourier constants in Subsection 2.3.1. These constants are closely related to the order parameter. Consequently we can from its behaviour determine the behaviour of the order parameter. To analyse the Fourier constants we look at the eigenvalues of the equation in Subsection 2.3.2 and at its continuous spectrum in Subsection 2.3.3. We derive conditions on the coupling strength K and the noise strength D for which the eigenvalues and the values in the continuous spectrum are in the left half of the complex plane and for which the system is thus linearly stable.

2.3.1 Derivation of the Evolution Equations

Following the approach of Strogatz and Mirello [7], we now consider solutions close to the incoherent solution. Thus let

$$\rho(\theta, \omega, t) = \frac{1}{2\pi} + \varepsilon \eta(\theta, \omega, t), \quad (18)$$

where $\varepsilon \ll 1$ (, but $\epsilon \neq 0$). By the normalization property (16), we have that

$$\begin{aligned} \int_{-\pi}^{\pi} \left(\frac{1}{2\pi} + \epsilon \eta(\theta, \omega, t) \right) d\theta &= 1 \\ \Rightarrow 1 + \epsilon \int_{-\pi}^{\pi} \eta(\theta, \omega, t) d\theta &= 1 \\ \Rightarrow \int_{-\pi}^{\pi} \eta(\theta, \omega, t) d\theta &= 0. \end{aligned}$$

By substituting (18) into the Fokker-Planck Equation (15) we obtain

$$\varepsilon \frac{\partial \eta}{\partial t} = \varepsilon D \frac{\partial^2 \eta}{\partial \theta^2} - \frac{\partial}{\partial \theta} \left[v \left(\frac{1}{2\pi} + \varepsilon \eta \right) \right]. \quad (19)$$

We will rewrite this equation in terms of the order parameter and consider the evolution equation at $\mathcal{O}(\varepsilon)$. To find the value of the order parameter for the perturbation of the trivial solution we substitute (18) into our expression for the order parameter (17) and rewrite this:

$$\begin{aligned} re^{i\psi} &= \int_{-\pi}^{\pi} \int_{-\infty}^{+\infty} e^{i\theta} \rho(\theta, \omega, t) g(\omega) d\omega d\theta \\ &= \int_{-\pi}^{\pi} \int_{-\infty}^{+\infty} e^{i\theta} \left[\frac{1}{2\pi} + \varepsilon \eta(\theta, \omega, t) \right] g(\omega) d\omega d\theta \\ &= \underbrace{\frac{1}{2\pi} \int_{-\pi}^{\pi} e^{i\theta} d\theta}_{=0} \int_{-\infty}^{+\infty} g(\omega) d\omega + \int_{-\pi}^{\pi} \int_{-\infty}^{+\infty} e^{i\theta} \varepsilon \eta(\theta, \omega, t) g(\omega) d\omega d\theta \\ &= \varepsilon \int_{-\pi}^{\pi} \int_{-\infty}^{+\infty} e^{i\theta} \eta(\theta, \omega, t) g(\omega) d\omega d\theta. \end{aligned} \quad (20)$$

We denote the last integral by

$$\hat{r}e^{i\psi} = \int_{-\pi}^{\pi} \int_{-\infty}^{+\infty} e^{i\theta} \eta(\theta, \omega, t) g(\omega) d\omega d\theta. \quad (21)$$

Thus the relation between the original order parameter and \hat{r} , whose dynamics we will study later is $r = \varepsilon \hat{r}$. Using the relation we found for r , we look again at the Fokker-Planck equation. Note that only the last term depends on r since $v = \omega + Kr \sin(\psi - \theta)$. We can rewrite the last term of Equation 19 in the following way

$$\begin{aligned} \frac{\partial}{\partial \theta} \left[v \left(\frac{1}{2\pi} + \varepsilon \eta \right) \right] &= \frac{1}{2\pi} \frac{\partial v}{\partial \theta} + \varepsilon \frac{\partial}{\partial \theta} (\eta v) \\ &= \frac{1}{2\pi} \frac{\partial v}{\partial \theta} + \varepsilon \frac{\partial \eta}{\partial \theta} v + \varepsilon \frac{\partial v}{\partial \theta} \eta \\ &= \frac{1}{2\pi} \frac{\partial}{\partial \theta} [\omega + \varepsilon K \hat{r} \sin(\psi - \theta)] + \varepsilon \frac{\partial \eta}{\partial \theta} [\omega + \varepsilon K \hat{r} \sin(\psi - \theta)] \\ &\quad + \varepsilon \frac{\partial}{\partial \theta} [\omega + \varepsilon K \hat{r} \sin(\psi - \theta)] \eta \\ &= -\frac{1}{2\pi} \varepsilon K \hat{r} \cos(\psi - \theta) + \frac{\partial \eta}{\partial \theta} [\varepsilon \omega + \varepsilon^2 K \hat{r} \sin(\psi - \theta)] \\ &\quad - \varepsilon^2 K \hat{r} \cos(\psi - \theta) \eta \\ &= -\frac{1}{2\pi} \varepsilon K \hat{r} \cos(\psi - \theta) + \varepsilon \omega \frac{\partial \eta}{\partial \theta} + \mathcal{O}(\varepsilon^2). \end{aligned} \quad (22)$$

We substitute 22 back into the Fokker-Planck equation (19) to obtain

$$\begin{aligned} \varepsilon \frac{\partial \eta}{\partial t} &= \varepsilon D \frac{\partial^2 \eta}{\partial \theta^2} + \frac{1}{2\pi} \varepsilon K \hat{r} \cos(\psi - \theta) + \varepsilon \omega \frac{\partial \eta}{\partial \theta} + \mathcal{O}(\varepsilon^2) \\ \Rightarrow \frac{\partial \eta}{\partial t} &= D \frac{\partial^2 \eta}{\partial \theta^2} + \frac{1}{2\pi} K \hat{r} \cos(\psi - \theta) - \omega \frac{\partial \eta}{\partial \theta} + \mathcal{O}(\varepsilon). \end{aligned} \quad (23)$$

We will now consider 23 at its lowest order in ϵ . Thus we analyse

$$\frac{\partial \tilde{\eta}}{\partial t} = D \frac{\partial^2 \tilde{\eta}}{\partial \theta^2} + \frac{1}{2\pi} K \hat{r} \cos(\psi - \theta) - \omega \frac{\partial \tilde{\eta}}{\partial \theta}, \quad (24)$$

where we drop the tilde again in the following. To analyse Equation (24) we write η in terms of its full Fourier series with respect to θ :

$$\begin{aligned} \eta(\theta, \omega, t) &= \sum_{-\infty}^{\infty} c_n e^{in\theta} \\ &= c_0 + c_1 e^{i\theta} + c_{-1} e^{-i\theta} + \underbrace{\sum_2^{\infty} c_n e^{in\theta}}_{:= \eta^\perp(\theta, \omega, t)} + \underbrace{\sum_{-\infty}^{-2} c_n e^{in\theta}}_{:= \eta^\perp(\theta, \omega, t)} \\ &= ce^{i\theta} + c^* e^{-i\theta} + \eta^\perp(\theta, \omega, t), \end{aligned} \quad (25)$$

where we write $c := c_1$, with $*$ we denote the complex conjugate, and $c_0 = \int_{-\pi}^{\pi} \eta(\theta, \omega, t) d\theta = 0$. We write the first harmonics separately since these two terms are the only ones to contribute to the coherence $r(t)$. This is due to the simplification Kuramoto assumed in that the coupling is purely sinusoidal. Recall that r is related to \hat{r} by $r = \epsilon \hat{r}$ and notice that in (24) the only term with \hat{r} is $\frac{1}{2\pi} K \hat{r} \cos(\psi - \theta) = \text{Re}(\hat{r} e^{i\psi} e^{-i\theta})$. Thus higher order terms in η such as $c_2 e^{2in\theta}$ do not contribute to \hat{r} and hence r .

The second and higher harmonics can be considered separately [7]. In our analysis in the next subsection we concern ourselves with the fundamental amplitude $c(\omega, t)$. Inserting the Fourier

expression (25) into our expression for the order parameter (21) we get

$$\begin{aligned}
\hat{r}e^{i\psi} &= \int_{-\pi}^{\pi} \int_{-\infty}^{+\infty} e^{i\theta} \eta(\theta, \omega, t) g(\omega) d\theta d\omega \\
&= \int_{-\pi}^{\pi} \int_{-\infty}^{+\infty} e^{i\theta} [ce^{i\theta} + c^*e^{-i\theta} + \eta^\perp(\theta, \omega, t)] g(\omega) d\omega d\theta \\
&= \int_{-\infty}^{+\infty} \int_{-\pi}^{\pi} e^{i\theta} [ce^{i\theta} + c^*e^{-i\theta}] g(\omega) d\theta d\omega + \int_{-\infty}^{+\infty} \int_{-\pi}^{\pi} e^{i\theta} \eta^\perp(\theta, \omega, t) g(\omega) d\theta d\omega \\
&= \int_{-\infty}^{+\infty} \left[\frac{1}{2i} ce^{i\theta} + c^* \right]_{\theta=-\pi}^{\pi} g(\omega) d\omega + \int_{-\infty}^{+\infty} \int_{-\pi}^{\pi} e^{i\theta} \left[\sum_2^{\infty} c_n e^{in\theta} + \sum_{-\infty}^{-2} c_n e^{in\theta} \right] g(\omega) d\theta d\omega \\
&= 2\pi \int_{-\infty}^{+\infty} c^* g(\omega) d\omega + \int_{-\infty}^{+\infty} \int_{-\pi}^{\pi} \left[\sum_2^{\infty} c_n e^{i(n+1)\theta} + \sum_{-\infty}^{-2} c_n e^{i(n+1)\theta} \right] g(\omega) d\theta d\omega \\
&= 2\pi \int_{-\infty}^{+\infty} c^* g(\omega) d\omega + \int_{-\infty}^{+\infty} \left[\sum_2^{\infty} \frac{c_n}{i(n+1)} e^{i(n+1)\theta} + \sum_{-\infty}^{-2} \frac{c_n}{i(n+1)} e^{i(n+1)\theta} \right]_{\theta=-\pi}^{\pi} g(\omega) d\omega \\
&= 2\pi \int_{-\infty}^{+\infty} c^* g(\omega) d\omega. \tag{26}
\end{aligned}$$

In the end most terms cancel out since for integers $n \in \mathbb{Z}$ it holds that $e^{i(n+1)\pi} = e^{-i(n+1)\pi}$.

Studying the stability we will look at both the eigenvalues and the continuous spectrum of the evolution equation of $c(t, \omega)$. The relation between the original order parameter and c is given by (20) and (26) and looks as follows:

$$re^{i\psi} = 2\pi\varepsilon \int_{-\infty}^{+\infty} c^* g(\omega) d\omega. \tag{27}$$

If we look at order $\mathcal{O}(\varepsilon)$ only, then $r(t)$ is determined by $c(t, \omega)$ through (27). If for example c grows exponentially, then so will r . From (27) we can also obtain an expression in terms of $c(t, \omega)$ for the cosine term in the Fokker-Planck equation for η (24) that was derived earlier.

$$\begin{aligned}
\hat{r} \cos(\psi - \theta) &= \operatorname{Re} [\hat{r} e^{i\psi - i\theta}] \\
&= 2\pi \operatorname{Re} \left[e^{-i\theta} \int_{-\infty}^{+\infty} c^*(t, \omega) g(\omega) d\omega \right] \\
&= 2\pi \left[\frac{1}{2} e^{i\theta} \int_{-\infty}^{+\infty} c(t, \omega) g(\omega) d\omega + \frac{1}{2} e^{-i\theta} \int_{-\infty}^{+\infty} c^*(t, \omega) g(\omega) d\omega \right] \\
&= \pi e^{i\theta} \int_{-\infty}^{+\infty} c(t, \omega) g(\omega) d\omega + c.c., \tag{28}
\end{aligned}$$

where *c.c.* denotes the complex conjugate of the term preceding it. To obtain the evolution equation of $c(t, \omega)$, we insert the expression of the term η (25), namely $\eta = ce^{i\theta} + c^*e^{-i\theta} + \eta^\perp(\theta, \omega, t)$, and that of $\hat{r} \cos(\psi - \theta)$ (28) into the Fokker-Planck equation for η (24). We denote

(double) derivatives with the subscripts t , θ and $\theta\theta$.

$$\begin{aligned}\frac{\partial \eta}{\partial t} &= D \frac{\partial^2 \eta}{\partial \theta^2} - \omega \frac{\partial \eta}{\partial \theta} + \frac{1}{2\pi} K \hat{r} \cos(\psi - \theta) \\ c_t e^{i\theta} + c_t^* e^{-i\theta} + \eta_t^\perp &= D(-ce^{i\theta} - c^* e^{-i\theta} + \eta_{\theta\theta}^\perp) - \omega(ice^{i\theta} - ic^* e^{-i\theta} + \eta_\theta^\perp) \\ &\quad + \frac{K}{2} \left(\int_{-\infty}^{\infty} c(t, v) g(v) dv \right) e^{i\theta} + c.c.\end{aligned}\tag{29}$$

In the next subsection we study the evolution equation of the fundamental harmonic.

2.3.2 Analysis of the Fundamental Harmonic (Eigenvalues)

From the equation derived above we can obtain the evolution equations for the different harmonics. To obtain the evolution equation for the fundamental harmonic we equate the coefficients of $e^{i\theta}$ on both sides of Equation 29 to obtain

$$\frac{\partial c}{\partial t} = -(D + i\omega)c(t, \omega) + \frac{K}{2} \int_{-\infty}^{\infty} c(t, v) g(v) dv.\tag{30}$$

Equation 30 again nicely describes the mean-field property of the system. For each frequency ω , $c(t, \omega)$ depends on the other frequencies through the term $c(t, v)$ in the integral. This integral is the same regardless of the frequency ω . Thus the dependence of $c(t, \omega)$ on the other frequencies is the same for each ω .

To find the eigenvalues λ we should solve

$$\frac{\partial c}{\partial t} = \lambda c(t, \omega).\tag{31}$$

Thus we look for solutions of the form $c(t, \omega) = b(\omega)e^{\lambda t}$. We substitute this expression for c into the evolution equation of c (30).

$$\begin{aligned}\frac{\partial}{\partial t} b(\omega) e^{\lambda t} &= -(D + i\omega)b(\omega)e^{\lambda t} + \frac{K}{2} e^{\lambda t} \int_{-\infty}^{\infty} b(v) g(v) dv \\ \Rightarrow \lambda b(\omega) &= -(D + i\omega)b(\omega) + \frac{K}{2} \int_{-\infty}^{\infty} b(v) g(v) dv \\ \Rightarrow b(\omega) &= \frac{\frac{K}{2} \int_{-\infty}^{\infty} b(v) g(v) dv}{\lambda + D + i\omega}\end{aligned}$$

The integral term does not depend on time or frequency. We can write

$$B = \frac{K}{2} \int_{-\infty}^{\infty} b(v) g(v) dv.\tag{32}$$

The solution should be self consistent. Substituting $b(\omega) = \frac{B}{\lambda + D + i\omega}$ into this expression for B we obtain:

$$\begin{aligned}B &= \frac{K}{2} \int_{-\infty}^{\infty} \frac{B}{\lambda + D + iv} g(v) dv \\ \Rightarrow 1 &= \frac{K}{2} \int_{-\infty}^{\infty} \frac{1}{\lambda + D + iv} g(v) dv,\end{aligned}\tag{33}$$

where $B = 0$ is not a solution since it would imply $c(t, \omega) = 0$ for all t and ω and $c(t, \omega) := 0$ is not an eigenfunction of (31). Next consider Kuramoto's assumptions on the frequency distribution that g is even, and that g is non-increasing for non-negative ω . Under these assumptions Equation 33 has at most one solution and if such a solution exists, it is necessarily real [7]. Thus we consider the real part of (33):

$$1 = \frac{K}{2} \int_{-\infty}^{\infty} \frac{\lambda + D}{(\lambda + D)^2 + v^2} g(v) dv. \quad (34)$$

We have obtained an equation describing the dependence of the eigenvalue λ on the noise strength D , the coupling strength K and the frequency distribution $g(\omega)$. Using this equation we can determine the stability of the original equation depending on these parameters. It gives the stability properties of Equation 30, which describes the evolution in time of Fourier coefficient $c(t, \omega)$ and is related to the order parameter by (27).

In the noise free case, $D = 0$, there can never be any negative eigenvalues since $\lambda < 0$ would make the right hand side of (34) negative. Hence the fundamental harmonic is never linearly stable for $D = 0$. More generally we have the condition that $\lambda > -D$ in order to have a positive right hand side.

To find the critical coupling, we substitute $\lambda = 0$ into Equation 34. Since at $\lambda = 0$, the stability changes from linearly stable to unstable.

$$\begin{aligned} 1 &= \frac{K_c}{2} \int_{-\infty}^{\infty} \frac{D}{D^2 + v^2} g(v) dv \\ &\Rightarrow K_c = 2 \left[\int_{-\infty}^{\infty} \frac{D}{D^2 + v^2} g(v) dv \right]^{-1}. \end{aligned}$$

We can find the critical coupling for the noiseless case when we let λ go to zero from above in Equation 34 for $D = 0$.

$$1 = \lim_{\lambda \rightarrow 0^+} \frac{K}{2} \int_{-\infty}^{\infty} \frac{\lambda}{\lambda^2 + v^2} g(v) dv.$$

As λ goes to 0 from above, $\frac{\lambda}{\lambda^2 + v^2}$ gets a sharper peak around $v = 0$. For positive values of λ , it holds that $\int_{-\infty}^{\infty} \frac{\lambda}{\lambda^2 + v^2} dv = \pi$. Thus we can write $\frac{\lambda}{\lambda^2 + v^2} \xrightarrow{\lambda \rightarrow 0^+} \pi\delta(v)$, where $\delta(v)$ is the Dirac delta function. For the critical coupling we then obtain

$$\begin{aligned} K_c &= 2 \left[\int_{-\infty}^{\infty} \pi\delta(v) g(v) dv \right]^{-1} \\ K_c &= \frac{2}{\pi g(0)} \end{aligned}$$

which is the same formula that Kuramoto found in his analysis of the noiseless model. For $K > K_c$ the eigenvalue is positive which means that the incoherent solution is unstable for such K . This in turn means that as $t \rightarrow \infty$ we expect the system to synchronise.

2.3.3 Analysis of the Fundamental Harmonic (Continuous Spectrum)

We continue to find the values for the continuous spectrum of the evolution equation for the first harmonic of η . Thus we look at Equation 30 again. The continuous spectrum of an operator L

Figure 1: The spectra of the first harmonic for $D = 0$.

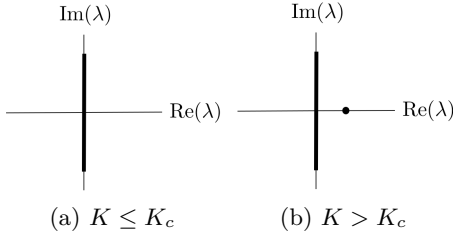
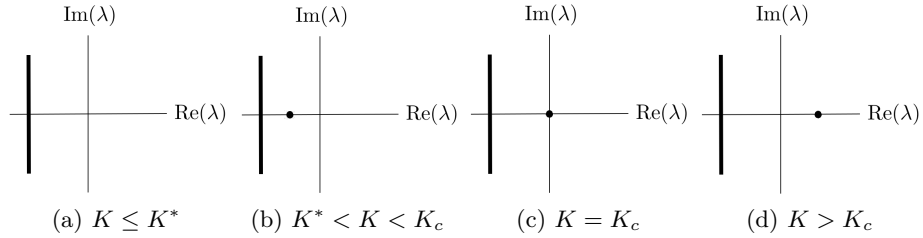


Figure 2: The spectra of the first harmonic for $D > 0$.



$\sigma_c(L)$ consists of those values λ for which $\lambda I - L$ is not surjective. (Here I is the identity operator.) The continuous spectrum consists of approximate eigenvalues that are neither eigenvalues nor do they lie in the residual spectrum. Equation 30 can be rewritten in terms of the operator L as

$$Lb = -(D + i\omega)b(\omega) + \frac{K}{2} \int_{-\infty}^{\infty} b(v)g(v)dv.$$

The operator $L - \lambda I$ is not surjective for all $\lambda \in \mathbb{C}$ such that for an arbitrary function $f(\omega)$ there is no solution $b(\omega)$ for the following equation

$$\begin{aligned} (L - \lambda I)b(\omega) &= f(\omega) \\ -(\lambda + D + i\omega)b(\omega) + \underbrace{\frac{K}{2} \int_{-\infty}^{\infty} b(v)g(v)dv}_{=B} &= f(\omega). \end{aligned} \quad (35)$$

If we denote the integral by B again, we see that if $\lambda + D + i\omega = 0$ for some frequency ω in the support of $g(\omega)$, then (35) is solvable only for constant functions $f(\omega)$. Thus in this case we cannot solve (35) for an arbitrary function $f(\omega)$. This means that the continuous spectrum consists at least of eigenvalues λ satisfying $\lambda + D + i\omega = 0$. Thus we have that

$$\{-D - i\omega : \omega \in \text{support}(g(\omega))\} \subseteq \sigma_c(L).$$

To see that this subset of $\sigma_c(L)$ actually equals the set $\sigma_c(L)$, we suppose that $\hat{\lambda}$ is not of this form. Then we can derive the solution

$$b(\omega) = \frac{B - f(\omega)}{\hat{\lambda} + D + i\omega}, \quad (36)$$

where B can be determined by self consistency as follows. Substitute the solution (36) into the equation for B given by (32)

$$B = \frac{K}{2} \int_{-\infty}^{\infty} \frac{B - f(v)}{\hat{\lambda} + D + iv} g(v) dv.$$

We rearrange terms to obtain:

$$\underbrace{B \left(1 - \frac{K}{2} \int_{-\infty}^{\infty} \frac{g(v)}{\hat{\lambda} + D + iv} dv \right)}_{\neq 0} = \frac{K}{2} \int_{-\infty}^{\infty} \frac{-f(v)}{\hat{\lambda} + D + iv} g(\omega) dv,$$

where the bracketed term is not equal to zero by the assumption that $\hat{\lambda}$ is not an eigenvalue and therefore does not satisfy (33). Thus we can solve for B and hence find a solution $b(\omega)$. Since we found a solution for $\hat{\lambda}$, it is not in the continuous spectrum. Therefore the continuous spectrum is given by

$$\sigma_c(L) = \{-D - i\omega : \omega \in \text{support}(g(\omega))\}.$$

Combining the continuous spectrum with the discrete spectrum found in the previous subsection we can determine when we have stability, neutral stability and instability in the system concerning only the first harmonic. When $D = 0$ the continuous spectrum lies on the imaginary axis. We then have two cases for the eigenvalue λ , as illustrated in Figure 1. For coupling equal to the critical coupling K_c $\lambda = 0$ and we have a neutral stability of the first harmonic of the incoherent solution, as shown in Figure 1a. For coupling strictly greater than K_c $\lambda > 0$ implying instability, as shown in Figure 1b. Thus we expect that the system synchronises for $K > K_c$ as $t \rightarrow \infty$.

When $D > 0$, the continuous spectrum has a negative real part. For the discrete spectrum we have four cases, as illustrated in Figure 2. In addition to before, now we can have $\lambda < 0$. This is the case when $K < K_c$, as shown in Figures 2a and 2b. Then both the continuous and discrete spectrum have negative real parts. Hence we have linear stability. The discrete spectrum is born when $D = -\lambda$, say at coupling K^* , as shown in Figure 2a. The discrete spectrum remains in the negative real half for coupling strictly smaller than K_c , as shown in Figure 2b. And thus the first harmonic of the incoherent solution remains linearly stable. In the case of no noise we only had neutral stability for coupling $K \leq K_c$. For the noise case have neutral stability when $K = K_c$, as shown in Figure 2c. For coupling greater than K_c the first harmonic of the incoherent solution becomes unstable. Thus we expect that the system synchronises for $K > K_c$ as $t \rightarrow \infty$. Note that K_c is dependent on D .

Thus starting near the incoherent solution with coupling below the critical coupling, the behavior according to the fundamental harmonic differs depending on the presence of noise. In case of noise the solution always stays close to the incoherent solution. Whereas in the absence of noise it does not and nor does it go farther and farther away from the incoherent solution. Thus we do not expect complete synchronisation nor complete incoherence in the noiseless case.

We will continue our analysis of the Kuramoto model in the next Section by considering a bimodal distribution for the natural frequencies of the oscillators. So far we only considered a unimodal frequency distribution.

3 Bimodal Frequency Distribution

In this section we will consider two types of bimodal distributions for the natural frequencies of the oscillators. We analyse the Kuramoto model for both a Lorentzian and a discrete bimodal distribution for the natural frequencies. For the latter we include additive noise as discussed in Section 2. Now that the frequencies are no longer distributed uniformly we will see that we can have different partially synchronised groups. The results of the time-frequency analysis for the Kuramoto model are in Subsection 6.3. For the discrete distribution we followed the approach of Bonilla et al.[17] and for the Lorenzian case we followed the approach of Martens et al. [18].

3.1 Discrete Bimodal Frequency Distribution

Before considering a more complex bimodal frequency distribution, we look at a discrete bimodal frequency distribution. We consider the Kuromato model with added white-noise as in Section 2. This distribution is studied by, among others, Okuda and Kuramoto [2]; and Bonilla, Neu and Spigler [17]. This type of distribution is described by

$$g(\omega) = \frac{\delta(\omega - \omega_0) + \delta(\omega + \omega_0)}{2},$$

where ω are the natural frequencies and $\delta(x)$ is the Dirac delta function. Half of the oscillators have a natural frequency ω_0 while the other half has natural frequency $-\omega_0$.

We study the Kuramoto model with added white noise as described in Subsection 2.1 with the only difference that we now consider a different distribution of natural frequencies. To find the values of K and D for which the model is linearly stable or unstable, we consider again Equation 33 and find the eigenvalues in case we take the density $g(\omega)$ as above.

$$\begin{aligned} 1 &= \frac{K}{2} \int_{-\infty}^{\infty} \frac{1}{\lambda + D + iv} g(v) dv \\ &\Rightarrow 1 = \frac{K}{2} \cdot \frac{1}{2} \left(\frac{1}{\lambda + D + i\omega_0} + \frac{1}{\lambda + D - i\omega_0} \right) \\ &\Rightarrow 1 = \frac{K}{2} \left(\frac{\lambda + D}{(\lambda + D)^2 + \omega_0^2} \right) \\ &\Rightarrow 0 = \lambda^2 + \left(2D - \frac{K}{2} \right) \lambda + D^2 - \frac{K}{2} D + \omega_0^2 \\ &\Rightarrow 0 = \left(\lambda + \left(D - \frac{K}{4} \right) \right)^2 - \frac{K^2}{16} + \omega_0^2 \end{aligned}$$

The eigenvalues we thus obtain are

$$\lambda_{\pm} = \frac{K}{4} - D \pm \frac{1}{4} \sqrt{K^2 - 16\omega_0}.$$

Both eigenvalues have negative real parts for sufficiently small coupling:

$$\text{If } K < 2D, \text{ then } \operatorname{Re}(\lambda_-) \leq \operatorname{Re}(\lambda_+) \leq -D + \frac{K}{2} < 0.$$

Thus for $K < 2D$, the incoherent solution is linearly stable for all ω_0 . On the other hand, for sufficiently large coupling, the system has one eigenvalue with positive real part:

$$\text{If } K > 4D, \text{ then } \operatorname{Re}(\lambda_+) \geq -D + \frac{K}{4} > 0.$$

Thus for $K > 4D$, the incoherent solution is linearly unstable for all ω_0 . The type of bifurcation differs depending on ω_0 . For $\omega_0 > D$, the incoherent solution becomes unstable by a bifurcation into solutions with time-periodic order-parameter. See for example [17] for a stability analysis of this branch of solutions.

In the case where $\omega_0 < D$, there are additional values for K on the interval $2D < K < 4D$ for which the incoherent solution is unstable. These follow from determining where the eigenvalue λ_+ becomes positive. Thus we equate λ_+ to zero:

$$\begin{aligned} 0 &= -D + \frac{K}{4} - \frac{1}{4}\sqrt{K^2 - 16\omega_0^2} \\ \Rightarrow 16D^2 - 8DK + K^2 &= K^2 - 16\omega_0^2 \\ \Rightarrow K &= 2D\left(\frac{\omega_0^2}{D^2} + 1\right). \end{aligned}$$

The eigenvalue λ_+ becomes positive when

$$K > K_c = 2D\left(\frac{\omega_0^2}{D^2} + 1\right).$$

Thus when $\omega_0 < D$, the incoherent solution becomes unstable for coupling greater than K_c .

3.2 Lorenzian Bimodal Frequency Distribution

We will carry out a stability analysis for the Kuramoto model without noise where the frequencies are distributed according to the sum of two Lorenzian distributions. We follow the approach suggested by Ott and Antonsen [11]. The idea is to consider solutions of the density equation that are of a certain form. The system can then be reduced exactly to a small number of ODE's. The resulting system represents only a selection of the solutions to the original system. For several distributions its bifurcation diagram can be constructed. Ott and Antonsen [11, 18] motivate their ansatz by noting that both the incoherent solution and the partially synchronised state are of the form they propose.

3.2.1 Derivation

We consider the noiseless Kuramoto model for $j = 1, 2, 3, \dots$ given by

$$\begin{aligned} \dot{\theta}_j &= \omega_j + Kr \sin(\psi - \theta_j) \\ &= \omega_j + \text{Im}(ze^{-i\theta_j}) \\ &= \omega_j + \frac{K}{2i}(ze^{-i\theta_j} - z^*e^{i\theta_j}) \end{aligned}$$

where we consider the limit as the number of oscillators N goes to infinity. Thus the order parameter is given by (17) as before:

$$z = re^{i\psi} = \int_{-\pi}^{\pi} \int_{-\infty}^{+\infty} e^{i\theta} \rho(\theta, \omega, t) g(\omega) d\omega d\theta.$$

We start with considering the continuity equation for the density of the oscillators

$$\frac{\partial \rho}{\partial t} + \frac{\partial}{\partial \theta}(\rho \nu) = 0,$$

into which we substitute the velocity v as follows:

$$\frac{\partial \rho}{\partial t} + \frac{\partial}{\partial \theta} \left(\rho \left(\omega + \frac{K}{2i} (ze^{-i\theta} - z^* e^{i\theta}) \right) \right) = 0. \quad (37)$$

Note that this corresponds to the Fokker-Planck equation (15) discussed earlier with $D = 0$ since we consider the noiseless case here. We look at the Fourier expansion of the density ρ and take its coefficients c_n to be of the form $c_n = a(\omega, t)^n$. This is the ansatz proposed by Ott and Antonsen. Solutions of this form are those in the Poisson kernel of the unit circle. There are some restrictions on $a(\omega, t)$. These will be discussed later. The Fourier expansion of ρ that we consider is

$$\rho = \frac{1}{2\pi} \left(1 + \sum_{n=1}^{\infty} a(\omega, t)^n e^{in\theta} + c.c. \right), \quad (38)$$

where *c.c.* denotes the complex conjugate of the preceding term. The partial derivatives of this expression with respect to t and θ are as follows

$$\frac{\partial \rho}{\partial t} = \frac{1}{2\pi} \left(\sum_{n=1}^{\infty} n \frac{\partial a}{\partial t} a^{n-1} e^{in\theta} + c.c. \right)$$

and

$$\frac{\partial \rho}{\partial \theta} = \frac{1}{2\pi} \left(\sum_{n=1}^{\infty} in a^n e^{in\theta} + c.c. \right).$$

The continuity equation (37) for ρ then becomes:

$$\begin{aligned} 0 &= \left(\sum_{n=1}^{\infty} n \frac{\partial a}{\partial t} a^{n-1} e^{in\theta} + c.c. \right) \\ &\quad + \left(\sum_{n=1}^{\infty} in a^n e^{in\theta} + c.c. \right) \left(\omega + \frac{K}{2i} (ze^{-i\theta} - z^* e^{i\theta}) \right) \\ &\quad + \left(1 + \sum_{n=1}^{\infty} a(\omega, t)^n e^{in\theta} + c.c. \right) \frac{K}{2i} (-ize^{-i\theta} - iz^* e^{i\theta}). \end{aligned}$$

Now equating all terms with $e^{i\theta}$ we obtain:

$$0 = a^0 \frac{\partial a}{\partial t} + \omega i a + 2 \frac{K}{2i} zia^2 + a^2 (-iz) \frac{K}{2i} + \frac{K}{2i} (-iz^*),$$

which reduces to

$$\frac{\partial a}{\partial t} + \frac{K}{2} (a^2 z - z^*) + \omega i a = 0. \quad (39)$$

The same equation can be obtained equating for the other $e^{in\theta}$ terms. Thus if a satisfies this condition, then the Fourier series of $\rho(\omega, t)$ as in (38) satisfies the continuity equation.

The conditions on $a(\omega, t)$ as assumed by Ott and Antonsen [11] are as follows:

1. $|a(\omega, t)| \leq 1$
2. $a(\omega, 0)$ is analytically continuable for $\text{Im}(\omega) < 0$.
3. $|a(\omega, t)| \rightarrow 0$ as $\text{Im}(\omega) \rightarrow -\infty$.

Ott and Antonsen showed that if a solution to the system described by (39) and (40) satisfies these conditions for $t = 0$, then it will satisfy the conditions for all $0 \leq t < +\infty$. These conditions are used to for example apply Fubini's theorem in simplifying the order parameter to a single integral over ω (Condition 1). We then calculate this integral by applying the residue theorem to the integral over a path Γ that lies in the plane $\text{Im}(\omega) < 0$ and on the real axis. The integral we want to calculate is only over the real axis and we can choose the path in $\text{Im}(\omega) < 0$ such that the integral vanishes on it (Conditions 2 and 3).

The order parameter is given by

$$\begin{aligned}
z &= \int_{-\pi}^{\pi} \int_{-\infty}^{+\infty} e^{i\theta} \rho(\theta, \omega, t) g(\omega) d\omega d\theta \\
&= \int_{-\pi}^{\pi} \int_{-\infty}^{+\infty} e^{i\theta} \frac{1}{2\pi} \left(1 + \sum_{n=1}^{\infty} a(\omega, t)^n e^{in\theta} + c.c. \right) g(\omega) d\omega d\theta \\
&= \int_{-\pi}^{\pi} \frac{e^{i\theta}}{2\pi} d\theta \int_{-\infty}^{+\infty} g(\omega) d\omega + \int_{-\pi}^{\pi} \int_{-\infty}^{+\infty} \frac{1}{2\pi} \left(\sum_{n=1}^{\infty} a(\omega, t)^n e^{i(n+1)\theta} + c.c. \right) g(\omega) d\omega d\theta \\
&= \int_{-\pi}^{\pi} \int_{-\infty}^{+\infty} \frac{1}{2\pi} \left(a^*(\omega, t) e^{-i(1-1)\theta} \right) g(\omega) d\omega d\theta \\
&= \int_{-\infty}^{+\infty} a^*(\omega, t) g(\omega) d\omega,
\end{aligned} \tag{40}$$

To further study the system

$$\begin{aligned}
\frac{\partial a}{\partial t} + \frac{K}{2} (a^2 z - z^*) + \omega i a &= 0 \\
z^* &= \int_{-\infty}^{+\infty} a(\omega, t) g(\omega) d\omega,
\end{aligned} \tag{41}$$

we look at a particular distribution. Ott and Antonsen [11] analysed the system for a unimodal Lorentzian distribution. We now follow the approach of Martens [18] and consider a bimodal Lorentzian distribution

$$g(\omega) = \frac{\Delta}{2\pi} \left(\frac{1}{(\omega - \omega_0)^2 + \Delta^2} + \frac{1}{(\omega + \omega_0)^2 + \Delta^2} \right).$$

This is a sum of two Lorentzians which have width parameter Δ and centre frequencies $\pm\omega_0$. We substitute this frequency distribution into (41) and perform the integration. To avoid the singularities of $a(\omega, t)$, we will deform the integration path for ω . By the conditions on a , we know that a does not have singularities on the lower half plane $\text{Im}(\omega) < 0$. We will integrate over the contour Γ given by the real line and a large semi-circle in the lower half plane C^- . With 'large' we mean its radius goes to infinity, making that the integrand vanishes by Condition 3. The contour is negatively oriented resulting in a minus sign when calculating the residues. Writing $g(\omega)$ as its partial fraction expansion we will find that it has four poles, two of which lie inside the contour Γ .

The partial fraction expression of $g(\omega)$ is

$$g(\omega) = \frac{1}{4\pi i} \left(\frac{-1}{\omega + \omega_0 + i\Delta} + \frac{1}{\omega + \omega_0 - i\Delta} - \frac{1}{\omega - \omega_0 + i\Delta} + \frac{1}{\omega - \omega_0 - i\Delta} \right),$$

which has poles $\omega_{1,2} = \pm\omega_0 - i\Delta$ inside the contour Γ and poles $\omega_{3,4} = \pm\omega_0 + i\Delta$ outside the contour. These are the only singularities of the integrand that are inside the chosen contour Γ by the assumptions on a (Condition 2). To perform the integration in (41) we make use of the Residue Theorem as follows.

$$\begin{aligned} z^* &= \int_{\Gamma} a(\omega, t) g(\omega) d\omega - \int_{C^-} a(\omega, t) g(\omega) d\omega \\ &= \int_{\Gamma} a(\omega, t) \frac{1}{4\pi i} \left(\frac{-1}{\omega + \omega_0 + i\Delta} + \frac{1}{\omega + \omega_0 - i\Delta} - \frac{1}{\omega - \omega_0 + i\Delta} + \frac{1}{\omega - \omega_0 - i\Delta} \right) d\omega \\ &= -1 \cdot \left[-a(-\omega_0 - i\Delta, t) \frac{1}{4\pi i} (2\pi i) + 0 - a(\omega_0 - i\Delta, t) \frac{1}{4\pi i} (2\pi i) + 0 \right] \\ &= \frac{1}{2} [a(\omega_0 - i\Delta, t) + a(-\omega_0 - i\Delta, t)] \end{aligned}$$

For convenience we rewrite the order parameter.

$$\begin{aligned} z &= \frac{1}{2} [a^*(\omega_0 - i\Delta, t) + a^*(-\omega_0 - i\Delta, t)] \\ &= \frac{1}{2}(z_1 + z_2), \end{aligned}$$

where

$$z_{1,2} = a^*(\pm\omega_0 - i\Delta, t).$$

Now we consider the ODE we obtained earlier (39) for a^* at $(\pm\omega_0 - i\Delta, t)$. We use the notation in z_1 and z_2 just introduced. The derivatives of z_k with respect to their first arguments are denoted by \dot{z}_k for $k = 1, 2$.

$$\begin{aligned} \dot{z}_1 &= -\frac{K}{2} \left(\frac{1}{2}(z_1 + z_2)^* z_1^2 - \frac{1}{2}(z_1 + z_2) \right) - (\omega_0 - i\Delta) i z_1 \\ &= \frac{K}{4} (z_1 + z_2 - (z_1^* + z_2^*) z_1^2) - (\Delta + i\omega_0) z_1 \\ \dot{z}_2 &= -\frac{K}{2} \left(\frac{1}{2}(z_1 + z_2)^* z_2^2 - \frac{1}{2}(z_1 + z_2) \right) - (-\omega_0 - i\Delta) i z_2 \\ &= \frac{K}{4} (z_1 + z_2 - (z_1^* + z_2^*) z_2^2) - (\Delta - i\omega_0) z_2. \end{aligned}$$

This is the system we will analyse and study bifurcations of. It can be reduced to a three dimensional system by transforming to polar coordinates. We will do this here before starting the bifurcation analysis. In particular we change to the polar coordinates $z_1 = \varphi_1 e^{i\phi_1}$ and $z_2 = \varphi_2 e^{i\phi_2}$.

$$\begin{aligned} \dot{\varphi}_1 e^{i\phi_1} + \varphi_1 i e^{i\phi_1} \dot{\phi}_1 &= \frac{K}{4} (\varphi_1 e^{i\phi_1} + \varphi_2 e^{i\phi_2} - (\varphi_1 e^{-i\phi_1} + \varphi_2 e^{-i\phi_2}) \varphi_1^2 e^{2i\phi_1}) - (\Delta + i\omega_0) \varphi_1 e^{i\phi_1} \\ \dot{\varphi}_2 e^{i\phi_2} + \varphi_2 i e^{i\phi_2} \dot{\phi}_2 &= \frac{K}{4} (\varphi_1 e^{i\phi_1} + \varphi_2 e^{i\phi_2} - (\varphi_1 e^{-i\phi_1} + \varphi_2 e^{-i\phi_2}) \varphi_2^2 e^{2i\phi_2}) - (\Delta - i\omega_0) \varphi_2 e^{i\phi_2}. \end{aligned}$$

Multiplying the first equation by $e^{-i\phi_1}$ and the second by $e^{-i\phi_2}$ we obtain

$$\dot{\varphi}_1 + i\varphi_1 \dot{\phi}_1 = \frac{K}{4} \left(\varphi_1 + \varphi_2 e^{i(\phi_2 - \phi_1)} - \varphi_1^3 - \varphi_1^2 \varphi_2 e^{i(\phi_1 - \phi_2)} \right) - (\Delta + i\omega_0) \varphi_1 \quad (42)$$

$$\dot{\varphi}_2 + i\varphi_2 \dot{\phi}_2 = \frac{K}{4} \left(\varphi_1 e^{i(\phi_1 - \phi_2)} + \varphi_2 - \varphi_1 \varphi_2^2 e^{i(\phi_2 - \phi_1)} - \varphi_2^3 \right) - (\Delta - i\omega_0) \varphi_2. \quad (43)$$

For each equation we equate its real parts and introduce the phase difference $\psi = \phi_2 - \phi_1$:

$$\begin{aligned} \dot{\varphi}_1 &= \frac{K}{4} (\varphi_1 + \varphi_2 \cos \psi - \varphi_1^3 - \varphi_1^2 \varphi_2 \cos \psi) - \Delta \varphi_1 \\ &= \frac{K}{4} (1 - \varphi_1^2) (\varphi_1 + \varphi_2 \cos \psi) - \Delta \varphi_1 \\ \dot{\varphi}_2 &= \frac{K}{4} (\varphi_1 \cos \psi + \varphi_2 - \varphi_1 \varphi_2^2 \cos \psi - \varphi_2^3) - \Delta \varphi_2 \\ &= \frac{K}{4} (1 - \varphi_2^2) (\varphi_1 \cos \psi + \varphi_2) - \Delta \varphi_2. \end{aligned}$$

Similarly we equate the imaginary parts of complex equations above (42,43):

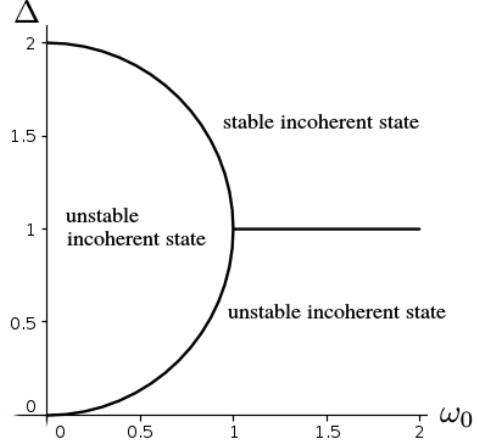
$$\begin{aligned} \varphi_1 \dot{\phi}_1 &= \frac{K}{4} (\varphi_2 \sin(\phi_2 - \phi_1) - \varphi_1^2 \varphi_2 \sin(\phi_1 - \phi_2)) - \omega_0 \varphi_1 \\ &= \frac{K}{4} ((\varphi_2 + \varphi_1^2 \varphi_2) \sin(\phi_2 - \phi_1)) - \omega_0 \varphi_1 \\ \varphi_2 \dot{\phi}_2 &= \frac{K}{4} (\varphi_1 \sin(\phi_1 - \phi_2) - \varphi_1 \varphi_2^2 \sin(\phi_2 - \phi_1)) - \omega_0 \varphi_2 \\ &= \frac{K}{4} ((-\varphi_1 - \varphi_1 \varphi_2^2) \sin(\phi_2 - \phi_1)) + \omega_0 \varphi_2. \end{aligned}$$

We divide both sides of first equation by φ_1 and both sides of the second by φ_2 in order to calculate $\dot{\psi}$:

$$\begin{aligned} \dot{\psi} &= \dot{\phi}_2 - \dot{\phi}_1 \\ &= \frac{K}{4} \left(\frac{-\varphi_1 - \varphi_1 \varphi_2^2}{\varphi_2} \sin(\phi_2 - \phi_1) \right) + \omega_0 - \frac{K}{4} \left(\frac{\varphi_2 + \varphi_1^2 \varphi_2}{\varphi_1} \sin(\phi_2 - \phi_1) \right) + \omega_0 \\ &= 2\omega_0 + \frac{K}{4} \left(\frac{-\varphi_1 - \varphi_1 \varphi_2^2}{\varphi_2} \sin(\psi) - \frac{\varphi_2 + \varphi_1^2 \varphi_2}{\varphi_1} \sin(\psi) \right) \\ &= 2\omega_0 - \frac{K}{4} \frac{\varphi_1^2 + \varphi_2^2 + 2\varphi_1^2 \varphi_2^2}{\varphi_1 \varphi_2} \sin(\psi). \end{aligned}$$

We have now reduced the order parameter z to a three dimensional system of ordinary differential equations. We did this by taking the Ott-Antonsen ansatz as the form of solutions of the continuity equation for the density of the oscillators. We could then write the order parameter z in terms of a and obtained an ordinary differential equation describing the evolution of a . For our bimodal Lorentzian distribution $g(\omega)$ we could perform the integration over the product $a(\omega, t)g(\omega)$ taking into account where these functions (might) have singularities. Finally we reduced the system from four dimensions to three by changing to polar coordinates. We thus

Figure 3: The boundary $B(\omega_0)$ between linear stability and no linear stability for the incoherent state.



obtained the following system.

$$\begin{aligned}\dot{\varphi}_1 &= \frac{K}{4}(1 - \varphi_1^2)(\varphi_1 + \varphi_2 \cos \psi) - \Delta \varphi_1 \\ \dot{\varphi}_2 &= \frac{K}{4}(1 - \varphi_2^2)(\varphi_1 \cos \psi + \varphi_2) - \Delta \varphi_2 \\ \dot{\psi} &= 2\omega_0 - \frac{K}{4} \frac{\varphi_1^2 + \varphi_2^2 + 2\varphi_1^2\varphi_2^2}{\varphi_1\varphi_2} \sin(\psi).\end{aligned}$$

A further restriction on the solutions considered by Martens [18] is to only consider symmetric solutions such that $\varphi_1(t) = \varphi_2(t)$. Then we obtain:

$$\begin{aligned}\dot{\varphi} &= \frac{K}{4}(1 - \varphi^2)(\varphi + \varphi \cos \psi) - \Delta \varphi \\ &= \frac{K}{4}\varphi \left(1 - \frac{4\Delta}{K} - \varphi^2 + (1 - \varphi^2) \cos \psi\right) \\ \dot{\psi} &= 2\omega_0 - \frac{K}{2}(1 + \varphi^2) \sin(\psi).\end{aligned}$$

3.2.2 Bifurcation Analysis around the Incoherent Solution

In the following analysis we look at the stability properties of the system depending on the parameters of the bimodal Lorentzian distribution. We start by finding the fixed points. For this we look at the system in its Cartesian coordinates. As a convenience for both the Cartesian

coordinate system and the polar coordinate system we scale its variables by:

$$\begin{aligned} q &= \varphi^2 \\ \tilde{t} &= \frac{K}{2} t \\ \tilde{\Delta} &= \frac{4\Delta}{K} \\ \tilde{\omega}_0 &= \frac{4\omega_0}{K}. \end{aligned}$$

This results in

$$\dot{z}_1 = (z_1 + z_2 - (z_1^* + z_2^*)z_1^2) - (\tilde{\Delta} + i\tilde{\omega}_0)z_1 \quad (44)$$

$$\dot{z}_2 = (z_1 + z_2 - (z_1^* + z_2^*)z_2^2) - (\tilde{\Delta} - i\tilde{\omega}_0)z_2 \quad (45)$$

and in polar coordinates:

$$\begin{aligned} q^{-\frac{1}{2}} \dot{q} \frac{K}{4} &= \frac{K}{4} q^{-\frac{1}{2}} (1 - \tilde{\Delta} - q + (1 - q) \cos \psi) \\ \Rightarrow \quad \dot{q} &= 1 - \tilde{\Delta} - q + (1 - q) \cos \psi \\ \frac{K}{2} \dot{\psi} &= \frac{K}{2} \tilde{\omega}_0 - \frac{K}{2} (1 + q) \sin(\psi) \\ \Rightarrow \quad \dot{\psi} &= \tilde{\omega}_0 - (1 + q) \sin(\psi). \end{aligned}$$

In the following we drop the tildes again. We mean the scaled variables unless mentioned otherwise. The first points we are interested in our bifurcation analyses are those for which we are in the incoherent state. Thus those states for which the order parameter z is zero and the oscillators are not synchronised. In polar coordinates this corresponds to $\varphi_1, \varphi_2 = 0$ or $q = 0$. To find the corresponding eigenvalues we linearize (44, 45). E.g. we drop terms of order 2 and higher.

$$\begin{pmatrix} \dot{z}_1 \\ \dot{z}_2 \end{pmatrix} = \begin{pmatrix} -(\Delta + i\omega_0) + 1 & 1 \\ 1 & -(\Delta - i\omega_0) + 1 \end{pmatrix} \begin{pmatrix} z_1 \\ z_2 \end{pmatrix}.$$

To find the eigenvalues of the matrix in the equation above we look at its characteristic equation:

$$\begin{aligned} (\lambda + \Delta + i\omega_0 - 1)(\lambda + \Delta - i\omega_0 - 1) - 1 &= 0 \\ \Rightarrow \quad (\lambda + \Delta)^2 + \omega_0^2 - 2(\lambda + \Delta) &= 0 \\ \Rightarrow \quad [(\lambda + \Delta) - 1]^2 - 1 + \omega_0^2 &= 0 \\ \Rightarrow \quad \lambda_{\pm} &= -\Delta + 1 \pm \sqrt{1 - \omega_0^2}. \end{aligned}$$

Thus we have found two eigenvalues λ_{\pm} for the incoherent state. Whenever the real part of these eigenvalues is less than zero, the incoherent state is stable. Since $\text{Re}(\lambda_+) \geq \text{Re}(\lambda_-)$ we look at when $\text{Re}(\lambda_+) < 0$. There are two cases:

Case 1. For $\omega_0 \leq 1$, $\text{Re}(\lambda_+) < 0$ iff $\Delta > 1 + \sqrt{1 - \omega_0^2}$.

Case 2. For $\omega_0 > 1$, $\text{Re}(\lambda_+) < 0$ iff $\Delta > 1$.

Thus the boundary between linear stability and no linear stability (see also Figure 3) is given the by:

$$B(\omega_0) = \begin{cases} 1 + \sqrt{1 - \omega_0^2} & \text{for } \omega_0 \leq 1 \\ 1 & \text{for } \omega_0 > 1. \end{cases}$$

4 Chimera State

An interesting phenomenon regarding synchronisation is a chimera state. Systems of coupled identical oscillators have been observed to spontaneously break up into a synchronised group and an unsynchronised group [19, 20]. Such states have mostly been found in systems with weak nonlocal coupling, but they can also exist in systems where this is not the case.

Until recently it was thought that more complex behavior such as partial synchronisation and incoherence would not occur in systems with identical oscillators [8]. Such systems were expected to either synchronise or remain in an incoherent state. However, Kuramoto and Battogtokh [1] recently discovered what we now know as chimera states in such a system.

The model they studied consisted of identical oscillators on a ring that were non-locally coupled. They observed an apparent stable state in which some oscillators synchronised while others kept moving incoherently. Abrams and Strogatz later named this a chimera state. To study chimera states in the Kuramoto model we consider a coupling discussed by Abrams, Mirello, Strogatz and Panaggio [6, 9]. They say this is the simplest system in which chimeras have been observed so far.

We start by rewriting the model using the Ott-Antonsen ansatz [11] as before and thus make some assumptions about the form of the solution. The idea is to bifurcate from a system with uniform global coupling towards a system with stronger coupling within a group than between groups. In the remaining of this Section we follow the approach as described by Abrams, Mirello and Strogatz [6].

4.1 Derivation

We divide the population of oscillators into different groups and the coupling we will consider differs between groups. The inter group coupling is stronger than the intra group coupling. Furthermore we include the phaselag α in the coupling which is the same for each oscillator. We consider two groups of N oscillators denoted by θ_i^1 and θ_i^2 for $i = 1, \dots, N$. The intragroup coupling is denoted by $K_{1,1} = K_{2,2} = \mu = \frac{1+A}{2}$ and the intergroup coupling is denoted by $K_{1,2} = K_{2,1} = \nu = \frac{1-A}{2}$, where $0 < A \leq 1$ and $\nu + \mu = 1$. This assures that $\mu > \nu$, e.g. stronger intergroup coupling than intragroup coupling. For $A = 0$ the model would equal the original Kuramoto model. Thus by increasing A from 0 we bifurcate away from global coupling.

The governing equations are

$$\dot{\theta}_i^1 = \omega + \frac{K_{1,1}}{N} \sum_{j=1}^N \sin(\theta_i^1 - \theta_j^1 + \alpha) + \frac{K_{1,2}}{N} \sum_{j=1}^N \sin(\theta_i^1 - \theta_j^2 + \alpha) \quad (46)$$

$$\dot{\theta}_i^2 = \omega + \frac{K_{2,2}}{N} \sum_{j=1}^N \sin(\theta_i^2 - \theta_j^2 + \alpha) + \frac{K_{2,1}}{N} \sum_{j=1}^N \sin(\theta_i^2 - \theta_j^1 + \alpha). \quad (47)$$

We also write the phase lag in terms of $\beta = \frac{\pi}{2} - \alpha$. This is done since for this type of system chimeras emerge in the limit $\beta \rightarrow 0$.

$$\begin{aligned}\dot{\theta}_i^1 &= \omega - \frac{1+A}{2N} \sum_{j=1}^N \cos(\theta_i^1 - \theta_j^1 - \beta) - \frac{1-A}{2N} \sum_{j=1}^N \cos(\theta_i^1 - \theta_j^2 - \beta) \\ \dot{\theta}_i^2 &= \omega - \frac{1+A}{2N} \sum_{j=1}^N \cos(\theta_i^2 - \theta_j^2 - \beta) - \frac{1-A}{2N} \sum_{j=1}^N \cos(\theta_i^2 - \theta_j^1 - \beta).\end{aligned}$$

Note that as A goes to zero we approach uniform global coupling. Looking at the continuum limit where the number of oscillators $N \rightarrow \infty$, the analysis is similar to what was done when studying the Kuramoto model with bimodal frequency distribution in Section 3.2. We again use the Ott-Antonsen ansatz. We now obtain two evolution equations of the densities ρ_1 for oscillators in the first group and ρ_2 for oscillators in the second group. Note that the superscripts are moved down. The continuity equations we consider are:

$$\frac{\partial \rho_\sigma}{\partial t} + \frac{\partial}{\partial \theta} (\rho_\sigma v_\sigma) = 0, \quad \text{for } \sigma = 1, 2. \quad (48)$$

The velocities v_1, v_2 are given by

$$v_\sigma(\theta, t) = \omega + K_{\sigma,1} \int_{-\pi}^{\pi} \sin(\theta_\sigma - \theta_1 - \alpha) \cdot \rho_1(\theta_1, t) d\theta_1 + K_{\sigma,2} \int_{-\pi}^{\pi} \sin(\theta_\sigma - \theta_2 - \alpha) \cdot \rho_2(\theta_2, t) d\theta_2. \quad (49)$$

For each group we define the complex order parameter as

$$z_\sigma(t) = K_{\sigma,1} \int_{-\pi}^{\pi} e^{i\theta_1} \cdot \rho_1(\theta_1, t) d\theta_1 + K_{\sigma,2} \int_{-\pi}^{\pi} e^{i\theta_2} \cdot \rho_2(\theta_2, t) d\theta_2. \quad (50)$$

We can rewrite the velocity (49) in terms of the order parameter as follows, where the integrals are still over the interval from $-\pi$ to π .

$$\begin{aligned}v_\sigma(\theta, t) &= \omega + K_{\sigma,1} \int \frac{1}{2i} \left(e^{i(\theta_1 - \theta_\sigma - \alpha)} - e^{-i(\theta_1 - \theta_\sigma - \alpha)} \right) \cdot \rho_1(\theta_1, t) d\theta_1 \\ &\quad + K_{\sigma,2} \int \frac{1}{2i} \left(e^{i(\theta_2 - \theta_\sigma - \alpha)} - e^{-i(\theta_2 - \theta_\sigma - \alpha)} \right) \cdot \rho_2(\theta_2, t) d\theta_2 \\ &= \omega + K_{\sigma,1} \int \frac{1}{2i} e^{i(\theta_1 - \theta_\sigma - \alpha)} \cdot \rho_1(\theta_1, t) d\theta_1 \\ &\quad + K_{\sigma,2} \int \frac{1}{2i} e^{i(\theta_2 - \theta_\sigma - \alpha)} \cdot \rho_2(\theta_2, t) d\theta_2 \\ &\quad - K_{\sigma,1} \int \frac{1}{2i} e^{-i(\theta_1 - \theta_\sigma - \alpha)} \cdot \rho_1(\theta_1, t) d\theta_1 \\ &\quad - K_{\sigma,2} \int \frac{1}{2i} e^{-i(\theta_2 - \theta_\sigma - \alpha)} \cdot \rho_2(\theta_2, t) d\theta_2 \\ &= \omega + \frac{1}{2i} z_\sigma(t) e^{-i\theta_\sigma} e^{-i\alpha} - \frac{1}{2i} z_\sigma^*(t) e^{i\theta_\sigma} e^{i\alpha},\end{aligned}$$

where with a $*$ we denote the complex conjugate. Following the approach of Ott and Antonsen, we consider only densities of the form of a Poisson Kernel:

$$\rho_\sigma(\theta, t) = \frac{1}{2\pi} \left[1 + \sum_{n=1}^{\infty} (a_\sigma(\omega, t) e^{i\theta_\sigma})^n + \sum_{n=1}^{\infty} (a_\sigma^*(\omega, t) e^{-i\theta_\sigma})^n \right]. \quad (51)$$

The function $a(\omega, t)$ is assumed to satisfy the same conditions in Section 3.2:

1. $|a(\omega, t)| \leq 1$
2. $a(\omega, 0)$ is analytically continuable for $\text{Im}(\omega) < 0$.
3. $|a(\omega, t)| \rightarrow 0$ as $\text{Im}(\omega) \rightarrow -\infty$.

Computing the terms of the continuity equations (48) for densities of this form (51), we obtain the following:

$$\begin{aligned}\frac{\partial \rho_\sigma}{\partial t} &= \frac{1}{2\pi} \left[\sum_{n=1}^{\infty} n [a_\sigma(\omega, t)]^{n-1} e^{ni\theta} \dot{a}_\sigma(\omega, t) + \sum_{n=1}^{\infty} n [a_\sigma^*(\omega, t)]^{n-1} e^{-in\theta} \dot{a}_\sigma^*(\omega, t) \right] \\ \frac{\partial \rho_\sigma}{\partial \theta} &= \frac{1}{2\pi} \left[\sum_{n=1}^{\infty} ni a_\sigma^n(\omega, t) e^{i\theta(n-1)} - \sum_{n=1}^{\infty} ni (a_\sigma^*)^n(\omega, t) e^{-i\theta(n+1)} \right] \\ \frac{\partial v_\sigma}{\partial \theta} &= \frac{1}{2i} (-iz_\sigma(t) e^{-i\theta} e^{-i\alpha} - iz_\sigma^*(t) e^{i\theta} e^{i\alpha}) \\ &\quad - \frac{1}{2} (z_\sigma(t) e^{-i\theta} e^{-i\alpha} + z_\sigma^*(t) e^{i\theta} e^{i\alpha})\end{aligned}$$

where with θ we denoted θ_σ . Substituting these terms in the continuity equations (48), we obtain:

$$\begin{aligned}0 &= \frac{\partial \rho_\sigma}{\partial t} + \frac{\partial}{\partial \theta} (\rho_\sigma v_\sigma) \\ &= \frac{1}{2\pi} \left[\sum_{n=1}^{\infty} n [a_\sigma(\omega, t)]^{n-1} e^{ni\theta} \dot{a}_\sigma(\omega, t) + \sum_{n=1}^{\infty} n [a_\sigma^*(\omega, t)]^{n-1} e^{-in\theta} \dot{a}_\sigma^*(\omega, t) \right] \\ &\quad + \frac{1}{2\pi} \left[\sum_{n=1}^{\infty} ni (a_\sigma(\omega, t))^n e^{i\theta n} - \sum_{n=1}^{\infty} ni (a_\sigma^*)^n(\omega, t) e^{-i\theta n} \right] \\ &\quad \cdot \left(\omega + \frac{1}{2i} z_\sigma(t) e^{-i\theta_\sigma} e^{-i\alpha} - \frac{1}{2i} z_\sigma^*(t) e^{i\theta_\sigma} e^{i\alpha} \right) \\ &\quad + \frac{1}{2\pi} \left[1 + \sum_{n=1}^{\infty} (a_\sigma(\omega, t) e^{i\theta})^n + \sum_{n=1}^{\infty} (a_\sigma^*(\omega, t) e^{-i\theta})^n \right] \\ &\quad \cdot \left(-\frac{1}{2} [z_\sigma(t) e^{-i\theta} e^{-i\alpha} + z_\sigma^*(t) e^{i\theta} e^{i\alpha}] \right), \quad \text{for } \sigma = 1, 2.\end{aligned}$$

Equating all coefficients of the $e^{i\theta}$ we obtain

$$\begin{aligned}0 &= \dot{a}_\sigma(\omega, t) + \omega \cdot ia_\sigma(\omega, t) + \frac{2}{2i} i (a_\sigma(\omega, t))^2 z_\sigma(t) e^{-i\alpha} - \frac{1}{2} z_\sigma^*(t) e^{i\alpha} - \frac{1}{2} (a_\sigma(\omega, t))^2 z_\sigma(t) e^{-i\alpha} \\ &= \dot{a}_\sigma(\omega, t) + \omega \cdot ia_\sigma(\omega, t) + \frac{1}{2} (a_\sigma(\omega, t))^2 z_\sigma(t) e^{-i\alpha} - \frac{1}{2} z_\sigma^*(t) e^{i\alpha}, \quad \text{for } \sigma = 1, 2.\end{aligned}$$

Dropping the notation of dependence on ω and t this becomes:

$$\frac{da_\sigma}{dt} + \omega i a_\sigma + \frac{1}{2} (a_\sigma^2 z_\sigma e^{-i\alpha} - z_\sigma^* e^{i\alpha}) = 0, \quad \text{for } \sigma = 1, 2. \quad (52)$$

Equating the coefficients for $e^{kn\theta}$ any $k \neq 0$ results in the same equation (52). In the case where $k = 0$ we obtain a the trivial statement $\frac{1}{2i} z_\sigma a_\sigma i e^{-i\alpha} + \frac{1}{2i} z_\sigma^* a_\sigma i e^{i\alpha} - \frac{1}{2} z_\sigma a_\sigma e^{-i\alpha} - \frac{1}{2} z_\sigma^* a_\sigma e^{i\alpha} = 0$.

Thus if these equations (52) are satisfied together with the conditions for a , then ρ_σ as in (51) is a solution to our system given by (46,47).

We can rewrite the order parameter that appears in (52) in terms of a_σ as well by substituting the Ott-Antonsen ansatzes (51) into (50).

$$\begin{aligned} z_\sigma(t) = & K_{\sigma,1} \int_{-\pi}^{\pi} e^{i\theta_1} \cdot \frac{1}{2\pi} \left[1 + \sum_{n=1}^{\infty} (a_1(t)e^{i\theta_1})^n + \sum_{n=1}^{\infty} (a_1^*(t)e^{-i\theta_1})^n \right] d\theta_1 \\ & + K_{\sigma,2} \int_{-\pi}^{\pi} e^{i\theta_2} \cdot \frac{1}{2\pi} \left[1 + \sum_{n=1}^{\infty} (a_2(t)e^{i\theta_2})^n + \sum_{n=1}^{\infty} (a_2^*(t)e^{-i\theta_2})^n \right] d\theta_2, \quad \text{for } \sigma = 1, 2. \end{aligned}$$

Most of the terms will be zero. For any $m \neq 0$ we namely have that the integral $\int_{-\pi}^{\pi} e^{im\theta_\sigma} d\theta_\sigma = 0$. Thus we obtain:

$$\begin{aligned} z_\sigma(t) = & K_{\sigma,1} \int_{-\pi}^{\pi} e^{i\theta_1} \cdot \frac{1}{2\pi} a_1^*(t)e^{-i\theta_1} d\theta_1 \\ & + K_{\sigma,2} \int_{-\pi}^{\pi} e^{i\theta_2} \cdot \frac{1}{2\pi} a_2^*(t)e^{-i\theta_2} d\theta_2 \\ = & K_{\sigma,1} \cdot a_1^*(t) + K_{\sigma,2} \cdot a_2^*(t), \quad \text{for } \sigma = 1, 2. \end{aligned}$$

Substituting these expressions for z_1 and z_2 into (52) we get

$$\begin{aligned} 0 = & \frac{da_\sigma}{dt} + \omega i a_\sigma + \frac{1}{2} a_\sigma^2 e^{-i\alpha} (K_{\sigma,1} \cdot a_1^* + K_{\sigma,2} \cdot a_2^*) \\ & - \frac{1}{2} e^{i\alpha} (K_{\sigma,1} \cdot a_1 + K_{\sigma,2} \cdot a_2), \quad \text{for } \sigma = 1, 2. \end{aligned} \tag{53}$$

We rewrite (53) into polar coordinates $(\varphi_\sigma, \phi_\sigma)$ where we take $a_\sigma = \varphi_\sigma e^{-i\phi_\sigma}$ for $\sigma = 1, 2$ as follows:

$$\begin{aligned} 0 = & -i\varphi_\sigma e^{-i\phi_\sigma} \frac{d\phi_\sigma}{dt} + e^{-i\phi_\sigma} \frac{d\varphi_\sigma}{dt} + \omega i \varphi_\sigma e^{-i\phi_\sigma} \\ & + \frac{1}{2} \varphi_\sigma^2 e^{-2i\phi_\sigma} e^{-i\alpha} (K_{\sigma,1} \cdot \varphi_1 e^{i\phi_1} + K_{\sigma,2} \cdot \varphi_2 e^{i\phi_2}) \\ & - \frac{1}{2} e^{i\alpha} (K_{\sigma,1} \cdot \varphi_1 e^{-i\phi_1} + K_{\sigma,2} \cdot \varphi_2 e^{-i\phi_2}) \\ \Rightarrow 0 = & -i\varphi_\sigma \frac{d\phi_\sigma}{dt} + \frac{d\varphi_\sigma}{dt} + \omega i \varphi_\sigma \\ & + \frac{1}{2} \varphi_\sigma^2 e^{-i\phi_\sigma} e^{-i\alpha} (K_{\sigma,1} \cdot \varphi_1 e^{i\phi_1} + K_{\sigma,2} \cdot \varphi_2 e^{i\phi_2}) \\ & - \frac{1}{2} e^{i\phi_\sigma} e^{i\alpha} (K_{\sigma,1} \cdot \varphi_1 e^{-i\phi_1} + K_{\sigma,2} \cdot \varphi_2 e^{-i\phi_2}), \quad \text{for } \sigma = 1, 2, \end{aligned} \tag{54}$$

where in the last step we multiplied both sides by $e^{-i\phi_\sigma}$. Now equating imaginary parts we obtain:

$$\begin{aligned} 0 = & -\varphi_\sigma \frac{d\phi_\sigma}{dt} + \omega \varphi_\sigma \\ & + \frac{1}{2} \varphi_\sigma^2 \varphi_1 K_{\sigma,1} \sin(\phi_1 - \phi_\sigma - \alpha) + \frac{1}{2} \varphi_\sigma^2 \varphi_2 K_{\sigma,2} \sin(\phi_2 - \phi_\sigma - \alpha) \\ & - \frac{1}{2} \varphi_1 K_{\sigma,1} \sin(\phi_\sigma + \alpha - \phi_1) - \frac{1}{2} K_{\sigma,2} \varphi_2 \sin(\phi_\sigma + \alpha - \phi_2), \quad \text{for } \sigma = 1, 2. \end{aligned}$$

For $\sigma = 1$ this simplifies to

$$\begin{aligned} 0 &= -\varphi_1 \frac{d\phi_1}{dt} + \omega\varphi_1 \\ &\quad - \frac{1}{2}\varphi_1^2\varphi_1 K_{1,1} \sin(\alpha) + \frac{1}{2}\varphi_1^2\varphi_2 K_{1,2} \sin(\phi_2 - \phi_1 - \alpha) \\ &\quad - \frac{1}{2}\varphi_1 K_{1,1} \sin(\alpha) - \frac{1}{2}\varphi_2 K_{1,2} \sin(\phi_1 + \alpha - \phi_2) \\ &= -\varphi_1 \frac{d\phi}{dt} + \omega\varphi_1 - \frac{\varphi_1^2 + 1}{2} (\varphi_1 K_{1,1} \sin(\alpha) + \varphi_2 K_{1,2} \sin(\phi_2 - \phi_1 - \alpha)). \end{aligned}$$

Similarly for $\sigma = 2$ we obtain

$$0 = -\varphi_2 \frac{d\phi_2}{dt} + \omega\varphi_2 + \frac{\varphi_2^2 + 1}{2} (\varphi_1 K_{2,1} \sin(\phi_1 - \phi_2 - \alpha) - \varphi_2 K_{2,2} \sin(\alpha)).$$

Equating real parts of (54):

$$\begin{aligned} 0 &= \frac{d\varphi_\sigma}{dt} + \frac{1}{2}\varphi_\sigma^2\varphi_1 K_{\sigma,1} \cos(\phi_1 - \phi_\sigma - \alpha) + \frac{1}{2}\varphi_\sigma^2\varphi_2 K_{\sigma,2} \cos(\phi_2 - \phi_\sigma - \alpha) \\ &\quad - \frac{1}{2}\varphi_1 K_{\sigma,1} \cos(\phi_\sigma + \alpha - \phi_1) - \frac{1}{2}K_{\sigma,2}\varphi_2 \cos(\phi_\sigma + \alpha - \phi_2), \quad \text{for } \sigma = 1, 2. \end{aligned}$$

For $\sigma = 1$ this simplifies to

$$\begin{aligned} 0 &= \frac{d\varphi_1}{dt} + \frac{1}{2}\varphi_1^2\varphi_1 K_{1,1} \cos(-\alpha) + \frac{1}{2}\varphi_1^2\varphi_2 K_{1,2} \cos(\phi_2 - \phi_1 - \alpha) \\ &\quad - \frac{1}{2}\varphi_1 K_{1,1} \cos(\alpha) - \frac{1}{2}K_{1,2}\varphi_2 \cos(\phi_1 + \alpha - \phi_2), \\ &= \frac{d\varphi_1}{dt} + \frac{\varphi_1^2 - 1}{2} (\varphi_1 K_{1,1} \cos(\alpha) + \varphi_2 K_{1,2} \cos(\phi_2 - \phi_1 - \alpha)). \end{aligned}$$

Similarly for $\sigma = 2$ we obtain

$$0 = \frac{d\varphi_2}{dt} + \frac{\varphi_2^2 - 1}{2} (\varphi_1 K_{2,1} \cos(\phi_1 - \phi_2 - \alpha) + \varphi_2 K_{2,2} \cos(\alpha)).$$

We now continue with the analysis of this system as done by [6].

4.2 Analysis of Chimera State

In the previous subsection we obtained the equations describing the evolution of the oscillator densities for each group. We now consider the case where one of the groups is perfectly synchronised. The dynamics for group 1 is described by the equations

$$0 = \frac{d\varphi_1}{dt} + \frac{\varphi_1^2 - 1}{2} (\varphi_1 K_{1,1} \cos(\alpha) + \varphi_2 K_{1,2} \cos(\phi_2 - \phi_1 - \alpha)) \quad (55)$$

$$0 = -\varphi_1 \frac{d\phi_1}{dt} + \omega\varphi_1 - \frac{\varphi_1^2 + 1}{2} (\varphi_1 K_{1,1} \sin(\alpha) + \varphi_2 K_{1,2} \sin(\phi_2 - \phi_1 - \alpha)), \quad (56)$$

and the dynamics for group 2 is described by

$$0 = \frac{d\varphi_2}{dt} + \frac{\varphi_2^2 - 1}{2} (\varphi_1 K_{2,1} \cos(\phi_1 - \phi_2 - \alpha) + \varphi_2 K_{2,2} \cos(\alpha)) \quad (57)$$

$$0 = -\varphi_2 \frac{d\phi_2}{dt} + \omega\varphi_2 + \frac{\varphi_2^2 + 1}{2} (\varphi_1 K_{2,1} \sin(\phi_1 - \phi_2 - \alpha) - \varphi_2 K_{2,2} \sin(\alpha)). \quad (58)$$

Recall that we assumed solutions to the continuity equations for each oscillator density ρ_1 , ρ_2 are of the form given by (51). Suppose we assume that all oscillators in group 1 are in perfect synchrony. Then for some θ_1 the value of the oscillator density ρ_1 should go to 1 and for all other values of θ_1 it should go to 0. That is, all oscillators in group 1 are nearly at the same phase. So ρ_1 should approximate the delta function as the number of oscillators goes to infinity. In our polar coordinates the oscillator density is rewritten to

$$\begin{aligned}\rho_1(\theta_1, t) &= \frac{1}{2\pi} \left[1 + \sum_{n=1}^{\infty} (\varphi_1 e^{i\theta_1 - i\phi_1})^n + \sum_{n=1}^{\infty} (\varphi_1 e^{i\phi_1 - i\theta_1})^n \right] \\ &= \frac{1}{2\pi} \sum_{n=-\infty}^{\infty} \varphi_1^n e^{in(\theta_1 - \phi_1)}.\end{aligned}\quad (59)$$

Without loss of generality we can assume that the oscillators in group 1 are synchronised at $\theta_1 = \phi_1$. Then (59) goes to the delta function $\delta(\theta_1 - \phi_1)$ for $\varphi_1 \rightarrow 1$,

$$\begin{aligned}\rho_1(\theta_1, t) &\rightarrow \sum_{n=-\infty}^{\infty} \delta(\theta_1 - \phi_1 - 2\pi n) \\ &= \delta(\theta_1 - \phi_1).\end{aligned}$$

Thus taking $\varphi_1 = 1$ corresponds to perfect synchronisation of the oscillators in group 1. Then $\dot{\varphi}_1 = 0$ and Equation 55 is trivially satisfied while Equation 56 reduces to

$$0 = -\frac{d\phi_1}{dt} + \omega - \mu \sin(\alpha) + \varphi_2 \nu \sin(\phi_2 - \phi_1 - \alpha). \quad (60)$$

Note that we substituted the intergroup coupling $K_{1,1} = K_{2,2} = \mu$ and the intragroup coupling $K_{1,2} = K_{2,1} = \nu$. The dynamics for group 2 given by Equations 57 and 58 reduce to

$$0 = \frac{d\varphi_2}{dt} + \frac{\varphi_2^2 - 1}{2} (\nu \cos(\phi_1 - \phi_2 - \alpha) + \varphi_2 \mu \cos(\alpha)) \quad (61)$$

$$0 = -\varphi_2 \frac{d\phi_2}{dt} + \omega \varphi_2 + \frac{\varphi_2^2 + 1}{2} (\nu \sin(\phi_1 - \phi_2 - \alpha) - \varphi_2 \mu \sin(\alpha)). \quad (62)$$

We can rewrite the system (60,61,62) in terms of $r = \varphi_2$ and $\psi = \phi_1 - \phi_2$ as follows.

$$\begin{aligned}0 &= -\frac{d\phi_1}{dt} + \omega - \mu \sin(\alpha) - r\nu \sin(\psi + \alpha) \\ 0 &= \frac{dr}{dt} + \frac{r^2 - 1}{2} (\nu \cos(\psi - \alpha) + r\mu \cos(\alpha)) \\ 0 &= -r \frac{d\phi_2}{dt} + \omega r + \frac{r^2 + 1}{2} (\nu \sin(\psi - \alpha) - r\mu \sin(\alpha)).\end{aligned}$$

We can rewrite these equations to obtain expressions for the derivatives with respect to time of r and $\psi = \phi_1 - \phi_2$:

$$\begin{aligned}\dot{r} &= \frac{dr}{dt} = \frac{1 - r^2}{2} (r\mu \cos(\alpha) + \nu \cos(\psi - \alpha)) \\ \dot{\psi} &= \frac{d\psi}{dt} = \frac{d\phi_1}{dt} - \frac{d\phi_2}{dt} \\ &= \omega - \mu \sin(\alpha) - r\nu \sin(\psi + \alpha) - \omega - \frac{r^2 + 1}{2r} (\nu \sin(\psi - \alpha) - r\mu \sin(\alpha)) \\ &= \frac{r^2 + 1}{2r} (r\mu \sin(\alpha) - \nu \sin(\psi - \alpha)) - \mu \sin(\alpha) - r\nu \sin(\psi + \alpha).\end{aligned}\quad (63)$$

Now we look at where the system has a fixed point (e.g. $\dot{r} = 0$ and $\dot{\psi} = 0$). Firstly $\dot{r} = 0$ when $r = 1$. Substituting this in the equation for $\dot{\psi}$ we find $\dot{\psi}|_{r=1} = -\nu \sin(\psi - \alpha) - \nu \sin(\psi + \alpha)$. Since $\nu > 0$, this expression is zero for $\psi = n\pi$ for $n \in \mathbb{Z}$. The fixed point $(r, \psi) = (1, 0)$ corresponds to the perfectly synchronised state of all oscillators.

The fixed point $(r, \psi) = (1, \pi)$ corresponds to the state in which the oscillators in group 2 are perfectly synchronised with each other, but not with group 1. The two synchronised groups are actually anti-phase. We observed this behavior in our numerical experiments as well. Each of the order parameters φ_1 and φ_2 is close to 1, yet the order parameter over all the oscillators together is close to 0.

Apart from the trivial fixed point there may exist fixed points that correspond to the chimera states. In a chimera state one of the order parameters, say φ_1 , equals 1 while the other order parameter $\varphi_2 (= r)$ does not equal 1. This means that the oscillators in group 1 are completely synchronised while those in group 2 are not.

Thus we are looking for a fixed point where $r \neq 1$ and where the other order parameter still has $\varphi_1 = 1$. From $\dot{r} = 0$ and $r \neq 1$ we obtain

$$\mu r \cos(\alpha) + \nu \cos(\psi - \alpha) = 0.$$

Substituting the expressions in terms of A for μ and ν and solving for A :

$$\begin{aligned} \frac{1+A}{2}r \cos(\alpha) + \frac{1-A}{2} \cos(\psi - \alpha) &= 0 \\ \Rightarrow A r \cos(\alpha) + r \cos(\alpha) + \cos(\alpha - \psi) - A \cos(\alpha - \psi) &= 0 \\ \Rightarrow A[r \cos(\alpha) - \cos(\alpha - \psi)] &= -r \cos(\alpha) - \cos(\alpha - \psi) \\ \Rightarrow A &= \frac{r \cos(-\alpha) + \cos(-\alpha + \psi)}{\cos(-\alpha + \psi) - r \cos(-\alpha)}. \end{aligned}$$

We make the substitution $\alpha = \frac{\pi}{2} - \beta$:

$$A = \frac{\sin(\beta + \psi) + r \sin(\beta)}{\sin(\beta + \psi) - r \sin(\beta)}.$$

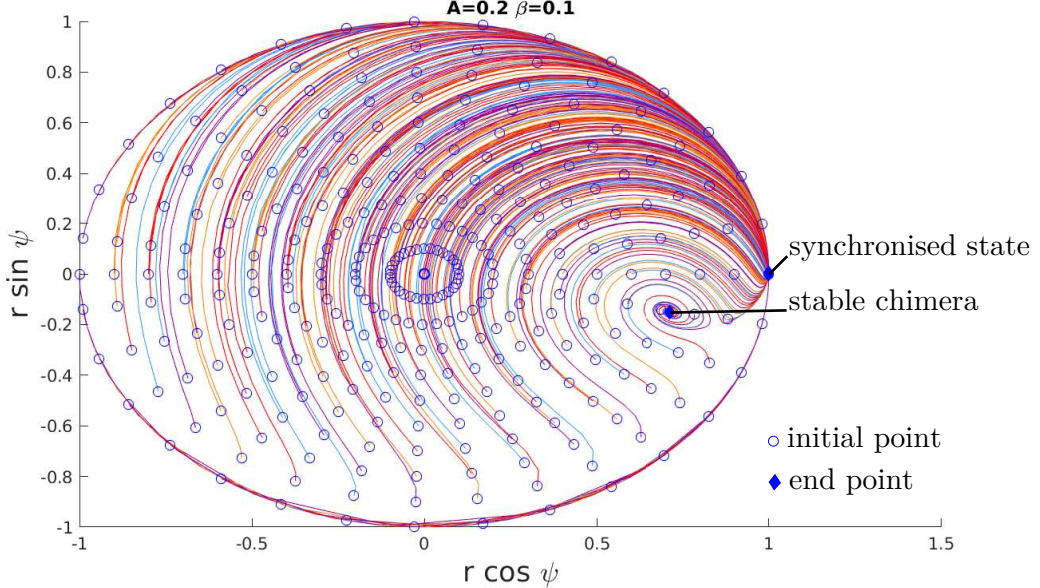
The other condition of a fixed point is that $\dot{\psi} = 0$. Thus we take the expression for $\dot{\psi}$ as in (63); and substitute $\alpha = \frac{\pi}{2} - \beta$, $\mu = \frac{1+A}{2}$ and $\nu = \frac{1-A}{2}$. Then we substitute the expression for A just obtained. The calculations can be found in Appendix A. We obtain:

$$r^2 = \frac{\sin(2\beta + \psi)}{\sin(2\beta - \psi) - 2 \sin(\psi)}.$$

Since $r = \varphi_2$ is a partial order parameter it takes on values between 0 and 1. Thus we consider the positive solution for r . Recall that φ_2 came from writing a_2 in terms of its polar coordinates, where $\varphi \geq 0$ is its radius. So the order parameter for the second group is

$$r = \sqrt{\frac{\sin(2\beta + \psi)}{\sin(2\beta - \psi) - 2 \sin(\psi)}}.$$

Figure 4: Here we have plotted 363 trajectories of (64) from different starting points (blue circles) until end time $T = 10^4$. The end of each trajectory is indicated with a blue solid diamond. The trajectories end up either at stable chimera or at the fixed point (synchronised state). The coupling parameter is $A = 0.2$, and the phase lag $\beta = 0.1$



4.3 Bifurcation Analysis for Chimera State

We have obtained an expression for the order parameter of the oscillators in group $\sigma = 2$ which we can use to study the dynamics of this group. The system we consider in this Subsection was found in the previous Subsection (63) and is given by

$$\begin{aligned}\dot{r} &= f_1(r, \psi) = \frac{1-r^2}{2} (r\mu \cos(\alpha) + \nu \cos(\psi - \alpha)) \\ \dot{\psi} &= f_2(r, \psi) = \frac{r^2+1}{2r} (r\mu \sin(\alpha) - \nu \sin(\psi - \alpha)) - \mu \sin(\alpha) - r\nu \sin(\psi + \alpha),\end{aligned}$$

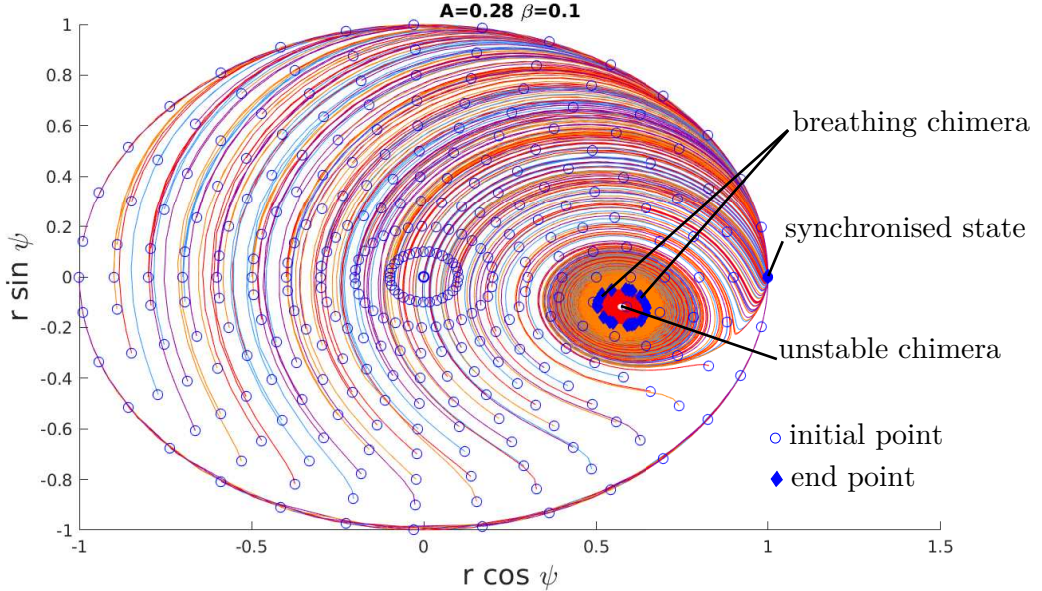
in terms of $\beta = \frac{\pi}{2} - \alpha$ this becomes:

$$\begin{aligned}\dot{r} &= f_1(r, \psi) = \frac{1-r^2}{2} (r\mu \sin(\beta) + \nu \sin(\beta + \psi)) \\ \dot{\psi} &= f_2(r, \psi) = \frac{r^2+1}{2r} (r\mu \cos(\beta) + \nu \cos(\beta + \psi)) - \mu \cos(\beta) - r\nu \cos(\psi - \beta).\end{aligned}\quad (64)$$

4.3.1 Phase Plane Analysis

We study the phase plane of the system given by (64) for different values of the coupling parameter A . Recall that setting $A = 0$ would correspond to the original Kuramoto model. As A is increased we bifurcate from uniform coupling towards pure intergroup coupling. In order to allow for easy comparison with the results of Abrams, Mirello and Strogatz [6], we use parameters corresponding to those in their order parameter plots.

Figure 5: Here we have plotted 363 trajectories of (64) from different starting points (blue circles) until end time $T = 10^4$. The end of each trajectory is indicated with a blue solid diamond. The trajectories end up either in the limit cycle (breathing chimera) or the fixed point (synchronised state). With the limit cycle we mean the cycle on which several of the blue diamonds are spread out. Trajectories inside the limit circle move away from the unstable point (unstable chimera) towards the limit cycle as well. The coupling parameter is $A = 0.28$, and the phase lag $\beta = 0.1$

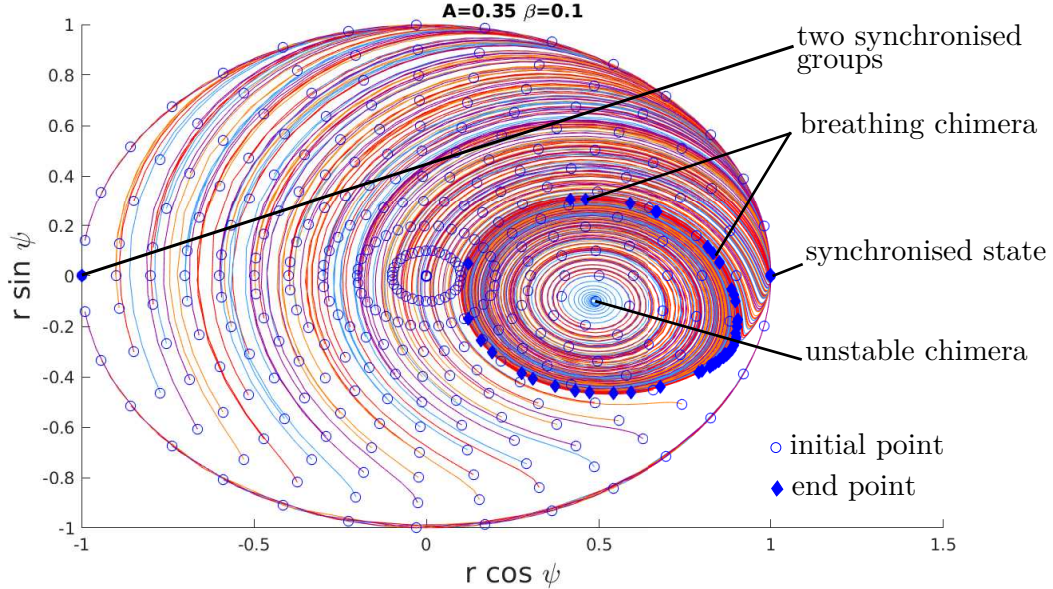


We start by considering the parameters $A = 0.2$ and $\beta = 0.1$ in Figure 4. Each paths starting point is indicated by a blue open circle. The ends are indicated by blue filled diamonds. The stable points / cycles could thus be found by looking for solid blue diamonds. First of all we can confirm the trivial fixed point where all oscillators are synchronised. When all oscillators are synchronised, the phase difference between the groups ψ equals 0 and order parameter of the second group r equals 1. Thus we find this point at coordinates $r \cos(\psi) = 1$, $r \sin(\psi) = 0$. Another point to which several paths converge is indicated as a stable chimera. At this point the order parameter of the second group $r < 1$ and the phase difference between the groups $\psi > 0$. Recall that we set the order parameter of the first group to 1. Thus we observed one synchronised group in coexistence with an incoherent group, e.g. a chimera state.

The second set of parameters we consider are $A = 0.28$ and $\beta = 0.1$. The phase plane is shown in Figure 5. This phase plane differs from that in Figure 4 in that the chimera is now unstable. Trajectories starting from or close to the chimera now move outwards and towards the limit cycle that is called 'breathing chimera'. We can see that several trajectories have their endpoints on this limit cycle around the chimera by the blue diamonds. The completely synchronised state is stable as well. Most trajectories end up in this state.

As we increase the coupling parameter A to 0.35, the limit cycle increases its period. The phase plane is shown in Figure 6. We also notice that the trajectory starting at $(r, \psi) = (1, \pi)$

Figure 6: Here we have plotted 363 trajectories of (64) from different starting points (blue circles) until end time $T = 10^4$. The end of each trajectory is indicated with a blue solid diamond. The trajectories end up either in the limit cycle (breathing chimera) or the fixed point (synchronised state). Trajectories inside the limit cycle move away from the unstable point (unstable chimera) towards the limit cycle as well. This is more clear now that the limit cycle is greater than in Figure 5. Note the presence of an unstable fixed point, namely for $r = 1, \psi = \pi$. Thus the two groups are synchronised with a phase difference of ϕ between them. The coupling parameter is $A = 0.35$, and the phase lag $\beta = 0.1$



stays there in this simulation. This state corresponds to two groups synchronised in anti-phase with each other. Trajectories slightly perturbed from this do however still go to the synchronised state.

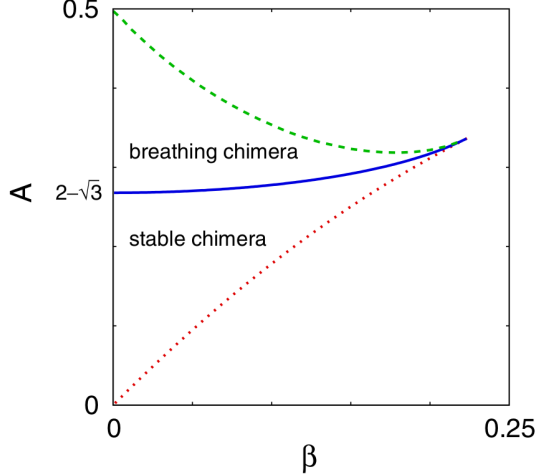
4.3.2 Bifurcation Curves

We will linearise the system around the fixed solution where $\varphi_1 = 1$; and $\varphi_2 = r$ and ψ are constant. To find where the bifurcations occur we summarise the approach of Abrams, Mirello and Strogatz [6] and look for Saddle-Node bifurcations as well as Hopf Bifurcations. In case of the Saddle-Node bifurcation we need to find where the determinant of the Jacobian is zero. In case of the Hopf bifurcation need to find where the trace of the Jacobian is zero and in addition the determinant of the Jacobian is positive. We linearise (64) around the fixed points that satisfy

$$A = \frac{\sin(\beta + \psi) + r \sin(\beta)}{\sin(\beta + \psi) - r \sin(\beta)}$$

$$r = \sqrt{\frac{\sin(2\beta + \psi)}{\sin(2\beta - \psi) - 2 \sin(\psi)}}. \quad (65)$$

Figure 7: "Stability diagram for chimera states. Bifurcation curves: saddle-node (dotted line) and supercritical Hopf (solid line), both found analytically; homoclinic (dashed line), found numerically." Source: [6].



The partial derivatives are as follows:

$$\begin{aligned}\frac{\partial f_1}{\partial r} &= -r(r\mu \sin(\beta) + \nu \sin(\beta + \psi)) + \frac{1 - r^2}{2}(\mu \sin(\beta)) \\ \frac{\partial f_1}{\partial \psi} &= -\frac{1 - r^2}{2}\nu \cos(\beta + \psi) \\ \frac{\partial f_2}{\partial r} &= r\mu \cos(\beta) - \frac{1 - r^2}{2r^2}\nu \cos(\beta + \psi) - \nu \cos(\psi - \beta) \\ \frac{\partial f_2}{\partial \psi} &= \frac{r^2 + 1}{2r}(-\nu \sin(\beta + \psi)) + r\nu \sin(\psi - \beta).\end{aligned}$$

Its Jacobian J is given by

$$J = \begin{pmatrix} \frac{\partial f_1}{\partial r} & \frac{\partial f_1}{\partial \psi} \\ \frac{\partial f_2}{\partial r} & \frac{\partial f_2}{\partial \psi} \end{pmatrix}.$$

Setting the determinant of the Jacobian to zero, Abrams, Mirello and Strogatz [6] find that this simplifies to

$$\sin(\beta) + \frac{\sin(2\beta + \psi)[\sin(\beta - 2\psi) + 2\sin(\beta + 2\psi)]}{\sin(2\beta - \psi) + 2\sin(\psi)} = 0,$$

where they used the expressions for A and r we found above (65). They find an approximation for the root ψ in terms of β and substitute this into the expression for A to obtain the curve for the saddle node bifurcation. The numerical curve is shown in Figure 7. Similarly the Hopf curve is found by setting the trace of the Jacobian to zero.

Figure 7 shows that the appearance of chimera states depends on the phase lag and the inter/intra group coupling. For a chimera state to appear, β should be small (corresponding to sufficient phase lag $\alpha = \pi/2 - \beta$). At $\beta = 0$ both fully synchronised states and the asymmetric states may appear [8]. These states correspond to the case where $r = 1$. Thus the order parameters of each of the groups is 1. There are two types of states for which this holds. Either all oscillators are synchronised in phase ($r = 1$ and $\psi = 0$) or oscillators within each group are synchronised while the groups are not synchronised in phase with each other ($r = 1$ and $\psi = \pi$).

As we increase β from 0, two bifurcations appear. An unstable chimera bifurcates from the fully synchronised state ($r = 1$ and $\psi = 0$). Secondly, a stable chimera bifurcates from the asymmetric state ($r = 1$ and $\psi = \pi$). If β is increased further a saddle node bifurcation occurs and the previously stable chimera becomes unstable.

There is another way through which the stable chimera state loses its stability. Namely through a Hopf bifurcation followed by a homoclinic bifurcation. If $\beta > 0$ small enough and increase from $0 < A < 2 - \sqrt{3}$, we encounter a supercritical Hopf bifurcation around $A = 2 - \sqrt{3}$. The state observed after this bifurcation is referred to as a breathing chimera. The order parameter of the incoherent group $re^{i\psi}$ follows a limit cycle in the complex plane [8]. The diameter of this limit cycle increases as A increases. When increasing A even further, we encounter a homoclinic bifurcation. The breathing chimera disappears as the limit cycle of its order parameter collides with the unstable chimera state.

Recall that a value of A close to zero corresponds to a system where the coupling is close to uniform. On the other hand, a value of A close to 1 corresponds to a system with intergroup and no intra group coupling. From Figure 7 we conclude that we need coupling that is close to uniform coupling to observe stable chimera's.

5 Time-frequency Analysis

We will introduce time-frequency analysis based on wavelets. This method works especially well for analysing rapidly varying dynamics. It works similarly to the windowed Fourier transform but has some advantages which we will discuss here. In principle the analysis of frequencies is mathematically defined for infinite time signals. The limitations of this type of analysis done on finite time signals have been described by Carmona [21].

In our time-frequency analysis we will analyse the order parameter that was derived earlier, i.e.

$$re^{i\psi} = \frac{1}{N} \sum_{j=1}^N e^{i\phi_j}.$$

We summarise both the basic and windowed Fourier transforms first to motivate the use of wavelets for our analysis.

5.1 Basic Fourier Transform

The basic Fourier transform decomposes a signal, a complex time signal in our case, into its frequencies. The Fourier transform expresses a signal as a sum of sinusoids. This results in

a decomposition of frequencies. If a certain frequency is present in a signal, the Fourier representation will have a peak at this frequency. There is no information about the location in time or the duration of this frequency. We only know if a frequency is present in the signal or not.

Thus there is no time related information. However, in our problem we would like to analyse exactly that. We are interested in the occurrence of synchronisation in the system, therefore we need the present frequencies to be linked the time at which they appeared.

5.2 Windowed Fourier Transform

The windowed Fourier transform uses the same principles but instead of looking at the signal as a whole, it is split up into different windows. The function is multiplied by some window function that is localized in time. Each window is then analysed separately. Thus obtaining for each window information about the present frequencies. The difficulty in this analysis is choosing the window size. For if the windows are too small, the frequency might not be measured accurately. Yet if the windows are too wide, we obtain less information about the time related to the frequencies. This is known as Heisenberg's uncertainty principle.

5.3 Continuous Wavelet Transform

The disadvantage of using fixed window functions is the information obtained is located at uniformly distributed points in time as well as uniformly distributed points in frequency. Morlet and Grossmann therefore developed a theory using basis functions that are localised in both time and frequency similar to what Gabor had developed previously. The basis that Morlet and Grossman used in addition allowed for a non-uniform coverage in the time-frequency space [22].

Instead of decomposing the signal by using sinusoids, we will use wavelets. The main difference with sinusoids is that wavelets are localised on a finite time interval only. When analysing for a certain frequency this wavelet is stretched or shrunk and thus automatically adjusts its window. The adaptation of wavelets in the method ensures that the length of the window is adjusted according to the frequency. This way rapid variations are better captured. Whereas events that happen on short timescales, e.g. timescales less than the length of the window, would be missed by the original time-frequency method. The continuous wavelet transform works especially well to analyse signals with a big variation between the frequencies present.

The mother wavelet we will consider in our analysis is the Analytic Morlet wavelet. This wavelet is described in for example [23]. The mother wavelet is a generator function $\psi(t)$ that will be scaled and shifted in the following way:

$$\psi_{a,b}(t) = a^{-1/2} \psi\left(\frac{t-b}{a}\right),$$

where $a > 0$, b are real. The mother wavelet can be scaled by varying a and shifted by varying b . The factor $a^{-1/2}$ ensures that regardless of its scaling, each wavelet has the same length $\|\psi(t)\|$.

The Analytic Morlet mother wavelet $\psi(t)$ is given by

$$\psi(t) = \pi^{-1/4} e^{i\omega_0 t} e^{-t^2/2}.$$

The daughter wavelets are then generated by transforming and scaling the mother wavelet. The parameter ω_0 controls the number of local cycles. We take $\omega_0 = 6$ according to [23] to satisfy

the admissibility condition. The admissible condition requires that in order to be considered a wavelet, an integrable function should have an average of zero [24]. For more details on for example the minimum scaling and spacing used by the continuous wavelet transform that is implemented here, we refer to the documentation of Matlabs Wavelet Toolbox [12, 13]. The scaling factor σ determines how much we stretch or compress the mother wavelet. The wavelet transform for a signal $S(t)$ is given by

$$L_\psi S(a, b) = \langle f, \psi_{a,b} \rangle = a^{-1/2} \int_{-\infty}^{\infty} S(t) \psi^* \left(\frac{t-b}{a} \right) dt,$$

where we denoted the complex conjugate of $\psi(t)$ by $\psi^*(t)$. The continuous wavelet transform for the signal $S(t) = e^{2\pi v t i}$ is for example given by

$$\begin{aligned} L_\psi S(a, b) &= a^{-1/2} \int_{-\infty}^{\infty} e^{2\pi v t i} \psi^* \left(\frac{t-b}{a} \right) dt \\ &= a^{-1/2} \cdot a \cdot e^{2\pi v b i} \int_{-\infty}^{\infty} e^{2\pi (av) s i} \psi^*(s) ds \\ &= a^{1/2} e^{2\pi v b i} \bar{\psi}(av), \end{aligned}$$

where the Fourier transform $\bar{\psi}(av)$ of the Analytic Morlet wavelet is given by

$$\bar{\psi}(av) = \pi^{-1/4} H(v) e^{-(av - \omega_0)^2/2}.$$

Here $H(v)$ is the Heaviside step function ($H(v) = 1$ if $v > 0$, $H(v) = 0$ otherwise). We will be interested in the modulus of this transform which is given by

$$|L_\psi S(a, b)| = a^{1/2} \pi^{-1/4} H(v) e^{-(av - \omega_0)^2/2}.$$

5.4 Time-frequency Analysis: Some Examples

To demonstrate the use of the time-frequency analysis that will be used to analyse the Kuramoto model we first introduce a few examples. Firstly consider the time signal given simply by $S(t) = e^{it}$. Its graph and time-frequency plot are shown in Figure 8. The highest amplitude frequencies are colour coded in yellow. The lowest amplitude frequencies are coloured dark blue. In this case we observe a yellow constant line indicating that the signal has a constant frequency.

The frequency is normalised and given in cycles per sample. We are mainly interested in the presence of a dominant frequency. This presence indicates synchronisation. At what frequency these synchronised oscillators are then moving is of less interest. We can however convert the normalised frequency to frequencies again by dividing by the time step that was taken. In the case of the sine as well as in following analysis we take a time step $\Delta t = 0.1$. Thus we calculate the dominant frequency in Figure 8b as follows: $f \approx 0.0156/0.1 = 0.156$, or $0.98/2\pi$.

Now consider the time signal give by $S(t) = e^{i(t+0.1t^2)}$. Its graph is given in Figure 9a. The frequency of the signal increases in time, as can be seen in the time-frequency plot in Figure 9b. Note that the normalized frequency axis has logarithmic scaling. We compute the time by multiplying the time in samples (X-axis in time-frequency plots) by the time step.

Figure 8: An example to demonstrate the time-frequency analysis. We analyse the signal $S(t) = e^{it}$ for $0 < t < 30$.

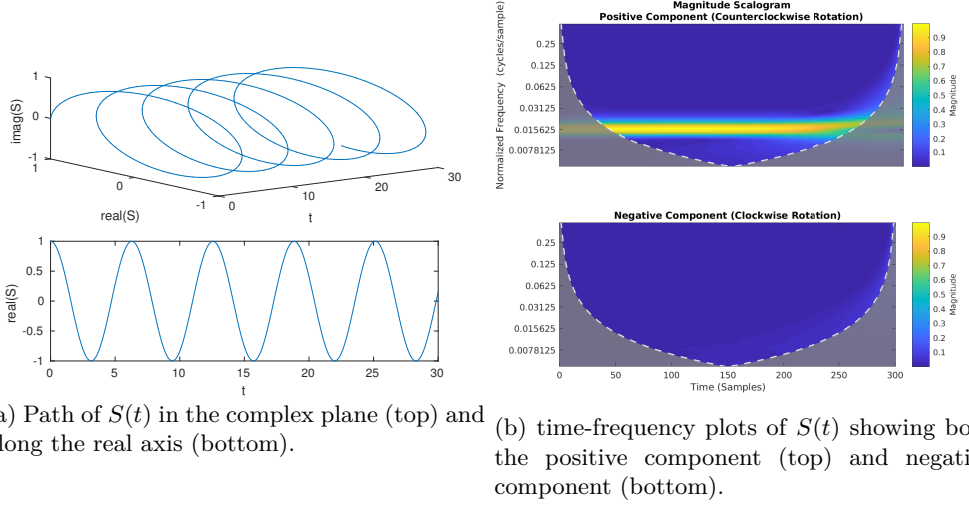
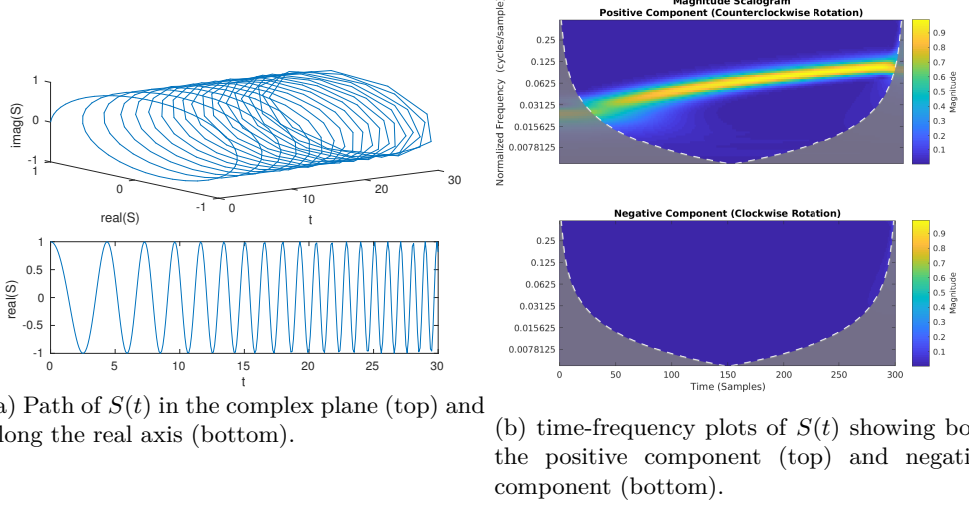


Figure 9: An example to demonstrate the time-frequency analysis. We analyse the signal $S(t) = e^{i(t+0.1t^2)}$ for $0 < t < 30$.



6 Numerical Solutions

In this Section we will simulate a large number of oscillators for the different models discussed in this thesis. To simulate the Kuramoto model with noise, we use the Monte Carlo method together with the Euler-Maruyama method. We simulate many trajectories for each of which we add the appropriate white noise term at each time step. For each of these trajectory we then find the value of the order parameter at every time point. The average of all those order parameters is then plotted and analysed by time-frequency analysis. We follow the sectioning as

before. We start with the Original Kuramoto model in Subsection 6.1, secondly we consider the Kuramoto model with added white noise in Subsection 6.2, thirdly we consider the Kuromoto model with a bimodal frequency distribution in Subsection 6.3 and conclude with the model that was discussed in Section 4 in which we expect a chimera state in Subsection 6.4.

6.1 The Original Kuramoto Model

We consider the original Kuramoto model and perform time-frequency analysis on the path of the complex order parameter. We let the initial phases be uniformly distributed, thus we start close to the incoherent solution. We check its stability by increasing K from zero. The natural frequencies are taken from a Lorenzian distribution with width parameter Δ . We can calculate the critical coupling using the formula that was derived earlier (12). The critical coupling is thus given by $K_c = 2\Delta$.

In our first experiment we take width parameter $\Delta = 0.025$ and mean frequency $\omega_0 = 0.3$. Usually a zero mean frequency is taken for simplification, since we can without loss of generality move into a moving frame of the actual frequency. We take a non-zero mean frequency such that we can apply time-frequency analysis on the signal. The critical coupling in the limit of infinitely many oscillators is $K_c = 2 \cdot 0.025 = 0.05$. We therefore consider coupling constants $K = 0.04 < K_c$ and $K = 0.1 > K_c$. For coupling larger than K_c , we can use Equation 13 as derived by Kuramoto to determine the value of the radial or the order parameter:

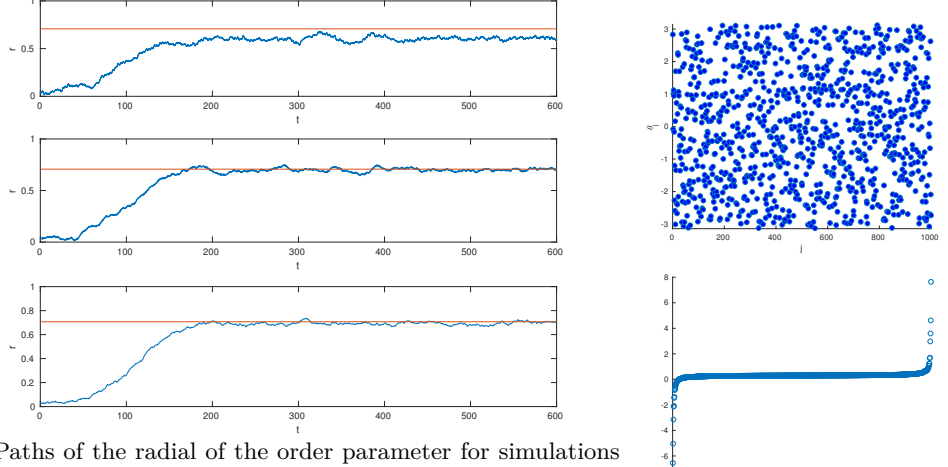
$$r = \sqrt{1 - \frac{0.05}{0.1}} = \frac{1}{2}\sqrt{2} \approx 0.71.$$

We attempt to confirm these values for the critical coupling as well as the supposed value of r by simulating the oscillators and calculating the order parameter. We then perform time-frequency analysis to confirm incoherence or synchronisation and to get familiar with the application of this method. Figure 10 shows the radial of the order parameter as well as the time-frequency analysis of the complex order parameter for sufficient coupling $K = 0.1 > K_c$. We increase the number of oscillators from top to bottom and notice that the radial of the order parameter approaches the value $r = 0.71$ that was computed with Kuramoto's formula. So if we want a certain degree of synchronisation $0 < r < 1$, then we can calculate the required coupling that should be present for the desired level of synchronisation to appear.

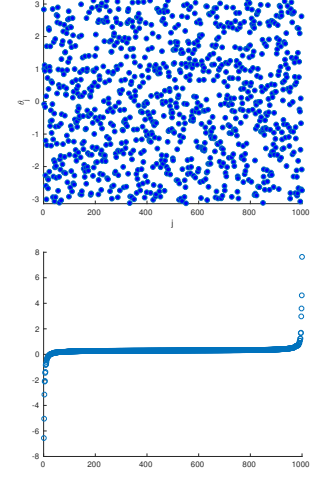
For completion we also look at a value for the coupling for which the Kuramoto model does not synchronise. In Figure 11 the oscillators have similar natural frequencies and there is coupling between them. Yet the radius r of the order parameter stays very small. The oscillators are close to synchronisation in frequency, but not synchronised in phase at all. Had there not been any coupling present between the oscillators, then each of them would move with its own natural frequency and the time-frequency plot would show several yellow and / or light blue lines. The time-frequency plot now indicates that the frequencies of the oscillators change over time.

Considering now a uniform discrete distribution for the oscillators and no noise. As a mean frequency we take $\omega_0 = 0.3$. Thus all oscillators have this frequency. We consider 100 oscillators again and take a coupling $K = 0.1$. The results are shown in Figure 12. All oscillators synchronise quickly in both frequency and phase. The radius of the order parameter goes to 1, indicating that all oscillators have the same phase. The clear straight yellow line in the time-frequency plot indicates one dominant frequency.

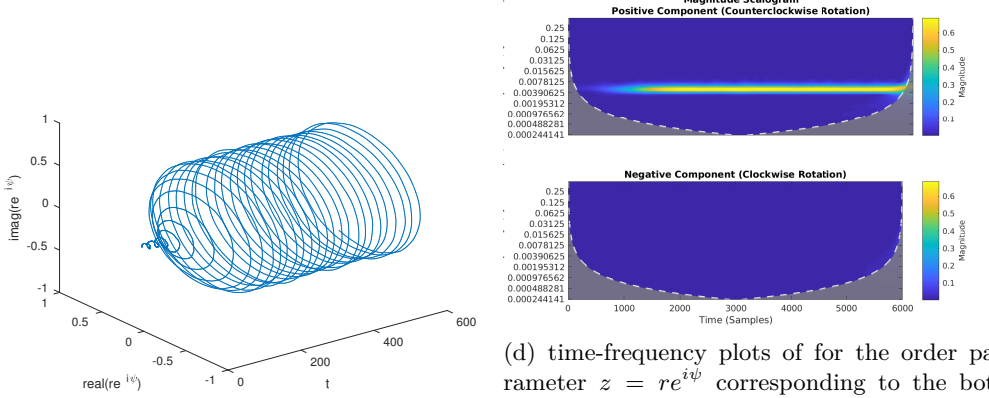
Figure 10: Simulations of the Kuramoto model with Lorenzian distribution ($\omega_0 = 0.3$, $\Delta = 0.025$) with coupling strength $K = 0.1$.



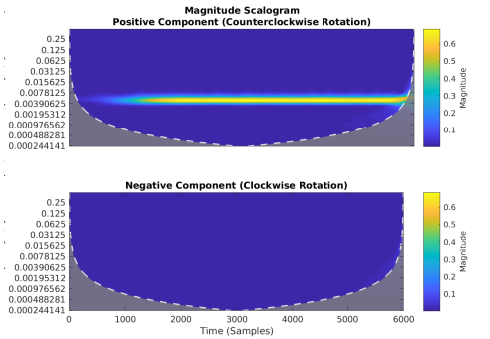
(a) Paths of the radial of the order parameter for simulations of the Kuramoto model as well as a line indicating the value of $r = 0.71$. We start with 250 oscillators (top) and increase this number to 500 (middle) and 1000 (bottom). As the number of oscillators increases the approximation to $r = 0.71$ is observed to improve.



(b) Distribution of the initial phases (top) and of the natural frequencies (bottom)



(c) Path of the order parameter in the complex plane for 1000 oscillators. See (d) for its time-frequency analysis.



(d) time-frequency plots of for the order parameter $z = re^{i\psi}$ corresponding to the bottom plot of 1000 oscillators showing both the positive component (top) and negative component (bottom). We note one dominant frequency in the positive direction at approximately $0.5^{7.5} \cdot 0.1 \approx 0.3/2\pi$.

Figure 11: Simulations of the Kuramoto model with Lorenzian distribution ($\omega_0 = 0.3$, $\Delta = 0.025$) with coupling strength $K = 0.04$ and $N = 1000$ oscillators.

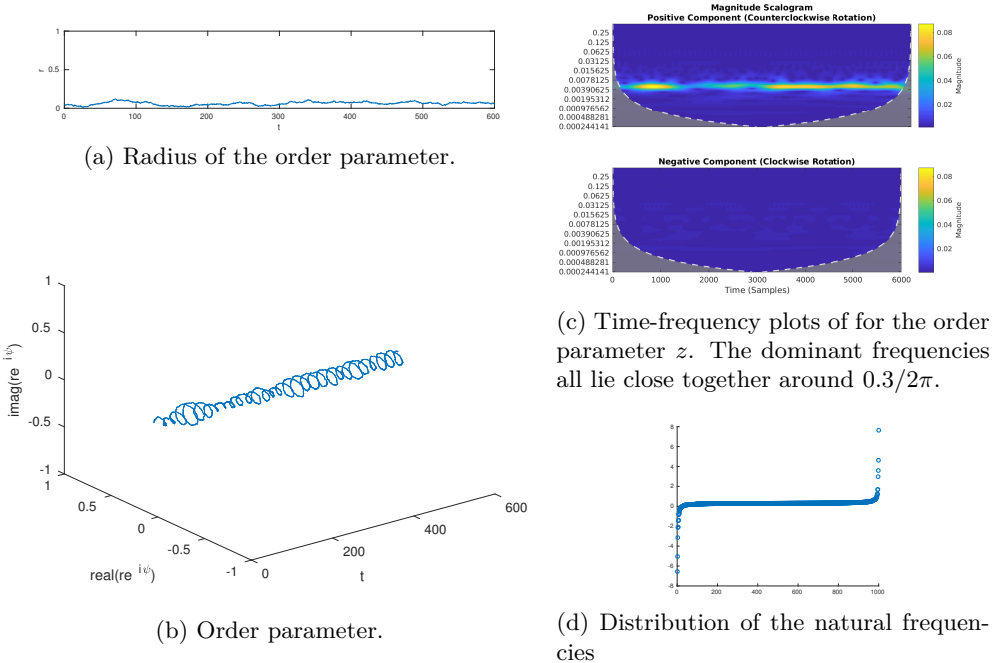
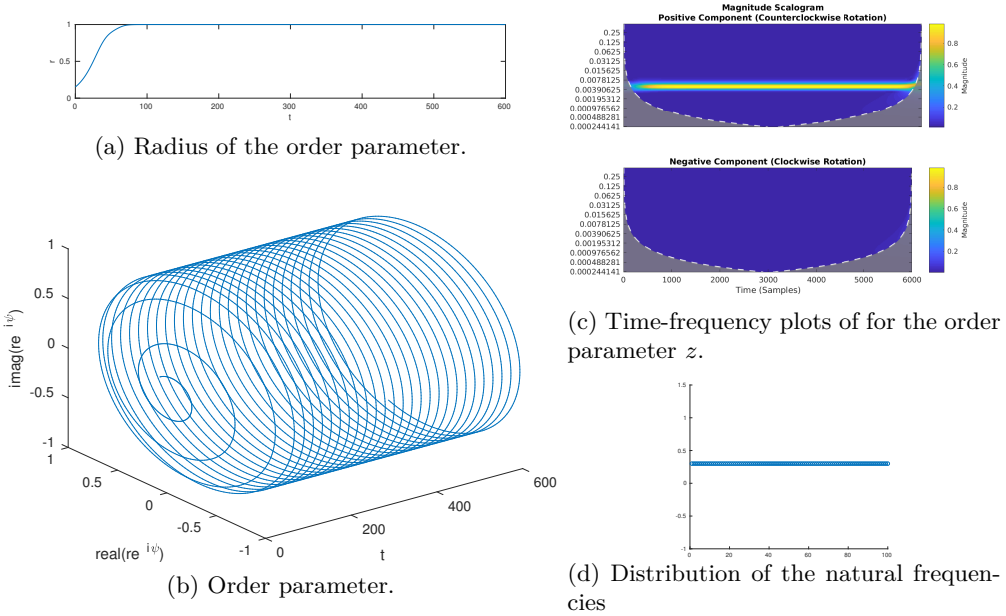


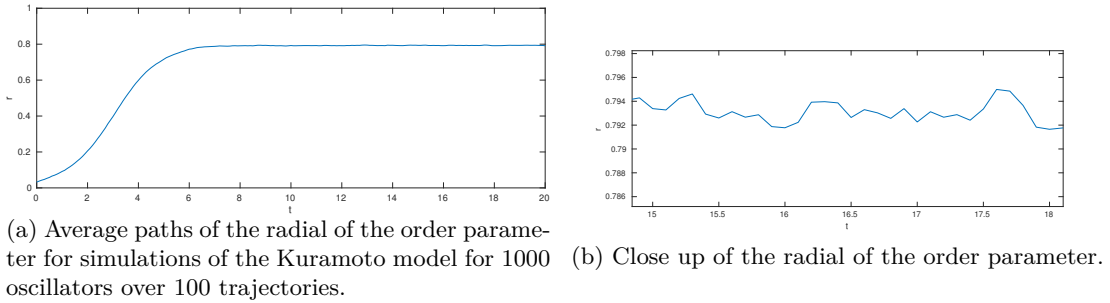
Figure 12: Simulations of the Kuramoto model with unimodal discrete distribution ($\omega_0 = 0.3$) with coupling strength $K = 0.1$, noise strength $D = 0$ and $N = 1000$ oscillators.



6.2 The Kuramoto Model with added White-Noise

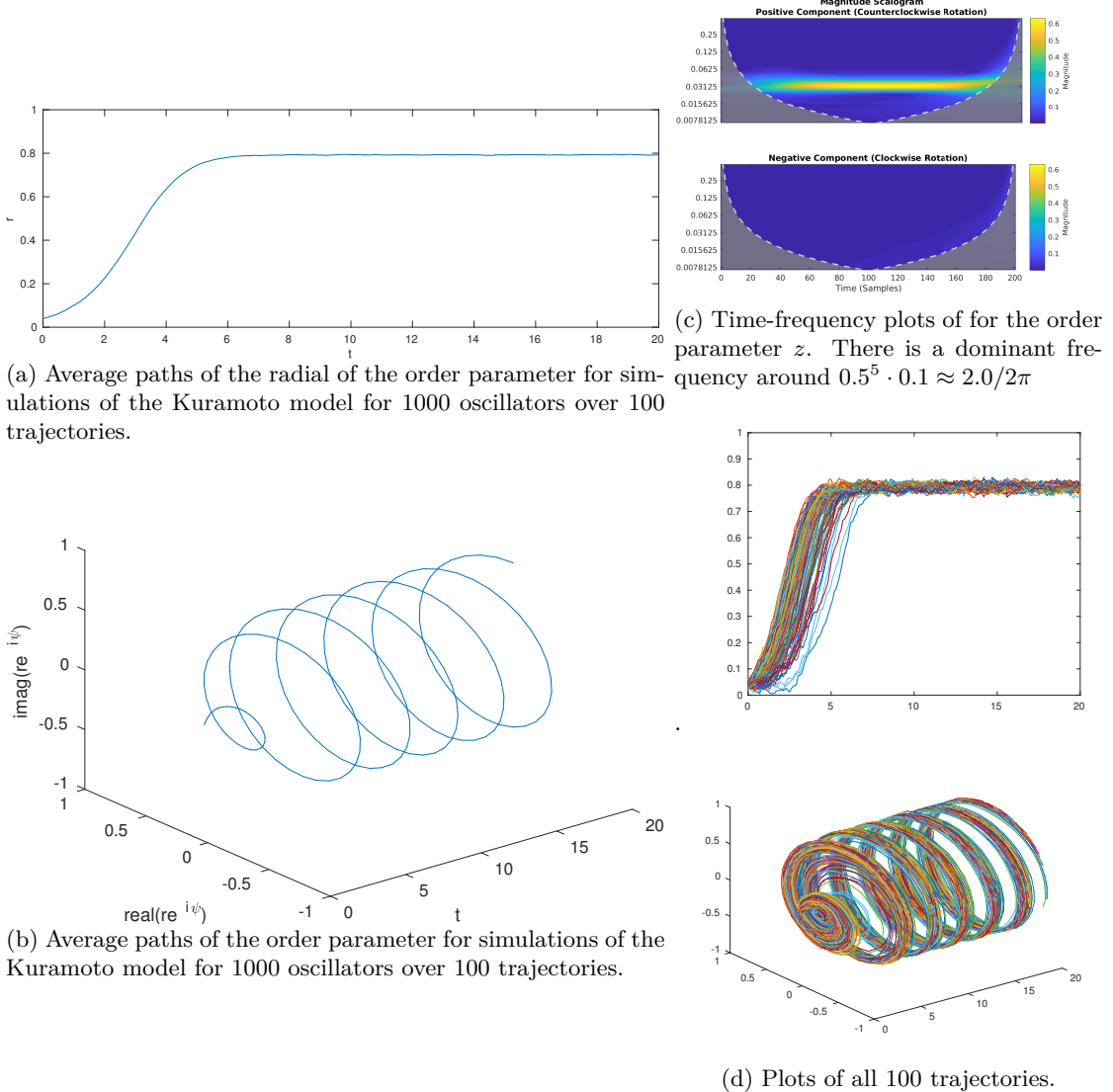
We now consider the Kuramoto model where a white-noise term is added as described in Section 2. We would like to compare the results to those in [4]. Thus we take the parameters corresponding to theirs. The noise strength we consider is $D = 1$, runtime $T = 20$, coupling strength $K = 4$. The initial phases are uniformly distributed and all natural frequencies equal zero. The variance we found when simulating 100 trajectories of 1000 oscillators is $1.018 \cdot 10^{-4}$. We show the radius of the order parameter in Figure 13a as well as a close up between $t = 15$ and $t = 18$ in Figure 13b. From the last Figure we observe that $0.792 < r < 0.795$ on this interval. A similar range was found in [4] on this interval ($0.788 < r < 0.795$).

Figure 13: Simulations of the Kuramoto model with unimodal discrete distribution ($\omega_0 = 0$) with coupling strength $K = 4$ and noise strength $D = 1$. (Only ω_0 is different with respect to Figure 14.)



In order to apply time-frequency analysis on the complex order parameter, we simulate oscillators with natural frequency $\omega_0 = 2$. We do this to be able to detect a frequency, but as we can imagine this as moving into a rotating frame, it does not affect the behaviour of the oscillators. We can see this by comparing the graphs of r in both cases to see that Figures 13a and 14a are nearly identical. The plots of Figure 14 were produced by taking 10^2 trajectories of 10^3 oscillators and resulted in a variance of $9.997 \cdot 10^{-5}$.

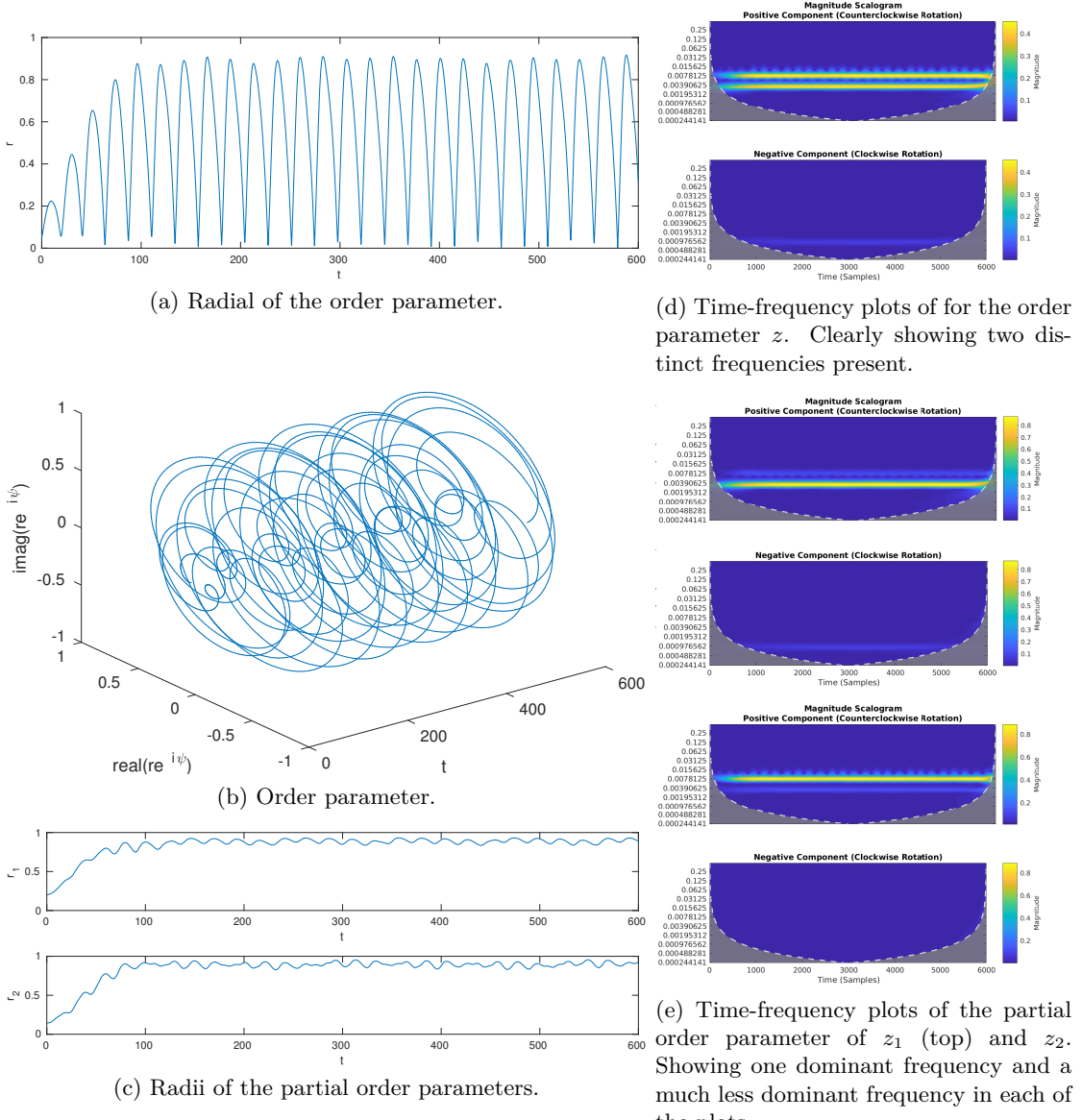
Figure 14: Simulations of the Kuramoto model with unimodal discrete distribution ($\omega_0 = 2$) with coupling strength $K = 4$ and noise strength $D = 1$. (Only ω_0 is different with respect to Figure 13.)



6.3 Bimodal Frequency Distribution

Now we consider a bimodal frequency distribution with central frequencies 0.2 and 0.5; and width parameter 0.015. The initial phases are uniformly distributed, the coupling strength is 0.15 and the noise strength is $D = 0$. In Figure 15 the corresponding plots are shown. The path of the radius of the order parameter over all oscillators oscillates between 0 and 0.9 while each of the radii of the partial order parameters oscillates only slightly between 0.8 and 0.9. The two dominant frequencies can also be extracted from the order parameter. The path of the order parameter in time is shown in Figure 15b and its time-frequency analysis is shown in Figure

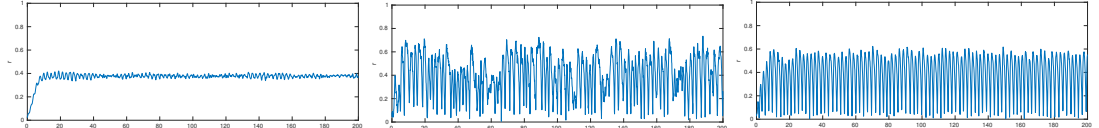
Figure 15: Simulations of the Kuramoto model with bimodal Lorenzian distribution (means 0.2, 0.5, $\Delta = 0.015$) with coupling strength $K = 0.1$, noise strength $D = 0$ and $N = 100$ oscillators.



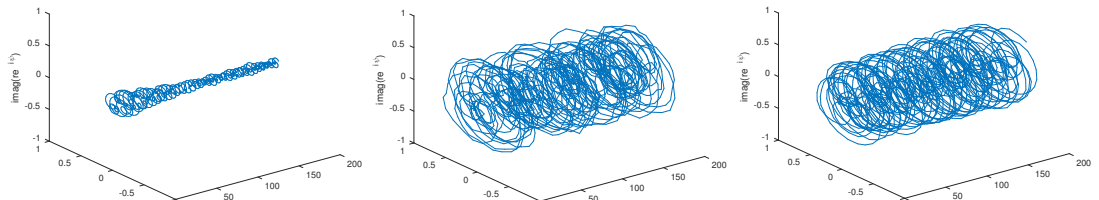
15d. This time-frequency plot shows two dominant frequencies, as expected. When increasing the coupling further (not shown), all oscillators synchronise and we obtain similar plots to those in Section 6.1. The difference is that we now have an intermediate state where we can observe two partially synchronised groups.

When adding noise to the model in addition to taking a bimodal frequency distribution, we obtained the plots in Figure 16. We simulated 1000 oscillators and applied the Monte Carlo

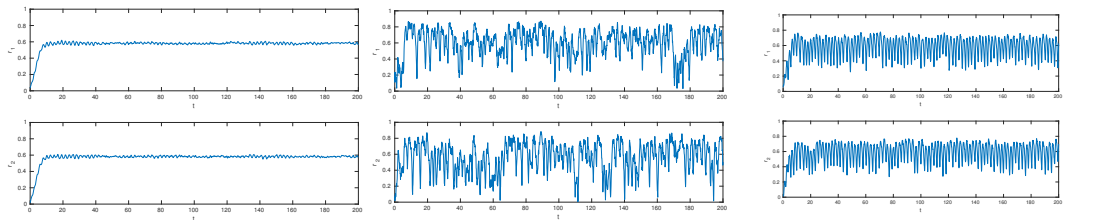
Figure 16: Simulations of the Kuramoto model with bimodal discrete distribution (means 0.2, 5) with coupling strength $K = 6.5$ and noise strength $D = 1$. We simulated 1000 oscillators for 100 trajectories (16a,16b,16c,16d) and compared this to 1 trajectory for 100 oscillators (16e,16f,16g,16h) as well as to 1 trajectory for 1000 oscillators (16i,16j,16k,16l).



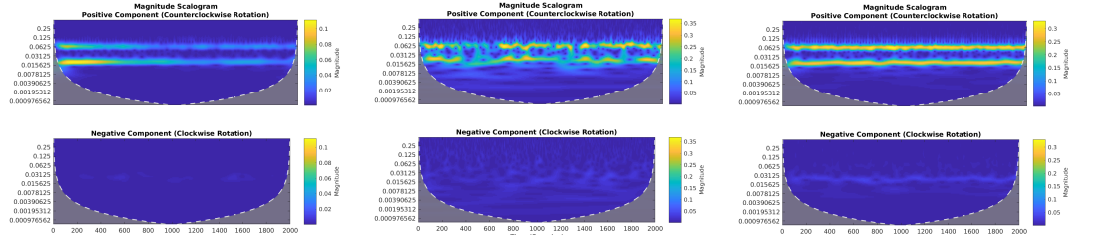
(a) Radial of the order parameter over 100 trajectories for 1000 oscillators. (e) Radial of the order parameter over 1 trajectory for 100 oscillators. (i) Radial of the order parameter over 1 trajectory for 1000 oscillators.



(b) Order parameter over 100 trajectories over 1000 oscillators. (f) Order parameter over 1 trajectory for 100 oscillators. (j) Order parameter over 1 trajectory for 1000 oscillators.



(c) Radii of the partial order parameters over 100 trajectories for 1000 oscillators. (g) Radii of the partial order parameters over 1 trajectory for 100 oscillators. (k) Radii of the partial order parameters over 1 trajectory for 1000 oscillators.



(d) Time-frequency analysis of the order parameter over 100 trajectories for 1000 oscillators. (h) Time-frequency analysis of the order parameter over 1 trajectory for 100 oscillators. (l) Time-frequency analysis of the order parameter of 1 trajectory for 1000 oscillators.

method for 100 trajectories. The time frequency analysis of the average order parameter over these 100 trajectories is shown in Figure 16d. From the average of the radii of the order parameters (Figure 16a), we expect strong synchronisation for all times after approximately $t = 10$.

Yet the dominant frequencies in the time frequency plot (Figure 16d) are not as strong (e.g. bright yellow) as in some of the other time-frequency plots we have seen. Moreover, there are two dominant frequencies present in the time-frequency plot though this is not implied by the plot of the radius of the order parameter.

This is due to the average of the complete order parameter having a low amplitude. Even though in each trajectory we have strong synchronisation in each group, they are not in phase with the other trajectories. Hence when we average over trajectories, this average will have a smaller radius than when we average just the radii over all trajectories. We would also expect oscillations in the radius r as in Figure 15 when two groups are partially synchronised. These oscillations are however also cancelled out by averaging over the trajectories.

Even though the Monte Carlo method does not achieve produce the desired for this particular set of parameters, the method still works when the frequencies of the oscillators are sufficiently large compared to the noise as in Figure 14. To achieve better accuracy for other parameters we might consider simulating more oscillators rather than different trajectories. Consider for example the difference between Figures 16l and 16h as we increase the number of oscillators from 100 to 1000, the amount of noise that can be detected in the time-frequency plot as light blue scattering is reduced significantly. At the same time the order parameter remains a useful tool to detect synchronisation when we do not average it over multiple paths.

6.4 Chimera State

We continue by simulating the Kuramoto model with location dependent coupling that was discussed in Section 4. Recall that in this model (46,47) the oscillators are divided into two groups. The intra group coupling is stronger than the inter group coupling. For the parameters $A = 0.2$ and $\beta = 0.1$ we found that the Chimera state is stable. These parameters correspond to the phase plot in Figure 4. To find the Chimera state we have to start at a state close to it. From Figure 4 we can make a guess for the phase difference and radius of the second group. The radius of the first group should be 1, so we set the initial phases of the first group identically to 0. The chimera state itself is located around $(r \cos(\psi), r \sin(\psi)) = (0.7131, -0.1518)$. Thus

Figure 17: Radii of the partial order parameters of the 'Chimera' model with uniform discrete distribution ($\omega_0 = 2$) with coupling parameters $A = 0.2$ and $\beta = 0.1$. $N = 200$ oscillators were simulated for $T = 4000$ and correspond to Figure 18.

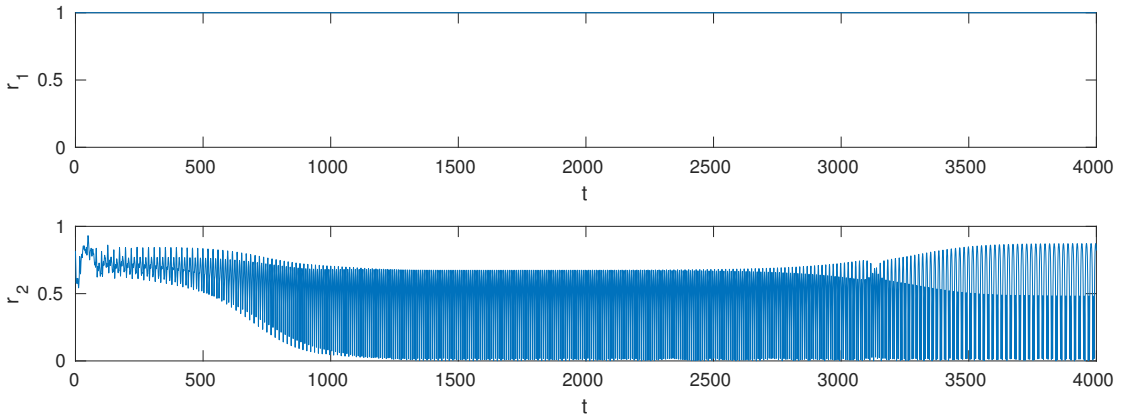
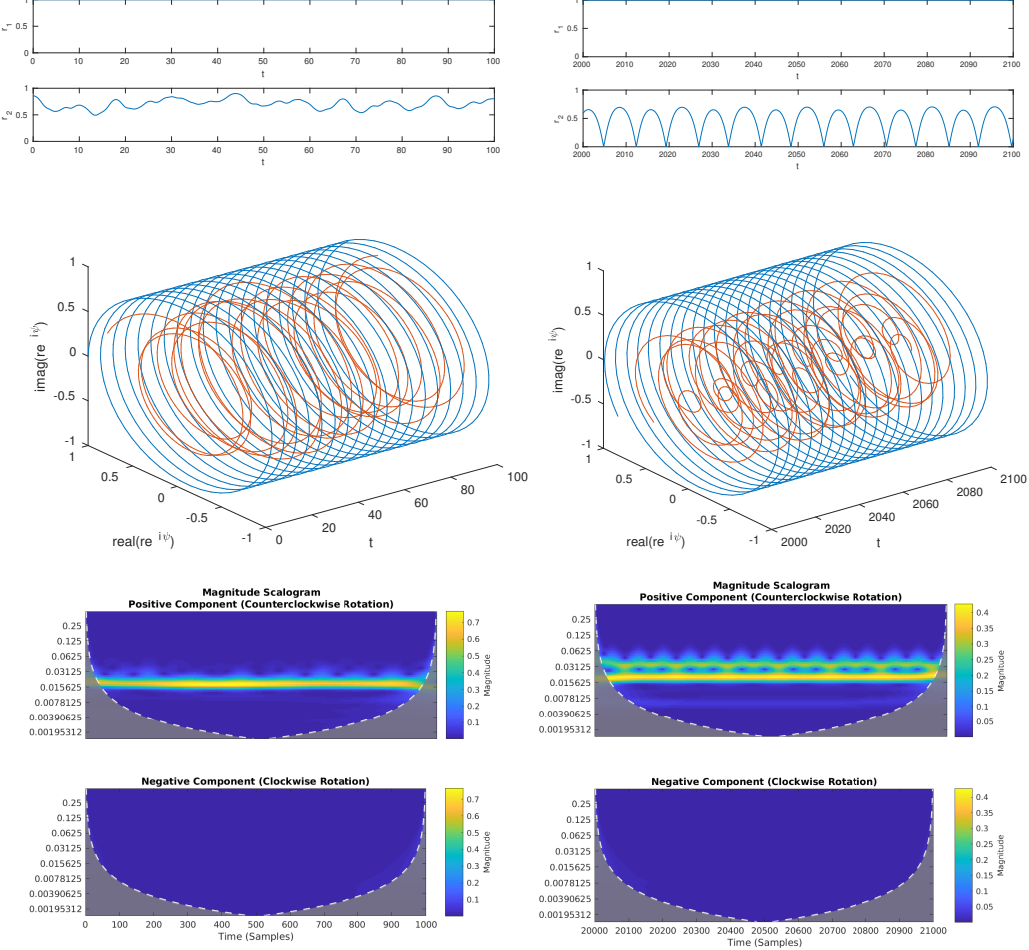


Figure 18: Simulations of the 'Chimera' model with uniform discrete distribution ($\omega_0 = 2$) with coupling parameters $A = 0.2$ and $\beta = 0.1$. $N = 200$ oscillators were simulated for $T = 4000$ and correspond to Figure 17.

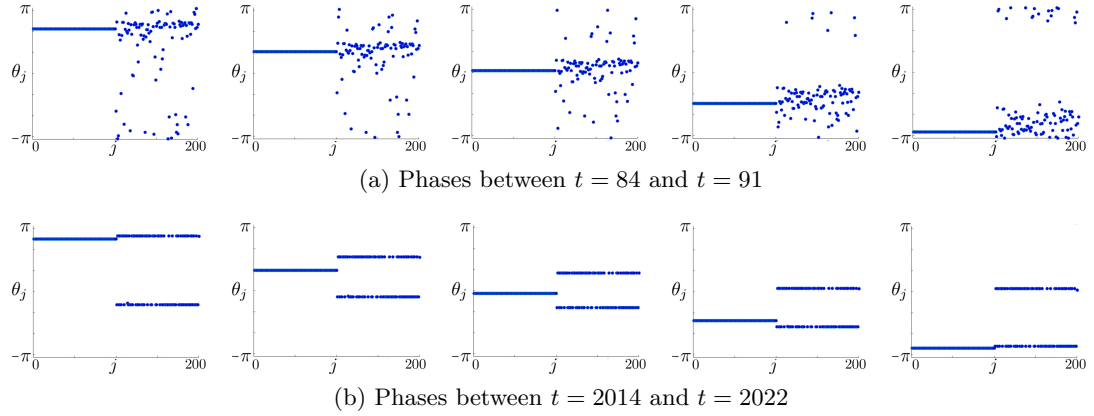


(a) Close up for $0 \leq t \leq 100$: radius (top), the partial order parameters z_1 in blue and z_2 in red (middle) and the time-frequency analysis of z_2 (bottom).
(b) Close up for $2000 \leq t \leq 2100$: radius (top), the partial order parameters z_1 in blue and z_2 in red (middle) and the time-frequency analysis of z_2 (bottom).

approximately at $(r, \psi) = (0.7291, -0.2100)$.

Since this order parameter and phase difference are local, it is only an indication of where the chimera state would be located in the original model. We choose the phases of the second group from a normal distribution with mean 0.4 and standard deviation 0.6. The natural frequencies are 2, the coupling parameter $A = 0.2$, the phase lag $\beta = 0.1$ and we simulate 200 oscillators. From the plot of the radius for the second group for $0 \leq t \leq 4000$ in Figure 17, we can see that the behaviour differs depending on time. The path for $0 \leq t \leq 100$ is shown in Figure 18a while that of times $2000 \leq t \leq 2100$ is shown in Figure 18b.

Figure 19: Distribution of phases corresponding to Figures 17 and 18. Each plot is the index of the oscillator vs. the phase between $-\pi$ and π .



For times $0 \leq t \leq 100$ the plots indicate that the state is close to a chimera state. The order parameter of this first group stays at radius $r_1 = 1$, while the order parameter of the second group has radius r_2 between 0.5 and 0.9. For a stable chimera this radius would have been constant rather than varied between 0.5 and 0.9. We have indeed not reached a stable chimera, since after a while the oscillations start to increase and the trajectory seems to end up in a breathing chimera. When we have a look at the phases themselves for different times, we can see more clearly what the behaviour of the oscillators looks like.

In Figure 19a we can see 5 plots of the phases of the oscillators at different times between $t = 84$ and $t = 91$. The indices of the oscillators are on the horizontal axis while their phases between $-\pi$ and π are on the vertical axis. The oscillators with indices 1 to 100 have the same phase in all frames. While for oscillators 101 to 200 this is not the case. Their phases are spread out over the whole interval on the first three frames. The last three frames show that there are moments where the phases of oscillators 101 through 200 are much more concentrated though not completely synchronised. At the last frame the order parameter of the second group $r_2 = 0.86$ while at the first frame $r_2 = 0.68$.

We now consider the phases for 5 different times between $t = 2014$ and $t = 2022$ in Figure 19b. The phases of oscillators 1 to 100 again have the same in all frames. As for oscillators 101 to 200, we see that the oscillators are split into two subgroups. Each of these subgroups is synchronised in phase. The frequency at which they are synchronised changes in time. Thus within group 2 we observe partial synchronisation even though all oscillators have the same natural frequency and all oscillators in group 2 are subjected to the same coupling.

We expected to find a chimera in which all oscillators in one of the groups would move incoherently, but we found a state in which two subgroups of oscillators move incoherently.

7 Concluding remarks

The phenomenon of synchronisation was introduced along with a manner to study it. We followed Kuramoto's analysis and obtained a value for the critical coupling when considering the model has infinitely many oscillators for different types of distributions by using the Ott-Antonsen ansatz.

We then followed Mirello's analysis of the Fokker-Planck equation that describes the oscillator density for the Kuramoto model with added white-noise. We considered a perturbation from the incoherent solution and derived a formula for the critical coupling. We also describe the types of stability depending on the noise strength.

We then looked at the effect of choosing a bimodal frequency distribution rather than a unimodal one as Kuramoto assumed in his analysis. For the Kuramoto model with noise we could perform the analysis for a discrete bimodal frequency distribution. Following Bonilla [17], we found a critical coupling depending on the noise strength and natural frequency of the oscillators. For the original Kuramoto model we could also perform the bifurcation analysis for a Lorenzian bimodal frequency distribution as done by Martens [18]. This way we can find conditions on the parameters of the distribution for which the incoherent state is stable.

We then considered a model in which the coupling is location dependent, the oscillators are identical, and there is a phase lag in the coupling. Following the approach of Abrams [6], we rewrite the system into a planar system for which we analysed a few phase plots. As we bifurcate from uniform coupling these plots indicate the presence of a stable chimera, then a breathing chimera, and then a breathing chimera with a longer period. Where a chimera is a state in which some oscillators are synchronised while others move incoherently.

For the above mentioned variations of the Kuramoto model, numerical analyses were performed on the complete systems of oscillators in Matlab, where in the noiseless case we applied time-frequency analysis on the order parameter.

In the case where we do not have global synchronisation but rather two or more clusters of oscillators synchronising separately, this cannot be concluded from simply looking at the order parameter of the complete population. When we take a bimodal frequency distribution or when we look at the 'chimera model', the order parameter can be analysed in time and frequency to provide information about partial synchronisation. Since we have set up the model and chosen the frequencies ourselves, we could compare the conclusions from the time-frequency plots with the paths of the partial order parameters. We concluded that using this analysis it is possible to detect global synchronisation as well as the synchronisation of separate clusters of oscillators.

References

- [1] Yoshiki Kuramoto and Dorjsuren Battogtokh. Coexistence of Coherence and Incoherence in Nonlocally Coupled Phase Oscillators. *Nonlinear Phenom. Complex Syst.*, 5(380-5), 2002.
- [2] Koji Okuda and Y Kuramoto. Mutual entrainment between populations of coupled oscillators. *Progress of theoretical physics*, 86(6):1159–1176, 1991.

- [3] L.L. Bonilla, C.J. Pérez Vicente, and R. Spigler. Time-periodic phases in populations of nonlinearly coupled oscillators with bimodal frequency distributions. *Physica D: Nonlinear Phenomena*, 113(1):79–97, 1998.
- [4] Juan A. Acebrón, L. L. Bonilla, Conrad J.Pérez Vicente, Félix Ritort, and Renato Spigler. The Kuramoto model: A simple paradigm for synchronization phenomena. *Reviews of Modern Physics*, 77(1):137–185, 2005.
- [5] Hidetsugu Sakaguchi. Desynchronization in a Self-Oscillating Medium. *Journal of Chemical Information and Modeling*, 80(5):743–748, 1988.
- [6] Daniel M. Abrams, Rennie Mirollo, Steven H. Strogatz, and Daniel A. Wiley. Solvable model for chimera states of coupled oscillators. *Physical Review Letters*, 101(8):1–4, 2008.
- [7] Steven H. Strogatz and Renato E. Mirollo. Stability of incoherence in a population of coupled oscillators. *Journal of Statistical Physics*, 63(3-4):613–635, 1991.
- [8] Mark J. Panaggio and Daniel M. Abrams. Chimera states: Coexistence of coherence and incoherence in networks of coupled oscillators. *Nonlinearity*, 28(3):R67–R87, 2015.
- [9] Mark J. Panaggio, Daniel M. Abrams, Peter Ashwin, and Carlo R. Laing. Chimera states in networks of phase oscillators: The case of two small populations. *Physical Review E*, 93(1):1–14, 2016.
- [10] Erik A. Martens, Christian Bick, and Mark J. Panaggio. Chimera states in two populations with heterogeneous phase-lag. *Chaos*, 26(9), 2016.
- [11] Edward Ott and Thomas M. Antonsen. Low dimensional behavior of large systems of globally coupled oscillators. *Chaos*, 18(3), 2008.
- [12] Michel Misiti, Yves Misiti, Georges Oppenheim, and Jean-Michel Poggi. Wavelet Toolbox User’s Guide 2018 <https://se.mathworks.com/help/wavelet/ref/cwtft.html#buu64ih-2>.
- [13] MATLAB. Release 2017b, The MathWorks, Inc., Natick, Massachusetts, United States.
- [14] Steven H. Strogatz and Ian Stewart. Coupled Oscillators and Biological Synchronization. *Scientific American*, 269(6):102–109, 1993.
- [15] Yoshiki Kuramoto. Rhythms and turbulence in populations of chemical oscillators. *Physica A: Statistical Mechanics and its Applications*, 106(1-2):128–143, 1981.
- [16] Steven H. Strogatz. From Kuramoto to Crawford: exploring the onset of synchronization in populations of coupled oscillators. *Physica D: Nonlinear Phenomena*, 143(1-4):1–20, 2000.
- [17] Luis L. Bonilla, John C. Neu, and Renato Spigler. Nonlinear stability of incoherence and collective synchronization in a population of coupled oscillators. *Journal of Statistical Physics*, 67(1-2):313–330, 1992.
- [18] E. A. Martens, E. Barreto, S. H. Strogatz, E. Ott, P. So, and T. M. Antonsen. Exact results for the Kuramoto model with a bimodal frequency distribution. *Physical Review E - Statistical, Nonlinear, and Soft Matter Physics*, 79(2):1–11, 2009.
- [19] Christian Bick and Erik A. Martens. Controlling chimeras. *New Journal of Physics*, 17(033030), 2015.

- [20] Gautam C. Sethia and Abhijit Sen. Chimera states: The existence criteria revisited. *Physical Review Letters*, 112(14), 2014.
- [21] Rene Carmona, W L Hwang, and B Torrésani. *Practical Time-Frequency Analysis: continuous wavelet and Gabor transforms, with an implementation in S*, volume 9. Academic Press, 1998.
- [22] Walter Deams and Paul Levrie. Abelprijs 2017 voor Yves Meyer. *Nieuw Archief voor Wiskunde*, 5-19(1):21–27, 2018.
- [23] C Torrence and G.P.Compo. A practical guide to wavelet analysis. *Bull. Amer. Meteor. Soc.*, 79(1):61–78, 1998.
- [24] M Farge. Wavelet Transforms And Their Applications To Turbulence. *Annual Review of Fluid Mechanics*, 24(1):395–457, 1992.

A Calculation of r^2 for Chimera Model

We set $\dot{\psi} = 0$, where $\dot{\psi}$ is as in Equation 63.

$$\begin{aligned}
0 &= \frac{r^2 + 1}{2r} [-r\mu \cos(-\beta) - \nu \cos(\psi + \beta)] + \mu \cos(-\beta) + r\nu \cos(\psi - \beta) \\
\Rightarrow 0 &= \frac{r^2 + 1}{2r} \left[-r \frac{1+A}{2} \cos(\beta) - \frac{1-A}{2} \cos(\psi + \beta) \right] + \frac{1+A}{2} \cos(\beta) + r \frac{1-A}{2} \cos(\psi - \beta) \\
\Rightarrow 0 &= A \cdot \left[-\frac{r^2 + 1}{2} \cos(\beta) + \frac{r^2 + 1}{2r} \cos(\psi + \beta) + \cos(\beta) - r \cos(\psi - \beta) \right] \\
&\quad - \frac{r^2 + 1}{2} \cos(\beta) - \frac{r^2 + 1}{2r} \cos(\psi + \beta) + \cos(\beta) + r \cos(\psi - \beta) \\
\Rightarrow 0 &= [\sin(\beta + \psi) + r \sin(\beta)] \cdot \left[-\frac{r^2 + 1}{2} \cos(\beta) + \frac{r^2 + 1}{2r} \cos(\psi + \beta) + \cos(\beta) - r \cos(\psi - \beta) \right] \\
&\quad + [\sin(\beta + \psi) - r \sin(\beta)] \cdot \left[-\frac{r^2 + 1}{2} \cos(\beta) - \frac{r^2 + 1}{2r} \cos(\psi + \beta) + \cos(\beta) + r \cos(\psi - \beta) \right] \\
\Rightarrow 0 &= -(r^2 + 1) \sin(\beta + \psi) \cos(\beta) - 2 \sin(\beta + \psi) \cos(\beta) \\
&\quad + (r^2 + 1) \sin(\beta) \cos(\psi + \beta) - 2r^2 \sin(\beta) \cos(\psi - \beta) \\
\Rightarrow 0 &= -(r^2 - 1) \sin(\beta + \psi) \cos(\beta) + (r^2 + 1) \sin(\beta) \cos(\psi + \beta) - 2r^2 \sin(\beta) \cos(\psi - \beta) \\
\Rightarrow 0 &= -r^2 [\sin(\beta + \psi) \cos(\beta) - \sin(\beta) \cos(\psi + \beta) + 2 \sin(\beta) \cos(\psi - \beta)] \\
&\quad + \sin(\beta + \psi) \cos(\beta) + \sin(\beta) \cos(\psi + \beta) \\
\Rightarrow r^2 &= \frac{\sin(\beta + \psi) \cos(\beta) + \sin(\beta) \cos(\psi + \beta)}{\sin(\beta + \psi) \cos(\beta) - \sin(\beta) \cos(\psi + \beta) + 2 \sin(\beta) \cos(\psi - \beta)}
\end{aligned}$$

The different terms in this fraction can be rewritten to simplify the expression. We will look at the numerator first.

$$\begin{aligned}
& \sin(\beta + \psi) \cos(\beta) + \sin(\beta) \cos(\psi + \beta) \\
&= \sin(\beta) \cos(\psi) \cos(\beta) + \cos(\beta) \sin(\psi) \cos(\beta) + \sin(\beta) \cos(\beta) \cos(\psi) - \sin(\beta) \sin(\psi) \sin(\psi) \\
&= \frac{1}{2} \sin(2\beta) \cos(\psi) + \cos^2(\beta) \sin(\psi) + \frac{1}{2} \sin(2\beta) \cos(\psi) - \sin^2(\beta) \sin(\psi) \\
&= \sin(2\beta) \cos(\psi) + \cos(2\beta) \sin(\psi) \\
&= \sin(2\beta + \psi)
\end{aligned}$$

Using similar trigonometric rules we can simplify the denominator as well.

$$\begin{aligned}
& \sin(\beta + \psi) \cos(\beta) - \sin(\beta) \cos(\psi + \beta) + 2 \sin(\beta) \cos(\psi - \beta) \\
&= \sin(\beta) \sin(\psi) \cos(\beta) + \cos^2(\beta) \sin(\psi) - \sin(\beta) \cos(\beta) \cos(\psi) + \sin(\beta) \sin(\psi) \\
&\quad + 2 \sin(\beta) \cos(\beta) \cos(\psi) + 2 \sin^2(\beta) \sin(\psi) \\
&= \frac{1}{2} \sin(2\beta) \cos(\psi) + \sin(\psi) - \frac{1}{2} \sin(2\beta) \cos(\psi) \\
&\quad + \sin(2\beta) \cos(\psi) + 2 \sin^2(\beta) \sin(\psi) \\
&= \sin(\psi) + \sin(2\beta) \cos(\psi) + 2 \sin^2(\beta) \sin(\psi) \\
&= \sin(2\beta) \cos(\psi) + (1 - 2 \sin^2(\beta)) \sin(\psi) - 2 \sin(\psi) \\
&= \sin(2\beta) \cos(\psi) + \cos(2\beta) \sin(\psi) - 2 \sin(\psi) \\
&= \sin(2\beta - \psi) - 2 \sin(\psi)
\end{aligned}$$

Thus the expression for r^2 reduces to

$$r^2 = \frac{\sin(2\beta + \psi)}{\sin(2\beta - \psi) - 2 \sin(\psi)}$$

B Matlab Code for Simulations

```

1 % Code to run the Kuramoto model with different options:
2 % - different frequency distributions
3 % - location dependent coupling ('Chimera model')
4 % - add a white-noise forcing term (Monte Carlo method)
5 %
6 % A model can be chosen by changing 'modeltype'. Either the
7 % parameter K (model 'k') or the parameters A and beta
8 % (model 'c') can then be changed
9 %
10 % The other parameters are the same for each model.
11 %
12 % Change for example the number of oscillators 'N' or the
13 % runtime 'T'. The initial phases are should be initialized
14 % as an N by 1 array 'X0'. Bi- and unimodal discrete and
15 % Lorenzian frequency distributions can be specified
16 % by 'w0', 'w0s', 'sd' and 'distribution'

```

```

17 %
18 % When adding a white-noise term (By changing 'D') , determine
19 % the number of trajectories by 'Na' and the number of
20 % trajectories to add per time by 'Nadd'. When you want
21 % to add more trajectories without resetting the variables
22 % change 'reset' to 0. Change 'reset' back to 1 when wanting to
23 % run a new experiment.
24 %
25 % The total number of trajectories produced (Monte Carlo) and
26 % the variances of the 3 different order parameters are
27 % displayed. Several figures are produced and saved under
28 % time specific names when the lines under "save
29 % figures" are commented out.
30 %
31 % Initializing 'plotpartial' to 1 will output extra
32 % plots for r1, r2, z1, z2 and their time-frequency plots.
33 %
34 % There are options to save figures and a movie of the phases
35 % automatically by setting 'save' and 'movie' to 1.
36
37 %% ----- Parameters
38 D = 1; % noise strength
39 T=20; % end time
40 N = 100; % number of oscillators (even)
41
42 %% ----- Type of Model -----
43 modeltype = 'k'; % 'c': Chimera model, 'k': Kuramoto model
44 plotpartial = 0; % if 1, plots for partial order parameters
45 % & time-frequency will be made
46
47 %% Original Kuramoto 'k'
48 K = 4;
49
50 %% Chimera model 'c'
51 A = 0.2;
52 beta = 0.1;
53
54 %% ----- Monte Carlo -----
55 Na = 10; % #trajectories
56 Nadd = 10; % number of trajectories to add each loop
57 reset = 10; % to add new trajectories: set to 0
58
59 %% ----- Options to save figures / movie -----
60 movie = 0;
61 save = 1;
62
63 % Timestep
64 t0=0; % initial time
65 dt = 0.1; % time step

```

```

66
67 %% ----- Initialising oscillator phases ----- %%
68 %% Completely uniform: (~incoherent solution)
69 X0 = 2*pi.*rand(N,1);
70
71 %% Close to chimera:
72 % X0(1:N/2)=zeros(N/2,1);
73 % X0(N/2+1:N)=0.6*randn(N/2,1)+0.4;
74
75 X0 = mod(X0+pi,2*pi)-pi;
76
77 %X0=Xf(:,steps+1); % Continue from previous endpoint
78
79 %% ----- Frequency distribution ----- %%
80 w0 = 2; % frequency mean
81 w0s = 5; % frequency mean 2
82 sd=0.015; % standard deviation
83 distribution = 'ud'; % *types of distributions:
84 % 'bl' bimodal lorentz 'ul' unimodal lorenz
85 % 'bd' bimodal discrete 'ud' unimodal
86 % discrete
87
88 if reset
89 [w, Ntotal,sqordersum,sqordersum1,sqordersum2, steps, ordersum,
...
90     ordersum1, ordersum2,ordercsum]= initialize(N, distribution, ...
91     w0,w0s,sd,T,t0,dt);
92 end
93
94 tic
95 [Xf,Ntotal,Var,Var1,Var2,sqordersum,sqordersum1,sqordersum2, ordersum
96     , ...
97     ordersum1, ordersum2,traj1order1,traj1order2,ordercsum]...
98 = RegularMonteCarlo(ordercsum, modeltype,A,beta,Nadd,Na,dt,N,w, ...
99 D,K, X0, t0,T,Ntotal, ordersum, ordersum1, ordersum2,sqordersum
100    , ...
101    sqordersum1,sqordersum2);
102 t=0:dt:T; % time discretisation
103 toc
104
105 disp(Ntotal) % total number of trajectories simulated
106 disp([Var Var1 Var2])
107
108 figures = []; % to store figure handles
109 figures = plotswave(ordercsum,plotpartial,figures, ordersum,ordersum1
110    , ...
111    ordersum2,t,Ntotal,traj1order1,traj1order2);
112
113
114
115
116
117
118
119
120
121
122
123
124
125
126
127
128
129
130
131
132
133
134
135
136
137
138
139
140
141
142
143
144
145
146
147
148
149
150
151
152
153
154
155
156
157
158
159
160
161
162
163
164
165
166
167
168
169
170
171
172
173
174
175
176
177
178
179
180
181
182
183
184
185
186
187
188
189
190
191
192
193
194
195
196
197
198
199
200
201
202
203
204
205
206
207
208
209
210
211
212
213
214
215
216
217
218
219
220
221
222
223
224
225
226
227
228
229
230
231
232
233
234
235
236
237
238
239
240
241
242
243
244
245
246
247
248
249
250
251
252
253
254
255
256
257
258
259
260
261
262
263
264
265
266
267
268
269
270
271
272
273
274
275
276
277
278
279
280
281
282
283
284
285
286
287
288
289
290
291
292
293
294
295
296
297
298
299
300
301
302
303
304
305
306
307
308
309
310
311
312
313
314
315
316
317
318
319
320
321
322
323
324
325
326
327
328
329
330
331
332
333
334
335
336
337
338
339
340
341
342
343
344
345
346
347
348
349
350
351
352
353
354
355
356
357
358
359
360
361
362
363
364
365
366
367
368
369
370
371
372
373
374
375
376
377
378
379
380
381
382
383
384
385
386
387
388
389
390
391
392
393
394
395
396
397
398
399
400
401
402
403
404
405
406
407
408
409
410
411
412
413
414
415
416
417
418
419
420
421
422
423
424
425
426
427
428
429
430
431
432
433
434
435
436
437
438
439
440
441
442
443
444
445
446
447
448
449
450
451
452
453
454
455
456
457
458
459
460
461
462
463
464
465
466
467
468
469
470
471
472
473
474
475
476
477
478
479
480
481
482
483
484
485
486
487
488
489
490
491
492
493
494
495
496
497
498
499
500
501
502
503
504
505
506
507
508
509
510
511
512
513
514
515
516
517
518
519
520
521
522
523
524
525
526
527
528
529
530
531
532
533
534
535
536
537
538
539
540
541
542
543
544
545
546
547
548
549
550
551
552
553
554
555
556
557
558
559
559
560
561
562
563
564
565
566
567
568
569
570
571
572
573
574
575
576
577
578
579
580
581
582
583
584
585
586
587
588
589
589
590
591
592
593
594
595
596
597
598
599
599
600
601
602
603
604
605
606
607
608
609
609
610
611
612
613
614
615
616
617
618
619
619
620
621
622
623
624
625
626
627
628
629
629
630
631
632
633
634
635
636
637
638
639
639
640
641
642
643
644
645
646
647
648
649
649
650
651
652
653
654
655
656
657
658
659
659
660
661
662
663
664
665
666
667
668
669
669
670
671
672
673
674
675
676
677
678
679
679
680
681
682
683
684
685
686
687
688
689
689
690
691
692
693
694
695
696
697
698
699
699
700
701
702
703
704
705
706
707
708
709
709
710
711
712
713
714
715
716
717
718
719
719
720
721
722
723
724
725
726
727
728
729
729
730
731
732
733
734
735
736
737
738
739
739
740
741
742
743
744
745
746
747
748
749
749
750
751
752
753
754
755
756
757
758
759
759
760
761
762
763
764
765
766
767
768
769
769
770
771
772
773
774
775
776
777
778
779
779
780
781
782
783
784
785
786
787
788
789
789
790
791
792
793
794
795
796
797
797
798
799
800

```

```

109 % % %% ----- Produce a scatterplot of the natural frequencies -----
110 %%%
111 figures(8)=figure; scatter(1:length(w),sort(w))
112 %% ----- Produce a scatterplot of the initial phases ----- %%
113 figures(1) = figure; scatter(1:N,(X0), 'MarkerFaceColor', 'b')
114 ylabel('|\theta_j|'); xlabel('j'); ylim([-pi pi])
115
116 %% ----- Produce movie of the phases of the oscillators ----- %%
117 if movie
118     ct=fix(clock);
119     h=figure;
120     v=VideoWriter([ num2str(ct(3)), '0', num2str(ct(2)), 't', ...
121         num2str(ct(4)), num2str(ct(5)), 'r.avi']);
122     open(v)
123     [~,~,st]=size(Xf);
124     for i = 1:st
125         scatter(1:N,mod(Xf(:,i)+pi,2*pi)-pi, 'MarkerFaceColor', 'b')
126         title(['r_1=', num2str(abs(ordersum1(i)),2), ', r_2=', ...
127             num2str(abs(ordersum2(i)),2), ', t=', num2str(t(i))]);
128         ylabel('|\theta_j|')
129         xlabel('j')
130         ylim([-pi pi])
131
132         frame = getframe(h);
133         writeVideo(v,frame);
134     end
135     close(v);
136 end
137
138 %% ----- Saving figures ----- %%
139 if save
140     ct=fix(clock);
141     %% Global order parameters:
142     saveas(figures(2),[num2str(ct(3)), '0', num2str(ct(2)), 't', ...
143         num2str(ct(4)), num2str(ct(5)), 'r'], 'epsc') % abs order
144     saveas(figures(3),[num2str(ct(3)), '0', num2str(ct(2)), 't', ...
145         num2str(ct(4)), num2str(ct(5)), 'rc'], 'epsc') % order
146     saveas(figures(5),[num2str(ct(3)), '0', num2str(ct(2)), 't', ...
147         num2str(ct(4)), num2str(ct(5)), 'rcw'], 'epsc') % wave order
148     %% Initial freq, phases
149     saveas(figures(1),[num2str(ct(3)), '0', num2str(ct(2)), 't', ...
150         num2str(ct(4)), num2str(ct(5)), 'X0'], 'epsc') %initial phases
151     saveas(figures(8),[num2str(ct(3)), '0', num2str(ct(2)), 't', ...
152         num2str(ct(4)), num2str(ct(5)), 'w'], 'epsc') % freq distr.
153     %% Partial order parameters:
154     if plotpartial
155         saveas(figures(4),[num2str(ct(3)), '0', num2str(ct(2)), 't', ...

```

```

156     num2str(ct(4)),num2str(ct(5)), 'r12'], 'epsc') % partial abs
157         order
158 saveas(figures(6),[num2str(ct(3)), '0', num2str(ct(2)), 't',...
159 num2str(ct(4)),num2str(ct(5)), 'rc1w'], 'epsc') % wave part.
160         order 1
161 saveas(figures(7),[num2str(ct(3)), '0', num2str(ct(2)), 't',...
162 num2str(ct(4)),num2str(ct(5)), 'rc2w'], 'epsc') % wave part.
163         order 2
164 saveas(figures(9),[num2str(ct(3)), '0', num2str(ct(2)), 't',...
165 num2str(ct(4)),num2str(ct(5)), 'rc12'], 'epsc') % partial order
166 end
167
168 function [w, Ntotal, sqordersum, sqordersum1, sqordersum2, steps, ...
169     ordersum, ordersum1, ordersum2, ordercsum]=...
170     initialize(N, distribution, w0, w0s, sd, T, t0, dt)
171
172 w = Distribution(distribution, N, w0, w0s, sd);
173 Ntotal = 0; % total number of trajectories simulated so
174     far
175 steps = (T-t0)/dt; % number of timesteps
176
177 %% Sums of (radial of) order parameter (squared) for MC method
178 ordersum=0;
179 ordersum1=0;
180 ordersum2=0;
181 sqordersum = 0;
182 sqordersum1 = 0;
183 sqordersum2 = 0;
184 ordercsum = 0;
185 end
186
187 function [w] = Distribution(distribution, N, w0, w0s, sd)
188     if distribution == 'bl'
189         %% bimodal lorenzian
190         unif = rand(N/2,1);
191         w1 = w0 + sd*tan(pi*(unif-0.5));
192         w2 = w0s + sd*tan(pi*(unif-0.5));
193         w = [w1 ; w2];
194     elseif distribution == 'ul'
195         %% unimodal lorenzian
196         unif = rand(N,1);
197         w = w0 + sd*tan(pi*(unif-0.5));
198     elseif distribution == 'bd'
199         %% bimodal discrete
200         w1 = w0*ones(N/2,1);
201         w2 = w0s*ones(N/2,1);
202         w = [w1 ; w2];
203     elseif distribution == 'ud'

```

```

201      %% unimodal discrete
202      w = w0*ones(N,1);
203  else
204      disp('choose distribution bl, ul, bd or ud')
205  end
206 end
207
208 function [g1] = Kuramoto(N,w,K, X)
209     [~, s2]=size(X);
210     g1=zeros(size(X)); % initialise
211     for z=1:s2 % runs over trajectories
212         [theta_j ,theta_i] = meshgrid(X(:,z));
213         g1 (:,z) = w + K/N*sum( sin(theta_j-theta_i) ,2);
214     end
215 end
216
217 function [g1] = KuramotoChimera(N,w,A,beta,X) % as in Abrams et al,
218 % 2008
219 M=N/2; % number of oscillators per group
220 [~, s2]=size(X);
221 g1 = zeros(size(X)); % initialise
222 for z=1:s2 % runs over trajectories
223     [theta_j ,theta_i] = meshgrid(X(:,z));
224     g1 (1:M, z) = w(1:M) - (1+A)/(2*M) *...
225         sum( cos(theta_i (1:M,1:M)-theta_j (1:M,1:M)-beta) ,2) ...
226         -(1-A)/(2*M) *...
227         sum( cos(theta_i (1:M,1:M)-theta_j (M+1:N,M+1:N)-beta) ,2) ;
228     g1 (M+1:N, z) = w(M+1:N) - (1+A)/(2*M) *...
229         sum( cos(theta_i (M+1:N,M+1:N)-theta_j (M+1:N,M+1:N)-beta) ...
230             ,2) ...
231             -(1-A)/(2*M) *...
232             sum( cos(theta_i (M+1:N,M+1:N)-theta_j (1:M,1:M)-beta) ,2) ;
233 end
234
235 function [Xf,Ntotal,Var,Var1,Var2,sqordersum,sqordersum1, ...
236 sqordersum2, ordersum, ordersum1, ordersum2, ...
237 traj1order1,traj1order2,ordercsum] = RegularMonteCarlo(ordercsum
238 , ...
239 modeltype,A,beta,Nadd,Na,dt,N,w,D,K, X0, t0,T,Ntotal, ...
240 ordersum, ordersum1, ordersum2,sqordersum,sqordersum1,sqordersum2
241 )
242 steps = (T-t0)/dt; % number of timesteps
243 %% ----- Monte-Carlo ----- %%
244 while Ntotal < Na % && (Yvar>epsilon || Zvar>epsilon)
245     % initial positions of all oscillators
246     Xf=ones(N, Nadd,steps+1).*X0;

```

```

246     for j=1:steps
247         % Brownian motion
248         dW = sqrt(dt)*randn(N,Nadd);
249         if modeltype == 'k'
250             g1 = Kuramoto(N,w,K,Xf(:,:,j));
251         elseif modeltype == 'c'
252             g1 = KuramotoChimera(N,w,A,beta,Xf(:,:,j));
253         else
254             error('Error. specify the type of model as c or k')
255         end
256         % Euler-Maruyana
257         Xf(:,:,j+1) = Xf(:,:,j) + g1*dt + sqrt(2*D).*dW;
258     end
259
260     %% ----- Order parameter ----- %%
261     ett=exp(1j*Xf);
262
263     %% ----- Partial order parameters ----- %%
264     ett1 = exp(1j*Xf(1:N/2,:,:));
265     ett2 = exp(1j*Xf(N/2+1:N,:,:));
266
267     %% ----- plotting different trajectories ----- %%
268     ettplot = 1/N*permute(sum(ett,1),[3 1 2]);
269     figure
270     for kk=1:Nadd
271         plot3(0:dt:T, real(ettplot(:,kk)), imag(ettplot(:,kk)));
272         hold on;
273         ylim([-1 1])
274         zlim([-1 1])
275     end
276     figure
277     for kk=1:Nadd
278         plot(0:dt:T, abs(ettplot(:,kk)));
279         hold on;
280         ylim([0 1])
281     end
282
283     %% ----- Order parameter for 1st trajectory ----- %%
284     traj1order1 = 1/(N/2)*sum(ett1(:,1,:),1);
285     traj1order2 = 1/(N/2)*sum(ett2(:,1,:),1);
286
287     ordercsum = ordercsum + sum((1/N*(sum(ett(:,:,1))),2);
288
289     %% ----- Calculate sums required for variance and mean ----- %%
290     ordersum= ordersum + sum(abs(1/N*(sum(ett(:,:,1))),2);
291     sqordersum= sqordersum + sum(abs(1/N*(sum(ett(:,:,steps+1),1)))
292         .^2,2);
293     ordersum1 = ordersum1 + sum(abs(1/(N/2)*(sum(ett1(:,:,1))),2);
294     ordersum2 = ordersum2 + ...

```

```

294     sum( abs(1/(N/2)*(sum( ett2 (:,:, :) ,1))),2) ;
295 sqordersum1= sqordersum1 + ...
296     sum( abs((1/(N/2)*(sum( ett1 (:,:, steps+1),1))).^2,2);
297 sqordersum2= sqordersum2 + ...
298     sum( abs((1/(N/2)*(sum( ett2 (:,:, steps+1),1))).^2,2);
299
300 Ntotal = Ntotal + Nadd;           % update number of paths simulated
301 end
302
303 %%—— Variances for absolute (partial) order parameters ——
304 Var = abs(sum(sqordersum)/Ntotal - ...
305             (sum(ordersum(1,1,steps+1))/Ntotal).^2);
306 Var1 = abs(sum(sqordersum1)/Ntotal - ...
307             (sum(ordersum1(1,1,steps+1))/Ntotal).^2);
308 Var2 = abs(sum(sqordersum2)/Ntotal - ...
309             (sum(ordersum2(1,1,steps+1))/Ntotal).^2);
310
311 Xf = Xf(:,1,:);
312 end
313
314 function [ figures]=plotswave(ordercsum , plotpartial , figures , ordersum
315 , ...
316 ordersum1 , ordersum2 , t , Ntotal , traj1order1 , traj1order2)
317
318 %%—— Complex order parameters for 1st trajectory —— %%
319 ordercomplex = permute(ordercsum,[3 2 1])/Ntotal;
320 ordercomplex1 = permute(traj1order1,[3 2 1]);
321 ordercomplex2 = permute(traj1order2,[3 2 1]);
322
323 %%—— Mean radius order parameter over all trajectories ——
324 %%——
325 orderabs = permute(ordersum,[3 2 1])/Ntotal;
326 orderabs1 = permute(ordersum1,[3 2 1])/Ntotal;
327 orderabs2 = permute(ordersum2,[3 2 1])/Ntotal;
328
329 %%—— Specifying figure sizes and positions —— %%
330 bdwidth = 5; topbdwidth=30;
331 set(0, 'Units' , 'pixels');
332 scnsize= get(0, 'ScreenSize');
333 pos1 = [bdwidth , 2/3*scnsize(4) + bdwidth , ...
334         scnsize(3)/2 - 2*bdwidth , scnsize(4)/3-(topbdwidth + bdwidth)
335         ];
336 pos2 = [pos1(1) + scnsize(3)/2 , pos1(2) , pos1(3) , pos1(4)];
337 pos3 = [pos1(1) , 0 , pos1(3)-300 , pos1(4)+250];
338 pos4 = [pos3(1)+ scnsize(3)/3 , pos3(2) , pos3(3) , pos3(4)];
339 pos5 = [pos3(1)+ 2*scnsize(3)/3 , pos3(2) , pos3(3) , pos3(4)];
340
341 %%—— Simple Plots —— %%

```

```

339 % radius of order parameter
340 figures(2) = figure('Position', pos1);
341 plot(t, orderabs)
342 xlabel('t')
343 ylabel('r')
344 ylim([0 1])
345
346 % order parameter
347 figures(3) = figure;
348 plot3(t, real(ordercomplex), imag(ordercomplex))
349 xlabel('t')
350 ylabel('real(re^{i\psi})')
351 zlabel('imag(re^{i\psi})')
352 ylim([-1 1])
353 zlim([-1 1])
354
355 %% —— Wavelet Toolbox Time–Frequency analysis —— %%
356 figures(5) = figure('Position', pos3);
357 cwt(ordercomplex, 'amor') % 'amor' is the analytic morlet
358 wavelet.
359
360 if plotpartial
361 % partial order parameters
362 figures(9) = figure;
363 plot3(t, real(ordercomplex1), imag(ordercomplex1))
364 hold on;
365 plot3(t, real(ordercomplex2), imag(ordercomplex2))
366 xlabel('t')
367 ylabel('real(re^{i\psi})')
368 zlabel('imag(re^{i\psi})')
369 ylim([-1 1])
370 zlim([-1 1])
371
372 % radius of partial order parameters
373 figures(4) = figure('Position', pos2);
374 plot(subplot(2,1,1), t, orderabs1)
375 xlabel('t')
376 ylabel('r_1')
377 ylim([0 1])
378 hold on;
379 plot(subplot(2,1,2), t, orderabs2)
380 xlabel('t')
381 ylabel('r_2')
382 ylim([0 1])
383
384 % wavelet toolbox time–frequency analysis for partial order
385 % parameters % for now only for 1 trajectory
386 figures(6) = figure('Position', pos4);
387 cwt(ordercomplex1, 'amor')

```

```

387     figures(7) = figure('Position', pos5);
388     cwt(ordercomplex2, 'amor')
389 end
390 end

```

C Matlab Code for Phase Plots

```

1 % Code to make phase plots for the Kuramoto model with
2 % location dependent coupling as described by Abrams,
3 % Mirello , Strogatz , Wiley (2008)
4
5 b=0.1;           % phase lag parameter
6 A=0.2;           % Coupling parameter
7 mu = (1+A)/2;    % intergroup coupling
8 nu = (1-A)/2;    % intragroup coupling
9 alpha=pi/2-b;    % phase lag
10
11 % The Kuramoto model with location dependen coupling:
12 f = @(t,Y) [(1-Y(1)^2)/2*(Y(1)*mu*cos(-alpha) + nu*cos(Y(2)+alpha)) ...
13          (Y(1)^2+1)/(2*Y(1))*(Y(1)*mu*sin(-alpha)-nu*sin(Y(2)+alpha)) -...
14          mu*sin(-alpha)-Y(1)*nu*sin(Y(2)-alpha)];
15
16 % Initialising figure , axis , title , colours
17 figure;
18 xlabel('r cos \psi', 'FontSize', 17);
19 ylabel('r sin \psi', 'FontSize', 17);
20 title(['A=' , num2str(A) , ' \beta=' , num2str(b)]);
21 hold on
22 colour= [ 1 0 0; 1 0.5 0; 0.6 0 0.6; 0.2 0.6 1]; % red orange purple
23          blue
24 i=1;      % to vary among the 4 colours
25
26 % Grid in terms of r and psi
27 rvec = [0.001 0.1:0.1:1];
28 psivec = [pi 0:0.2:pi 0:-0.2:-pi];
29
30 % store startpoints and endpoints to plot on top of trajectories
31 startpoints.y1 = zeros(length(rvec),length(psivec));
32 startpoints.y2 = zeros(length(rvec),length(psivec));
33 endpoints.y1 = zeros(length(rvec),length(psivec));
34 endpoints.y2 = zeros(length(rvec),length(psivec));
35
36 % running over grid , calculating and plotting trajectories
37 for r=1:length(rvec)
38     for psi=1:length(psivec)
39         [ts ,ys] = ode45(f,[0 ,3000],[rvec(r);psivec(psi)]);
40         plot(ys(:,1).*cos(ys(:,2)),ys(:,1).*sin(ys(:,2)), 'color' ,...
41               colour(i,1:3)); i=i+1; if i>4 i=1; end
42         startpoints.y1(r ,psi) = ys(1,1).*cos(ys(1,2));

```

```

42     startpoints.y2(r,psi) = ys(1,1).*sin(ys(1,2));
43     endpoints.y1(r,psi) = ys(length(ys),1).*cos(ys(length(ys),2))
44         ;
45     endpoints.y2(r,psi) = ys(length(ys),1).*sin(ys(length(ys),2))
46         ;
47 end
48 % running over grid, plotting start- and endpoints
49 for r=1:length(rvec)
50     for psi=1:length(psivec)
51         plot(startpoints.y1(r,psi),...
52             startpoints.y2(r,psi), 'bo') % starting point
53         plot(endpoints.y1(r,psi),...
54             endpoints.y2(r,psi), 'bd', 'MarkerFaceColor', 'b') % ending
55             point
56     end
57 end
58 hold off

```